Solid-State Studies on C_{60} Solvates

Jin Ye

Supervisors:

Prof. Dr. Josep Lluís TAMARIT MUR

Prof. Dr. Maria DEL BARRIO CASADO

Barcelona, September 2017

PhD programme in Computational and Applied Physics

DEPARTAMENT DE FISÍCA

UNIVERSITAT POLITÈCNICA DE CATALUNYA
BARCELONATECH
Departament de Física

Abstract

This thesis focuses on the thermodynamic and crystallographic characterization of C_{60} solvates, formed with small organic molecules ($CBr_2(CH_3)_2$, CBr_2Cl_2, CBr_2H_2, $CBrCl_2H$ and $CBrClH_2$) Nine different solvates are studied in this thesis. Chapter I provides an introduction concerning the physical and chemical properties of fullerene C_{60}, as well as the state of the art for solvates or co-crystals formed between C_{60} and organic materials. Chapter II provides information about the experimental techniques and the models used for the acquisition and analysis of experimental data, and also gives an introduction to the theoretical concepts of the refinement of X-ray Crystal Structures. The presentation, analysis and discussion of the obtained results are presented in the following five chapters, one for each organic solid under scrutiny. The last chapter is devoted to overall conclusions concerning the structural and thermodynamic common properties of the studied solvates. In addition, owing to the particularities of each studied solvates, together with those previously reported by the group and other works, correlations between properties that would allow the prediction of the formation of solvates and the fundamental physical reasons for the solvate formation and its properties, are presented. Going further into the details, some particular correlations involving the molecular symmetry (or pseudo-symmetry) of the host molecule and the overall solvate properties are described.

In Chapter III, the stable hexagonal solvate $C_{60}\cdot 2CBr_2H_2$, has been structurally and thermodynamically characterized. The solvate formed with CBr_2H_2 exhibits overall orientational order due to strong interactions between C_{60} and its solvent host molecule. The orientational order is consistent with the solvate's stability, which has a high negative excess volume and a high desolvation enthalpy.

Chapter IV deals with cubic co-crystals of $C_{60}\cdot 12CBr_2(CH_3)_2$, which were grown at room temperature in saturated solutions of FCC C_{60} and the solvent $CBr_2(CH_3)_2$ with C_{2v} molecular symmetry. The cubic co-crystals are found to be unstable in air and transform spontaneously into hexagonal co-crystals $C_{60}\cdot 2CBr_2(CH_3)_2$. The solvent molecules are positioned close to the prismatic hexagonal voids between the fullerene C_{60} molecules and they are orientationally disordered.

Chapter V describes the cubic co-crystals of $C_{60}\cdot 12CCl_2Br_2$, also unstable in air. These co-crystals transform spontaneously into the hexagonal co-crystals $C_{60}\cdot 2CCl_2Br_2$, the solvent molecules (C_{2v} symmetry) being positioned close to the prismatic hexagonal voids between the fullerene C_{60} molecules and also being orientationally disordered. The hexagonal solvates possess negative excess volume.

In Chapter VI, solvate $C_{60}\cdot 2CBrCl_2H$ is described. The solvent molecules, $CBrCl_2H$ display C_{3v} pseudo-symmetry axis (if one consider the halogen Br and Cl being interchangeable. The hexagonal solvate is stable in open air and undergoes a transformation on heating to another solvate of lower stoichiometry $C_{60}\cdot CBrCl_2H$ with a monoclinic structure. Paradoxically, according to the thermodynamics analysis, the measured desolvation enthalpies for both $C_{60}\cdot 2CBrCl_2H$ and $C_{60}\cdot CBrCl_2H$ do not exceed the sublimation enthalpy of pure $CBrCl_2H$.

Chapter VII is devoted to the characterization of solvate $C_{60}\cdot 2CBrClH_2$. The co-crystals are found to be monoclinic. This low-temperature monoclinic structure transforms reversibly on heating to a new hexagonal phase with the same stoichiometry. Both co-crystal structures form with a negative excess volume, which indicate the strong intermolecular interactions between the C_{60} and $CBrCl_2H$ in their solvate lattices. This result, in clear contradiction to the determined desolvation enthalpy, is clearly smaller than the sublimation enthalpies of the molecular structures of the involved species.

Chapter VIII, the last chapter, the overall experimental results are put together in order to derive common properties for the different studied solvates. To do so, the results of this thesis are analyzed in combination with previous reported results for molecular solvates, for which the solvent molecules have strong similarities to those studied in this work. Thus, we present a tentative overview of crystallographic and some thermodynamic results obtained in the frame of a systematic investigation on C_{60}:Solvent solvates. The results of this thesis represent a step in the direction of extending the current experimental knowledge of co-crystals C_{60}:Solvents. Moreover, the work makes a proposal in order to rationalize the structural properties of these solvates, which mainly consists of a prediction of the solvate volumes according to the van der Waals volumes of the involved chemical species.

Content

1. Introduction....1

1.1 Fulleride C_{60}....1

1.2 Intercalated compounds....3

1.3 Fullerenes in organic solvents: Solvates....5

1.4 References....8

2. Experimental techniques....16

2.1 Solvates Preparation....16

2.2 Scanning Electron Microscopy....17

2.3 Differential Scanning Calorimetry....18

2.3.1 Experimental systems and sample preparation....20

2.4 Thermogravimetric Analysis....22

2.4.1 Experimental system and sample preparation....24

2.5 X-ray Diffraction....25

2.5.1 Some basics concepts....25

2.6 Diffraction by crystals....28

2.6.1 Bragg equation....28

2.6.3 Experimental system and sample preparation....33

2.6.4 Analysis of the Experimental Profiles....35

2.7 References....40

3. The C_{60}:$CBr_2(CH_3)_2$ binary system....42

3.1 The solvent: 2,2-dibromo-propane....42

3.2 Study of the C_{60}:$CBr_2(CH_3)_2$ solvates.....43

3.3 Discussion and structural characterization..... 53

3.5 References.....59

4. The C_{60}:CBr_2Cl_2binary system.....61

4.1 The solvent: Dibromodichloromethane..... 61

4.2 Study of the C_{60}:CBr_2Cl_2 solvates.....62

4.3 Discussion and structural characterization..... 69

4.5 References.....75

5. The C_{60}:CBr_2H_2 binary system..... 76

5.1 The solvent: Dibromomethane.....76

5.2 Study of the C_{60}:CBr_2H_2 solvates.....77

5.3 Discussion and structural characterization..... 82

5.4 Conclusions.....90

5.5 References.....92

6. The C_{60}:$CBrCl_2H$ binary system.....94

6.1 The solvent: Bromodichloromethane.....94

6.2 Study of the C_{60}:$CBrCl_2H$ solvates..... 95

6.3 Discussion and structural characterization..... 103

6.5 Conclusions.....109

6.6 References.....110

7. The C_{60}:$CBrClH_2$ binary system.....111

7.1 The solvent: Bromochloromethane.....111

7.2 Study of the C_{60}:$CBrClH_2$ solvates..... 112

7.3 Discussion and structural characterization..... 118

7.4 Conclusions.....125

7.5 References.....126

8. Conclusion..... 127

1. Introduction

1.1 Fulleride C_{60}

Fullerene C_{60} was successively predicted by Osawa and Bochvar et al, [1, 2] in the early 1970's. Experimentally was registered for the first time in gaseous species produced by laser irradiation of graphite [3], but it would not be until 1990, Krätschmer et al. [4] proposed a method to produce C_{60} in macroscopic quantities. Fullerene is a molecule of carbon in the form of a hollow sphere, tube, and many other shapes. Spherical fullerenes, also referred to as Buckminsterfullerene or buckyball, resemble the balls used in association football. C_{60} belongs to the most studied and widely used compounds, also serve as a platform for producing advanced materials.

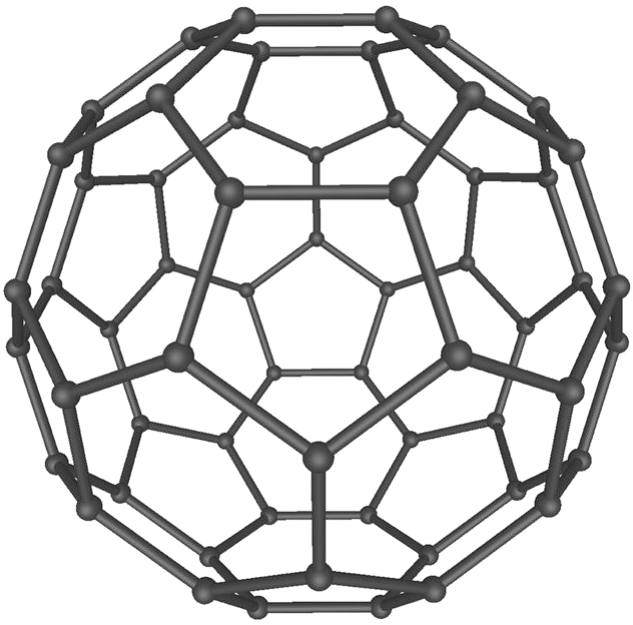

Fig. 1.1. The molecular structure of the C_{60} molecule.

The molecular structure of C_{60} is shown in Fig. 1.1. The C_{60} molecule consists of 60 carbon atoms arranged to obtain an icosahedral (symmetry I_h) with 20 hexagonal and 12 pentagonal faces.

Its molecular structure was first established based on the ^{13}C NMR measurements [5]: the spectrum comprises only one singlet [6].

All carbon atoms are equivalent and there are two types of C-C bonds: 30 short "double bonds" (6:6) that fuse two hexagons and 60 long "single bonds" that fuse a hexagon to a pentagon (6:5). The latter bond is characterized by a larger π-contribution and thus is shorter. The C-C distances in C_{60} are 1.40 Å (6/6) and 1.46 Å (5/6) according to gas electron diffraction data [7]. The corresponding mean values for 52 ordered molecular complexes of C_{60} calculated from the crystallographic data retrieved from the "Cambridge Structural Database" (CSD) are 1.39 Å (6/6) and 1.45 Å (5/6). The bond angles are 108° in pentagons and 120° in hexagons. The spherical excess defined as a difference between 360° and the sum of the bond angles at a certain carbon atom is, in the case of C_{60}, 12° for all carbon atoms. Pseudohexagonal faces are centers of three-fold rotation symmetry, pentagonal faces are centers of five-fold rotational symmetry, edges between two hexagonal faces are centers of two-fold rotational symmetry, and the entire molecule is symmetric under inversion.

Pure crystalline C_{60} can be obtained by resublimation in vacuo to eliminate the solvent molecules that can remain trapped in the interstitial cavities between C_{60} molecules in the crystal lattice.

At room temperature, C_{60} crystallize in an FCC cubic lattice(Fm $\bar{3}$ m) [8] where the molecules are rotationally disordered (Fig. 1.2). Upon a decrease in temperature the compound transforms at around 258 K to a new cubic structure (simple cubic Pa $\bar{3}$) where the molecular disorder is reduced at reorientational jumps about [111] direction. At the transition point, the lattice parameter changed from 14.1501(9) Å to 14.1015(6) Å that corresponds to a lattice contraction of 0.344(8) %. This dynamic disorder freezes at around 90 K.

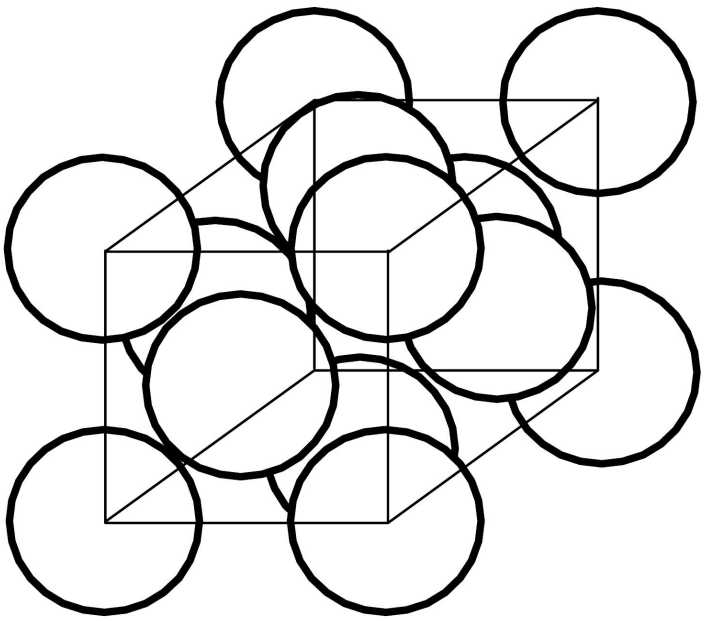

Fig. 1.2. Schematic representation of the crystal structure of the FCC phase of C_{60}.

Fullerenes, with their globular (quasi-spherical) shape, display an extremely rich variety of behaviors in the solid state: Orientational disorder phase with free-rotor (plastic crystalline phase) or merohedral disorder has been identified in the solid phase of C_{60} and their derivatives [9, 10].

1.2 Intercalated compounds

In the FCC structure of C_{60}, there are three interstitial sites per C_{60} molecule, one with octahedral symmetry and two with tetrahedral symmetry. These sites with the effective radius of 2.1 Å and 1.1 Å, respectively, are connected by channels of radius 0.7 Å. Because of the large diameter of the C_{60} molecules, the interstitial cavities are large enough to incorporate several atoms without too much distortion of the FCC packing. Moreover, the chemical

reactivity of the C_{60} is low and many atomic or molecular species can diffuse into the cavities of the C_{60} lattice without forming any chemical bond. There is a strong correlation between the dimensions of the intercalant atoms or molecules and their ability to intercalate into the interstitial sites in the fullerite lattice. The intercalation of rare gases into these sites had been carried out by Morosin et al. [11, 12]. For low stoichiometries, these compounds (co-crystals) can retain the same structure as pristine C_{60} at high and low temperature [13].

Intercalation of atomic and molecular gases gives rise to many novels and interesting phenomena in C_{60} lattices. The intercalation can lead to significant changes in the properties of C_{60} materials, through chemical reactions induced by temperature or pressure, the effects of those properties depend on the presence of intercalated impurity atoms or molecules. Intercalation can be used as a physical tool to study the properties of single molecules or their interactions with carbon or each other. Research into intercalation compounds of fullerites will probably continue to be of interest for many years to come [14].

During the investigation on Fullerite C_{60} with N_2 molecules by Galtsov et al. [13] showed that N_2 molecules intercalated into the C_{60} lattice cause increase in the lattice parameter. Both Tc (the orientational phase transition) and the associated change in the lattice parameter exhibit hysteresis. The peculiar behavior of solid C_{60}:N_2 solutions and solutions with atomic species are largely determined by the non-central component in the C_{60}:C_{60} intermolecular interaction [13], as well from the possible ordering of the molecular species in the octahedral sites at lower temperatures.

The effect of intercalation of C_{60} with helium and argon atoms on the fullerite structure was described by Stetsenko [15]. The evolution of the lattice parameters and the half-width for certain reflections as a function of the intercalation time of the helium atoms has shown that the voids in the C_{60} lattice were filled in two stages: the Helium atoms filled the octahedral voids relatively rapidly first, then fill the tetrahedral subsystem. The intercalants affected the half-width, intensity of the reflections, the lattice parameters, the phase transition temperature, the volume change at the transition and the thermal expansion coefficients of C_{60} [15].

Ohno et al. [16] believed that solid C_{60} will take up only minor amounts of iodine, resulting in the non-metallic product. However, Zhu et al. [17] using different experimental

conditions, prepared a highly crystalline $C_{60}{\cdot}I_4$, with alternating layers closely resembling of classic intercalation compounds. $C_{60}{\cdot}I_4$ was the first sample of fullerite intercalation compound with no electron transfer between C_{60} and the intercalate.

C_{60} can form intercalation compounds with alkali elements too. In the A_xC_{60} (A = Na, K, Rb, Cs) series there are materials with very interesting properties [18-24]. Intercalation of alkali elements results in a transfer of their valence electrons into the conduction bands, generating conduction and superconduction phenomena. Because of their unusual conducting and superconducting properties, these materials have attracted a lot of attentions. These properties are not restricted to the intercalation of inorganic elements, they also concern organic electronics. In spite of questionable experimental works like C_{60}:halogenomethane solvates, have been the focus on many studies [25]. The electronic structure of C_{60}:bromoform and C_{60}:chloroform solvates ($C_{60}{\cdot}2HCX_3$, X = Cl, Br) [26, 27] have provided a different electronic density of states (DOS). It was concluded, mainly from calculations, that DOS alone cannot account for a possible increase of the superconducting temperature upon intercalation of the chloroform and substitution by bromoform [25]. Coupling the vibrational modes of the C_{60} molecule and those of the haloform molecules has also been proposed as an additional possible mechanism.

1.3 Fullerenes in organic solvents: Solvates.

Crystals that can be obtained simply by slowly evaporating in the dark solutions of C_{60} in different organic solvents have been termed "solvates" by analogy with "hydrates", because a well-defined stoichiometry of the C_{60} and the solvent molecules give rise to a new lattice structure.

Following Krätschmer et al. [28], fullerenes are extracted by solvents, purified by chromatographic methods and crystallized by solvent evaporation. It soon appeared that the structural properties of the fullerenes so obtained depend on the solvents used because of the formation of solvates [29, 30]: The obtention of pure C_{60} depends on the stability of these

solvates. However, little is known about the structural properties of these compounds, probably as wrote by Gorun et al. "attempts to obtain crystals suitable for X-ray crystallography have been hampered by rotational and long-range disorder" [31], because the solvents can be retained (structurally or interstitially) strongly by FCC C_{60}. This leads to changes in the thermodynamic features of the SC-FCC C_{60} transition at 261 K [32] and in the X-ray diffraction patterns of FCC C_{60} which is related to stacking faults [33]. Also, solvates commonly exhibit incongruent melting giving rise to FCC C_{60} and its saturated solution. Only above the incongruent melting temperature does the saturated solution reflect the solubility of FCC C_{60}, whereas below this temperature the solubility of its solvate will be obtained [34-38]. Therefore, the stability and composition of fullerene solvates have been the focus of a large number of studies [39-47].

A large number of fullerene solvates containing aromatic solvents had been reported by Korobov et al., [44] which revealed that the solvate structures are “typical van-der-Waals complexes”, with small negative excess volumes and high packing coefficients. The excess volume and packing coefficients should correlate with the stabilities of the solvates. By now, the formation of the solid-state solvates was reported on C_{60} with benzene, CS_2, n-pentane, n-heptane, n-hexane, n-nonane, cyclohexane, CCl_4, other halogenated alkanes, toluene, bromobenzene, 1,2- and 1,3-dibromobenzenes, chlorobenzene, 1,3-dichlorobenzene, o-xylene, 1,2,4- and 1,3,5-trimethylbenzenes, tetralin, and other solvents, including alcohols [48].

For the solvates with 1:2 stoichiometry, the tetrahedral molecules such as C_{60}:2$YCCl_3$ (Y = H, CH_3, Br, Cl) and C_{60}:2$HCBr_3$, the results indicate that the van-der-Waals volume of the solvent molecules has a proportional relationship with the unit-cell volume of the solvates. However, for highly symmetrical solvent molecules, the particular external atoms of the solvent molecules seem not important, or, at least within the considered temperature ranges [46]. For example, solvates containing the solvent molecules as chloroform, $HCCl_3$, and bromoform, $HCBr_3$, with a C_{3v} symmetry possess a hexagonal crystal symmetry (P6/mmm), the C_{60} and the haloform molecules are stacked in alternating layers (the [001] hexagonal planes) [27].

Also for solvates with solvent molecules as $(CH_3)CCl_3$ and $BrCCl_3$ (C_{3v} symmetry too) or CCl_4 with the higher molecular symmetry (T_d), similar results were found for the crystal symmetry and for its crystal lattice anisotropy [49-53].

Fullerenes had attracted considerable attention in different fields of science, from the latest nanotechnologies (electronics, optics, fuel cells, etc.) to medicine or cosmetics, are the result of their unique properties, among which the high electron-acceptor ability and polarizability play outstanding roles. Thousands of papers are devoted to the application of fullerenes. They are used in the creation of liquid and solid compositions possessing useful properties [54-58], in biochemistry and biomedicine [59-68] analytical chemistry, [69, 70] and many other fields.

In this work, solvates of C_{60} with tetrahedral halogen-metahne derivative solvents: $CBr_2(CH_3)_2$ and CBr_2Cl_2, CBr_2H_2, $CBrCl_2H$ and $CBrClH_2$ are described. Comparison of different tetrahedral halogen-methanes polar solvents previously studied will be performed in order to shed light on the stability and other properties of these solvates. Consequently, the crystallographic packing and the crystal anisotropy of the solvates will be explained on the basis of the van-der-Waals volume of the constituents and a general relationship will be proposed.

1.4 References

[1] Osawa, E. Kagaku, Chemistry, 25, 1970, 854; Chemical Abstracts Service， 74， 1971，75698v.

[2] D. A. Bochvar, E. G. Galpern, DokladyAkademiiNauk SSSR 209, 1973, 610

[3] H. W. Kroto, J. R. Heath, S. C. O`Brien, R. F. Curl, R. E. Smalley, C_{60}: Buckminsterfullerene, Nature, 318, 1985, 162.

[4] W. Krätschmer, L. D. Lamb, K. Fostiropoulos, D. R. Huffman, Solid C_{60}: a new form of carbon, Nature, 347, 1990, 354.

[5] C. Piskotti, J. Yarger, A. Zettl, C_{36}. a new carbon solid, Nature, 393, 1998, 771.

[6] R. D. Johnson, G. Meijer, D. S. Bethune, C_{60} has icosahedral symmetry, Journal of the American, 122, 1990, 8983.

[7] K. Hedberg, L. Hedberg, D. S. Bethune, C. A. Brown, H. C. Dorn, R. D. Johnson, M. De, Vries, Bond lengths in free molecules of buckminsterfullerene, C_{60}, from gas-phase electron diffraction, Science, 254, 1991, 410.

[8] W. I. F. David, R. M. Ibberson, T. J. S. Dennis, J. P. Hare, K. Prassides, Structural Phase Transitions in the Fullerene C_{60}, Europhysics Letters, 18, 1992, 219.

[9] M Mehring, KF Thier, F Rachdi, T de Swiet, Localized and delocalized electronic states in A_1C_{60} (A = Rb, Cs), 38, 2000, 1625.

[10] I. S. Neretin, Y. L. Slovokhotov, Chemical crystallography of fullerenes, Russian chemical reviews, 73, 2004, 455.

[11] B. Morosin, J. D. Jorgensen, Simine Short, G. H. Kwei, J. E. Schirber, Ne-intercalated C_{60}:Pressure dependence of Ne-site occupancies, Physical Review B, 53, 1996, 1675.

[12] B. Morosin, Zhongbo Hu, J. D. Jorgensen, Simine Short, J. E. Schirber, G. H. Kwei, Ne intercalated C_{60}:Diffusion kinetics, Physical Review B, 59, 1999, 6051.

[13] N. N. Galtsov, A. I. Prokhvatilov, G. N. Dolgova, Intercalation of fullerite C_{60} with N_2 molecules. An investigation by X-ray powder diffraction, Low Temperature Physics, 33, 2007, 1159.

[14] B. Sundqvist, Interaction between and gases under pressure, Low Temperature Physics 29, 2003, 440.

[15] Y. E. Stetsenko, I. V. Legchenkova, K. A. Yagotintsev, A. I. Prokhvatilov, M. A. Strzhemechnyĭ, Intercalation of C_{60} fullerite with helium and argon at normal temperature and pressure, Low Temperature Physics, 29, 2003, 445.

[16] G. H. Kroll, P. J. Benning, Y. Chen, T. R. Ohno, J. H. Weaver, L. P. F. Chibante, R. E. Smalley, Interaction of O_2 with C_{60}: photon-induced oxidation, Chemical Physics Letters, 181, 1991, 112.

[17] Q. Zhu, J. E. Fischer, K. Kniaz, A. R. McGhie, O. Zhou, Intercalation of Solid C_{60} with Iodine, Nature, 355, 1992, 712.

[18] K. Holczer, O. Klein, S. M. Huang, R. B. Kaner, K. J. Fu, R. L. Whetten, F. Diederich, Alkali-fulleride superconductors-Synthesis, composition, and diamagnetic shielding, Science, 252, 1991, 1154.

[19] R. M. Fleming, A. P. Ramirez, M. J. Rosseinsky, D. W. Murphy, R. C. Haddon, S. M. Zahurak, A. V. Makhija, Relation of structure and superconducting transition temperatures in A_3C_{60}, Nature, 352, 1991, 787.

[20] R. C. Haddon, A. F. Hebard, M. J. Rosseinsky, D. W. Murphy, S. J. Duclos, K. B. Lyons, B. Miller, J. M. Rosamilia, R. M. Fleming, A. R. Kortan, S. H. Glarum, A. V. Nakhija, A. J. Muller, R. H. Eick, S. M. Zahurak, R. Tycko, G. Dabbagh, F. A. Thiel, Conducting Films of C_{60} and C_{70} by Alkali-Metal Doping, Nature, 350, 1991, 320.

[21] K. Holczer, R. L. Whetten, Superconducting and normal state properties of the A_3C_{60} compounds, Carbon, 30, 1992, 1261.

[22] J. E. Fisher, P. A. Heiney, Order and disorder in fullerene and fulleride solids, Journal of Physics and Chemistry of Solids, 54, 1993, 1725.

[23] S. V. Kozyrev, V. V. Rotkin, Fullerene: Structure, crystal lattice dynamics, electron structure, and properties (a review), Semiconductors 27, 1993, 777.

[24] V. N. Denisov, A. S. Lipin, B. N. Mavrin, A. A. Zakhidov, G. Ruani, R. Zamboni, C. Taliani, Raman scattering and lattice dynamics of fullerides MxC_{60}, Synthetic metals, 64, 1994, 341.

[25] R. Céolin, D.O. López, B. Nicolaï, P. Espeau, M. Barrio, H. Allouchi, J. Ll. Tamarit, Solid-state studies of C_{60} solvates formed with chlorodibromomethane, Chemical Physics, 342, 2007, 78.

[26] R. Windiks, A. Bill, B. Delley, V. Z. Kresin, Crystal structures and electronic properties of haloform-intercalated C_{60}, Physical Review B, 66, 2002, 195418.

[27] R. E. Dinnebier, O. Gunnarsson, H. Brumm, E. Koch, A. Huq, P. W. Stephens, M. Jansen, Structure of haloform intercalated C_{60} and its influence on superconductive properties, Science, 296, 2002 109.

[28] W. Krätschmer, L. D. Lamb, K. Fostiropoulos and D. R. Huffman, Solid C_{60}: a new form of carbon, Nature, 347, 1990, 354.

[29] K. Kikuchi, S. Suzuki, K. Saito, H. Shiromaru, I. lkemoto, Y. Achiba, A.A. Zakhidov, A. Ugawa, K. Imaeda, H. Inokuchi, K. Yakushi, Structure and superconductivity of single crystalline C_{60}, Physica C, 415, 1991, 185.

[30] B. Morosin, P. P. Newcomer, R. J. Banghman, E. L. Vinturini, D. Loy, J. E. Schirber, On the "orthorhombic form of C_{60}" molecular crystals containing CS_2, Physica C, 184, 1991, 21.

[31] S. M. Gorun, K. M. Creegan, R. D. Sherwood, D. M. Cox, V. W. Day, C. S. Day, R. M. Upton, C. E. Briant, Solvated C_{60} and C_{60}/C_{70} and the low-resolution single crystal X-ray structure of C_{60}, Journal of the Chemical Society, Chemical Communications, 21, 1991, 1556.

[32] Y. Miyazaki, M. Srai, R. Lin, A. Dworkin, H. Szwarc, J. Godard, Heat capacity of a giant single crystal of C_{60}, Chemical Physics Letters, 305, 1999, 293.

[33] G. B. M. Vaughan, Y. Chabre, D. Dubois, Effect of stacking disorder on the orientational ordering transition of solid C_{60}, Europhysics Letters, 31, 1995, 525.

[34] M. V. Korobov, A. L. Mirakian, N. V. Avramenko, E. F. Valeev, I. S. Neretin, Y. L. Lovokhotov, A. L. Smith, G. Olofsson, R. S. Ruoff, C_{60}·Bromobenzene Solvate: Crystallographic and Thermochemical Studies and Their Relationship to C_{60} Solubility in Bromobenzene, The Journal of Physical Chemistry B, 102, 1998, 3712.

[35] Y. Iwasa, K. Tanoue, T. Mitani, A. Izuoka, T. Sugawara, T. Yagi, High yield selective synthesis of C_{60} dimers. Chemical Communications, 13, 1998, 1411.

[36] R. Macovez, M. R. C. Hunt, J. Shan, A. Goldoni, T. Pichler, M. Pedio, P. Moras, C. Castellarin-Cudia, J. Schiessling, L. Venema, Metal-to-insulator transition in thin-film polymeric AC_{60}. New Journal of Physics, 11, 2009, 023035.

[37] A. L. Briseno, S. C. B. Mannsfeld, M. M. Ling, S. H. Liu, R. J. Tseng, C. Reese, M. E. Roberts, Y. Yang, F. Wudl, Z. N. Bao, Patterning organic single-crystal transistor arrays, Nature, 444, 2006, 913.

[38] W. L. Ma, C. Y. Yang, X. Gong, K. Lee, A. J. Heeger, Thermally stable, efficient polymer solar cells with nanoscale control of the interpenetrating network morphology, Advanced Functional Materials, 15, 2005, 1617.

[39] S. Cho, J. H. Seo, K. Lee, A. J. Heeger, Enhanced Performance of Fullerene n-Channel Field-Effect Transistors with Titanium Sub-Oxide Injection Layer, Advanced Functional Materials, 19, 2009, 19, 1459.

[40] L. D. Zheng, Y. Han, Solvated Crystals Based on [6,6]-Phenyl-C_{61}-butyric Acid Methyl Ester (PCBM) with the Hexagonal Structure and Their Phase Transformation. The Journal of Physical Chemistry B, 116, 2012, 1598.

[41] L. J. Wang, Solvated fullerenes, a new class of carbon materials suitable for high-pressure studies: A review. Journal of Physics and Chemistry of Solids, 84, 2015, 85.

[42] K. N. Semenov, N. A. Charykov, V. A. Keskinov, A. K. Piartman, A. A. Blokhin, A. A. Kopyrin, Solubility of Light Fullerenes in Organic Solvents. Journal of Chemical & Engineering Data, 55, 2010, 13.

[43] C. Smart, B. Eldridge, W. Reuter, J. A. Zimmerman, W. R. Creasy, N. Rivera, R. S. Ruoff, Extraction of giant fullerene molecules, and their subsequent solvation in low boiling point solvents. Chemical Physics Letters, 188, 1992, 171.

[44] M. V. Korobov, E. B. Stukalin, A. L. Mirakyan, I. S. Neretin, Y. L. Slovokhotov, A. V. Dzyabchenko, A. I. Ancharov, B. P. Tolochko, New solid solvates of C_{60} and C_{70} fullerenes: The relationship between structures and lattice energies. Carbon, 41, 2003, 2743.

[45] A. V. Dzyabchenko, V. Agafonov, V. A. Davydov, A Theoretical Study of the Pressure-Induced Dimerization of C_{60} Fullerene. The Journal of Physical Chemistry A, 103, 1999, 2812.

[46] L. Wang, B. Liu, H. Li, W. Yang, Y. Ding, S. V. Sinogeikin, M. Yue, Z. Liu, X. C. Zeng, W. L. Mao, Long-Range Ordered Carbon Clusters: A Crystalline Material with Amorphous Building Blocks, Science, 337, 2012, 825.

[47] V. D. Blank, S. G. Buga, M. Y. Popov, V. A. Davidov, H. Szwarc, A. Rassat, G. Fabre, Fullerene C_{60} Under the Influence of High Pressure Together with High Shear Stresses: How to Scratch Diamond, New Journal of Chemistry, 19, 1995, 253.

[48] O. N. Mchedlov-Petrossyan, Fullerenes in Liquid Media: An Unsettling Intrusion into the Solution Chemistry, Chemical Reviews, 113, 2013, 5149.

[49] R. Céolin, J. LlTamarit, M. Barrio, D. O. López, P. Espeau, H. Allouchi, R. J. Papoular, Solid state studies of the $C_{60}{\cdot}2(CH_3)CCl_3$ solvate, Carbon, 43, 2005, 417.

[50] M. Barrio, D.O. López, J.LlTamarit, P. Espeau, R. Céolin, Solid-State Studies of C_{60} Solvates Formed in the C_{60}-$BrCCl_3$ System, Chemistry of Materials, 15, 2003, 288.

[51] B. Keita, L. Nadjo, R. Céolin, V. Agafonov, D. Andre, H. Szwarc, J. Dugue, C. Fabre, A. Rassat, Atomic force microscopy characterization of stable faces in cubic C_{60} and hexagonal $C_{60}\cdot 2CCl_4$ single crystals, Chemical Physics Letters, 179, 1994, 595.

[52] R. Céolin, J. LlTamarit, M. Barrio, D. O. López, S. Toscani, H. Allouchi, V. Agafonov, H. Szwarc, Solid-state studies on a cubic 1: 1 solvate of C_{60} grown from dichloromethane and leading to another hexagonal C_{60} polymorph, Chemistry of Materials, 13, 2001, 1349.

[53] M. Barrio, D. O. López, J. LlTamarit, H. Szwarc, S. Toscani, R. Céolin, $C_{60}\cdot CCl_4$ phase diagram: polythermalbehaviour of solvates $C_{60}\cdot 12CCl_4$ and $C_{60}\cdot 2CCl_4$, Chemical Physics Letters, 260, 1996, 78.

[54] Y. M. Wang, P. V. Kamat, L. K. Patterson, Aggregates of fullerene C_{60} and C_{70} formed at the gas-water interface and in DMSO/water mixed solvents. A spectral study, The Journal of Physical, 97, 1993, 8793.

[55] K. G. Thomas, V. Biju, D. M. Guldi, P. V. Kamat, M. V. George, Photoinduced Charge Separation and Stabilization in Clusters of a Fullerene-Aniline Dyad, The Journal of Physical Chemistry B, 103, 1999, 8864.

[56] M. Becherer, B. Schade, C. Böttcher, A. Hirsch. Supramolecular Assembly of Self-Labeled Amphicalixarenes. Chemistry - A European Journal, 15, 1990, 1637.

[57] Y. Ren, P. Paira, T. R. Nayak, W. H. Ang, G. Pastorin, Synthesis of fullerene@gold core-shell nanostructures, Chemical Communications, 47, 2011, 7710.

[58] E. M. Pérez, Energy, supramolecular chemistry, fullerenes, and the sky, Pure and Applied Chemistry, 83, 2011, 201.

[59] E. Nakamura, H. Isobe, Functionalized fullerenes in water. The first 10 years of their chemistry, biology, and nanoscience, Accounts of chemical research, 36, 2003, 807.

[60] V. L. Colvin, The potential environmental impact of engineered nanomaterials, Nature biotechnology, 21, 2003, 1166.

[61] T. D. Ros, M. Prato, Medicinal chemistry with fullerenes and fullerene derivatives, Chemical Communications, 1999, 663.

[62] S. Bosi, T. D. Ros, G. Spalluto, M. Prato, Fullerene derivatives: an attractive tool for biological applications, European journal of medicinal, 38, 2003, 913.

[63] J. D. Fortner, D. Y. Lyon, C. M. Sayes, A. M. Boyd, J. C. Falkner, E. M. Hotze, L. B. Alemany, Y. J. Tao, W. Guo, K. D. Ausman, V. L. Colvin, J. B. Hughes, C_{60} in Water: Nanocrystal Formation and Microbial Response, Environmental Science & Technology, 39, 2005, 4307.

[64] R. Bakry, R. M. Vallant, M. Najam-ul-Haq, M. Rainer, Z. Szabo, C. W. Huck, G. K. Bonn, Medicinal applications of fullerenes, International Journal of Nanomedicine, 2, 2007, 639.

[65] N. Shinohara, T. Matsumoto, M. Gamo, A. Miyauchi, S. Endo, Y. Yonezawa, J. Nakanishi, Is Lipid Peroxidation Induced by the Aqueous Suspension of Fullerene C_{60} Nanoparticles in the Brains of Cyprinuscarpio?, Environmental Science & Technology, 43, 2009, 948.

[66] J. Lee, Y. Mackeyev, M. Cho, D. Li, J. H. Kim, L. J. Wilson, P. J. J. Alvarez, Photochemical and antimicrobial properties of novel C_{60} derivatives in aqueous systems, Environmental Science & Technology, 43, 2009, 6604.

[67] K. Mizuno, T. Zhiyentayev, L. Huang, S. Khalil, F. Nasim, G. P. Tegos, H. Gali, A. Jahnke, T. Wharton, M. R. J. Hamblin, Antimicrobial photodynamic therapy with functionalized fullerenes: quantitative structure-activity relationships, Journal of nanomedicine & nanotechnology, 2, 2011, 49.

[68] M. Carini, L. Djordjevic, T. D. Ros, Fullerenes in Biology and Medicine, Medicinal and Bio-Related Applications, 3, 2012, 1.

[69] Y. P. de Peña, M. Gallego, M. Valcarcel, Preconcentration of copper traces on C_{60}-C_{70} fullerenes by formation of ion pairs and chelates, Analytical Chemistry, 67, 1995, 2524.

[70] K. Scida, P. W. Stege, G. Haby, G. A. Messina, C. D. García, Recent applications of carbon-based nanomaterials in analytical chemistry: Critical review, AnalyticaChimicaActa, 691, 2011,6.

2. Experimental techniques

2.1 Solvates Preparation

The solvents, all of them are liquid at room temperature, involved in the formation of the solvates with fullerene studied in this work are:

- 2,2 Dibromopropane, $CBr_2(CH_3)_2$
- Dibromodichloromethane, CBr_2Cl_2
- Dibromomethane, CBr_2H_2
- Bromochloromethane, $CBrClH_2$
- Bromodichloromethane, $CBrCl_2H$

Table.2.1. Solvent properties.

Solvate	Molar mass (g/mol)	Density (Room T) (g/cm^3)	Origin	Purity
$CBr_2(CH_3)_2$	201.89	1.78	Aldrich	95%
CBr_2Cl_2	242.71	2.43	Across	98%
CBr_2H_2	173.84	2.50	Aldrich	≧99%
$CBrClH_2$	129.38	1.93	Aldrich	≧99.5%
$CBrCl_2H$	163.8	1.98	Aldrich	98%

The properties of their liquid phases related to this work are summarized in Table. 2.1. Fullerene C_{60} (M = 720.64 g/mol) was purchased from Term USA with a purity higher than 99.98%.

The co-crystals are obtained by mixing solid C_{60} with an excess of the corresponding solvent in screw-cap tubes. These tubes are stored in the dark, and they were periodically monitored by optical microscopy. The appearance of co-crystals is revealed by a change in color of the solution, and the appearance of crystals clearly is different from the bright powder characteristics of the C_{60}. Once the C_{60} powder has disappeared, the newly formed co-crystal is analyzed.

In order to characterize the new co-crystal, a number of techniques are used to provide the physical information about its composition (stoichiometry), crystal structure and thermal behavior. In this chapter, the used techniques are introduced:

- Scanning Electron Microscopy (SEM) is used to obtain information about the morphology of the new co-crystals, information closely related to that obtained by X-ray powder diffraction.
- X-ray powder diffraction measurements allow us to obtain the symmetry and lattice parameters as well as the structure of the co-crystals.
- The thermogravimetric analysis (TGA) provides information about the stoichiometry of the co-crystals.
- Differential scanning calorimetry (DSC) provides information about temperatures and energies involved in the possible transitions of the co-crystals.

2.2 Scanning Electron Microscopy

The Scanning Electron Microscopy (SEM) is a useful technique to study topography, morphology and composition of materials with high accuracy. In the scanning electron microscope, a stream of primary electrons is focused onto the sample surface resulting in a number of different particles or waves being emitted (secondary electrons, backscattered electrons, X-ray, photons, Auger electrons…). The secondary and backscattered electrons are used for imaging while the X-ray giving characteristic chemical information of the emitting atoms. The probed depth in EDX analysis is around 1 - 3 μm (shown in Fig. 2.1). The electrons are then collected by the detector and converted into signal which was displayed on a screen. In the present study, the scanning electron microscope used was a JEOL-7100F (scanning voltage 20kV) from the department of Materials Science of the Universitat Politècnica de Catalunya.

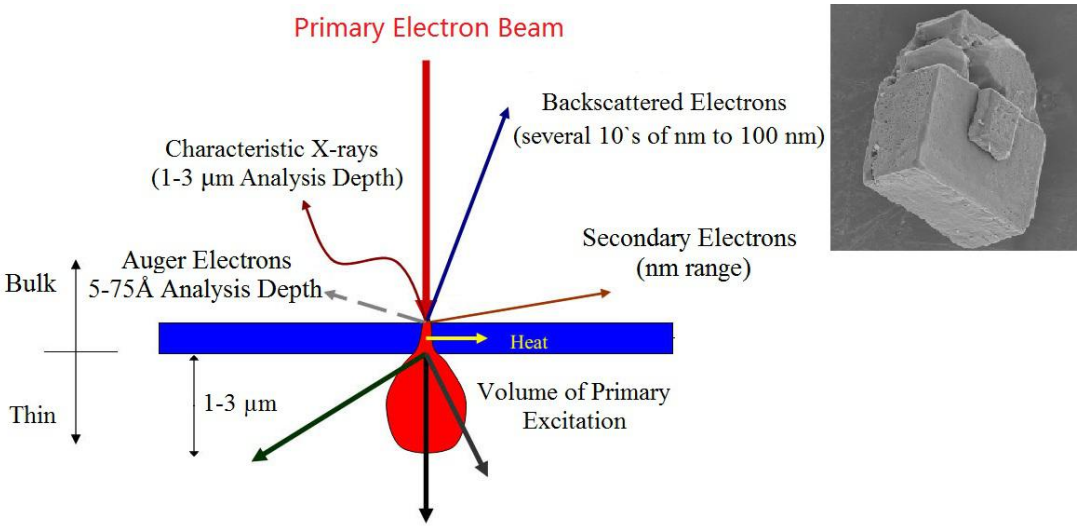

Fig. 2.1. Operating principle of a Scanning Electron Microscope. Insert: The SEM image of a cubic co-crystal.

2.3 Differential Scanning Calorimetry

To determine the temperatures and energies associated with thermodynamic changes of a substance such as fusion, solid-solid transition, crystallization, or desolvation, thermal analysis techniques are commonly used. In this technique, the substance is subjected to a controlled temperature program. In the classical DTA (Differential Thermal Analysis) the temperature difference between a sample and an inert reference material is measured when both are subjected to the same temperature program. As for the DSC (Differential Scanning Calorimetry) technique, the system measures the power needed to compensate the temperature difference between sample and reference along the temperature program [1]. Thanks to a previous calibration procedure, DTA signal is converted to power difference and thus, in both cases, the calorimetric signal has always the units of power.

In both cases, the thermal signal (power difference) is plotted as a function of time or temperature (assuming that heating rate is known) and this plot is called thermogram. An

endothermic event, such as a melting of the sample, yields a peak on the DTA or DSC signal Fig. 2.2. The initial peak temperature T_i, is the temperature (at time t_i) where the curve begins to deviate from the initial base line; the final temperature, T_f, is the temperature (at the time t_f) where the curve recovers the final baseline after the thermal effect finishes. The interpolated base line between these temperatures will be a horizontal straight line if the capacities of the initial and final phases are very similar. The temperature T_0 where the extrapolated ascending peak slope intersects the extrapolated initial base line is the onset temperature. The temperature T_0 is then the transition temperature.

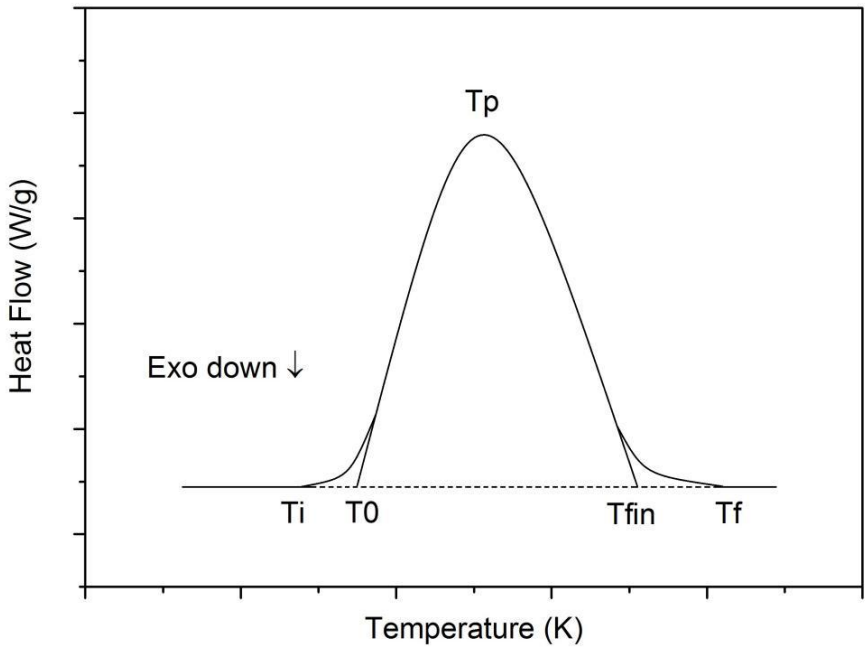

Fig. 2.2. Thermogram representing an endothermal event of a pure compound.

The area of the peak defined by the interpolated baseline and the peak is proportional to the enthalpy of transition, and to the mass of the sample [2] being the quotient between the area and the mass sample the enthalpy associated with the thermal transformation. For an

exothermal event, such as a crystallization, an inversed peak (downward) is obtained, the characteristic temperatures and energies being obtained in a similar manner. The enthalpy calibration procedure allows establishing the relationship between the enthalpy change measured (ΔH_{meas}) by the instrument for a given transition and the true transition enthalpy change of the sample (ΔH_{tr}), $\Delta H_{tr} = K \cdot \Delta H_{meas}$ of a reference well-known material. Between the recommended reference materials published by the International Confederation of Thermal Analysis IUPAC [3], the most commonly used is the melting process of Indium (T_m = 429.75 K and ΔH = 3.267 kJ/mol).

2.3.1 Experimental systems and sample preparation

Two experimental systems from TA Instruments, Q100 and TA2910 models, have been used. Both are DTA systems with an operating mode quite similar but with different cooling systems that allow to work down from 193 K and 113 K, respectively.

In Fig. 2.3A the calorimetric cell of both devices is shown. It consists mainly of a furnace temperature of which can be changed at a well-defined and controlled rate for the sample and reference temperature detectors. The sample is contained in a small crucible, called pan, designed to ensure a good thermal contact with the signal detectors. The inert material, called reference, is an empty pan.

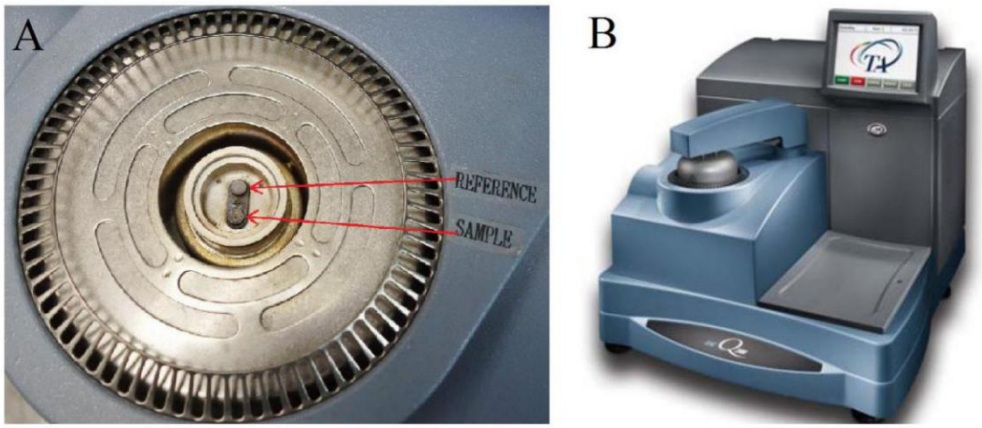

Fig. 2.3. Measuring cell (A) of the Q100 flux differential scanning calorimeter (B).

In relation to the measurements performed in the DTA systems, standard aluminum pans (from TA Instruments) or high pressure gold-plated stainless-steel (from Perkin-Elmer) sealed pans were used (Fig. 2.4). Due to the possible solvate instability out of the mother liquid, some measurements were performed over heterogeneous mixtures i.e., solvate co-crystals and liquid solution. In addition, the liquid, mainly composed of the solvent, has a high tendency to evaporate and, moreover, it was observed that this vapor rusts the standard aluminum pans. In these special cases the heterogeneous mixtures, co-crystals and mother liquor, were encapsulated in the aforementioned high pressure stainless-steel pans.

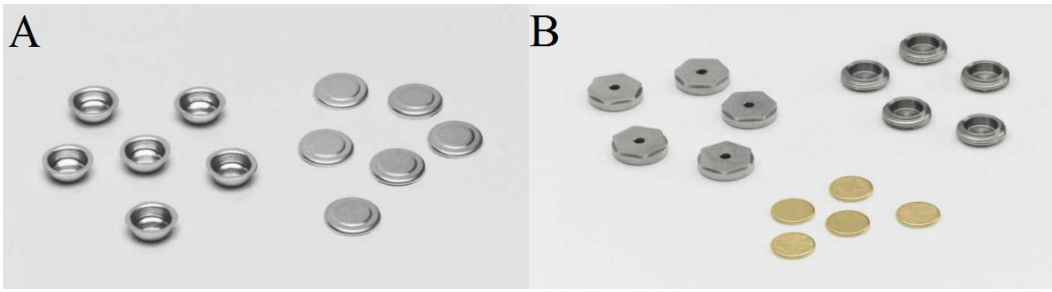

Fig. 2.4. Standard aluminum pans for DTA (A) and high pressure gold-plated stainless-steel (B) sealed pans.

The measurements over these mixtures allow us to obtain information about the temperature and energy transitions related to both the solvate and the liquid solution. This kind of measurements were performed in the TA2910 device, at a heating rate commonly of 2 K/min. The scanned temperature range was determined according to the crystallization and boiling point of the solvent.

To determine the desolvation enthalpy of the co-crystals, pierced aluminum pans (Fig. 2.5) were used, assuming that the rust is avoided in an open pan. The measurements were performed in the Q100 device at scanning rates ranged between 2 and 5 K/min from temperatures around room temperature to 400 K.

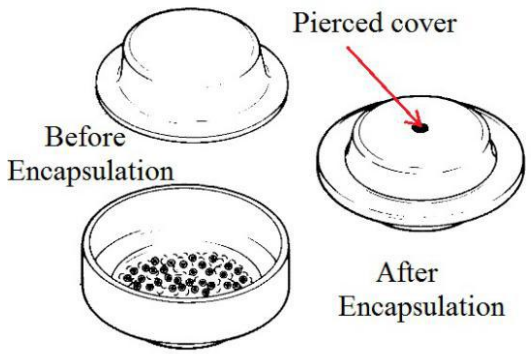

Fig. 2.5. Pierced aluminum pans for desolvation measurements (DSC and TGA devices).

2.4 Thermogravimetric Analysis

Thermogravimetric analysis (TGA) is a thermal weight-change analysis instrument, which is used to study changes in the mass of materials containing reactive or volatile molecular species as a function of time at a given temperature (isothermal regime), or as a function of temperature (scanning procedure as for the DTA or DSC techniques). The changes

in the mass can be caused by a variety processes such as decomposition, degradation, sublimation, vaporization, adsorption, desorption, oxidation, and reduction. The device can measure the loss of mass in the isothermal regime, or the changes in the mass that occur in response to programmed temperature changes. Both kinds of measurements have been used in this work depending on the thermal stability of the solvates, which allows obtaining their composition or stoichiometry of co-crystals. TGA is similar to DTA and DSC techniques: when the temperature of the system is submitted to a defined program, the resulting plot of the mass loss as a function of temperature (or time) is called thermograph or thermogram.

An example of a dynamic TGA measurement is shown in Fig. 2.6 where the variation of the mass is plotted as a function of the time or the temperature.

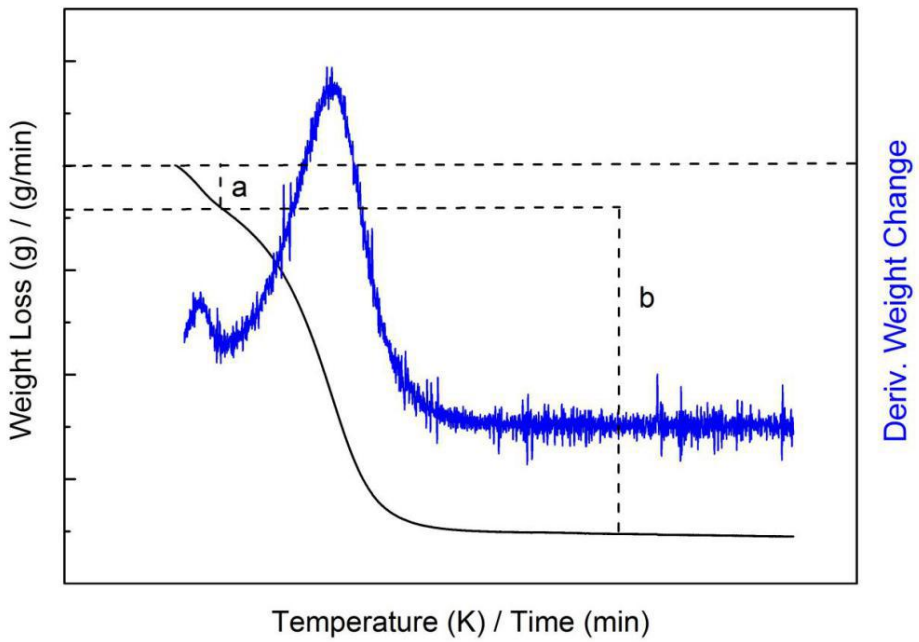

Fig. 2.6. Example of a TGA thermograph (left) and its first derivative of the mass loss (right y-axis) is displayed.

Due to the different decomposition rates or sublimation pressure vapors, the losses of

several components can be separated in a stepwise fashion, and the amounts of each component in the material can be determined. In Fig. 2.6, the mass loss is visible as a step-like decrease to the end of the process. Looking in more detail, it can be seen that this change can be deconvoluted into two smaller steps (a and b). While step "a" is not visible by naked eye in the TGA graph, it is clearly resolved in the derivative of the mass loss with respect to temperature or time.

2.4.1 Experimental system and sample preparation.

The system used in this work has been the Q50 device from TA instruments (Fig. 2.7). The figure shows the furnace and the balance with a platinum plate where the sample is located. This system has a single control/sample thermocouple positioned very close to the sample that allows measuring the temperature of the sample. To evacuate the vapor backflow a flux of inert gas is directed through the balance chamber. The vertical thermobalance is able to load a sample weight up to 1 g and the accuracy of the mass loss is better than 1 μg.

Fig. 2.7. Q50 Thermogravimetric analysis (TGA) from TA instruments.

The TGA measurements have been performed from room temperature to the stabilization of the loss of mass at around 400 - 500 K depending on the studied sample. The scanning heating rates were ranged between 2 - 5 K/min. For a better control of the sample mass, samples were encapsulated in pierced DSC aluminum pans and located on the platinum plate.

2.5 X-ray Diffraction

2.5.1 Some basics concepts

A crystal is a solid material whose constituents (such as atoms, molecules or ions) are arranged in an anisotropic, ordered microscopic structure, forming a crystal lattice that extends in all directions and that can be measured and quantified with crystallographic tools.

In a crystal lattice, there is a translational periodic arrangement of points in space called lattice and a motif that is an atom or group of atoms associated with each lattice points.

The smallest regularly-repeating block that contains the complete lattice pattern of a crystal is known as the unit cell. The unit cell shape of each crystal system can be described by the lengths of the unit vectors (a, b, c) and the angles between them (α, β, γ).

In 1849, Auguste Bravais found that all regular crystals could be described in terms of only 14 lattice types [4]. According to the symmetry and space rotations, lattices are classified into the 7 crystal systems. The system to which a crystal belongs can be identified from its external symmetry.

Symmetry is described in terms of transformations that leave an object apparently unchanged. These transformations are mediated by symmetry elements, and the action of transformation mediated by a symmetry element is called a symmetry operation. In a crystal, in addition to the trivial translation symmetry, another symmetry elements can appear, like rotation axes and mirrors and inversions planes. The combination of the last symmetries acting at a point results in 32 point groups. The combination of the point group symmetries with the translation symmetries introduced by the 14 Bravais lattices results in 230 space groups. The

space groups describe the way in which symmetry elements are arranged in space.

Table. 2.2. Seven different lattice systems and 14 different unit cells.

System	Axial lengths and angles	Bravais Lattice	Lattice Symbol
Cubic	Three equal axes at right angles $a = b = c$; $\alpha = \beta = \gamma = 90^o$	Simple Body-centered Face-centered	P I F
Tetragonal	Three axes at right angles, two equal $a = b \neq c$; $\alpha = \beta = \gamma = 90^o$	Simple Body-centered	P I
Orthorhombic	Three equal axes at right angles $a \neq b \neq c$; $\alpha = \beta = \gamma = 90^o$	Simple Body-centered Base-centered Face-centered	P I C F
Trigonal	Three equal axes, equally inclined	Simple	R
Hexagonal	Two equal coplanar axes at 120^o, third axis at right angles, $a = b \neq c$; $\alpha = \beta = 90^o$, $\gamma = 120^o$	Simple	P
Monoclinic	Three unequal axes, one pair not at right angles, $a \neq b \neq c$; $\alpha = \gamma = 90^o \neq \beta$	Simple Base-centered	P C
Triclinic	Three unequal axes, unequally inclined and none at right angles $a \neq b \neq c$; $\alpha \neq \beta \neq \gamma \neq 90^o$	Simple	P

•Primitive (P): lattice points on the cell corners.

• Body-Centered (I): lattice points on the cell corners with one additional point at the center of the cell.

• Face-Centered (F): lattice points on the cell corners with one additional point at the center of each of the faces of the cell.

•Base-Centered (A, B, or C): lattice points on the cell corners with one additional point at the center of each face of one pair of parallel faces of the cell (sometimes called end-centered).

Between the different notations that can be used to specify the symmetry of the crystal, the international notation will be used in this work. The international notation consists of two parts: The capital letter (P, A, B, C, I, F, or R) expresses the point group types; the second part is the symmetry element.

The arrangement and spacing of lattice planes produce diffraction from certain classes of planes in the structure which are always exactly 180° out of phase (see next paragraph Bragg's law) producing a phenomenon called systematic extinction or absence.Systematic absences in hkl reflections arise when symmetry elements containing translational components are present. Consequently, the systematic absences indicate the presence of centering and/or specific symmetry elements in the lattice and provide us information about the space group of the crystal.

The Miller indices can be used to specify directions and planes in a crystal. The orientation of a crystal plane can be determined by any three non-collinear points on this crystal face. The Miller indices (hkl) define the reciprocal axial intercepts of a plane of atoms in the unit cell (Fig. 2.8). The (hkl) plane of atoms intercepts the unit cell at $\frac{a}{h}$, $\frac{b}{k}$ and $\frac{c}{l}$. The direction of the vector d_{hkl} drawn from the origin of the unit cell that intersects the crystallographic plane (hkl) at a 90° angle represents the crystallographic direction commonly denoted by [hkl]. If a crystal plane is parallel to any axis, its intercept on that axis is at infinity, the reciprocal of which is zero.

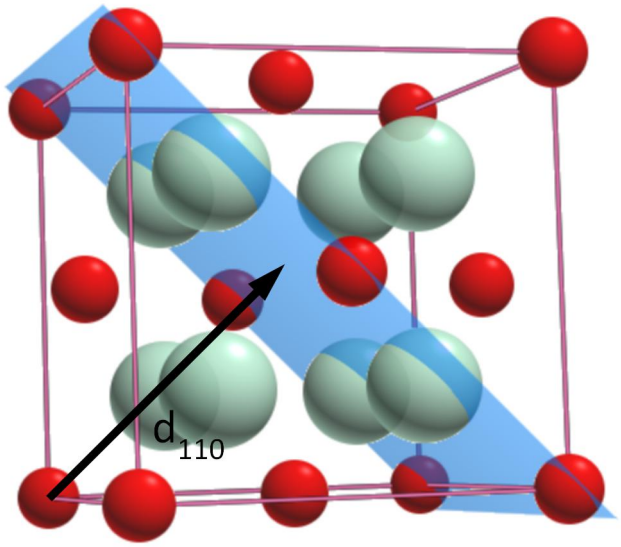

Fig. 2.8. Representation of the (1 1 0) crystal plane in a cubic lattice.

2.6 Diffraction by crystals

2.6.1 Bragg equation

Diffraction occurs when the light is scattered by a periodic array with long-range order, producing constructive interference at specific angles.The atoms in a crystal are arranged in a periodic array with long-range order and thus can produce diffraction. Moreover, the wavelength of X-ray is similar to the distance between atoms in a crystal. Then the scattering of X-ray from atoms produces a diffraction pattern, which contains information about the atomic arrangement within the crystal.

Bragg's law provides a simple model to understand what conditions are required for diffraction. For parallel planes of atoms, with a space d between the planes, constructive interference only occurs when Bragg's law is satisfied:

$$n\lambda=2d\sin\theta \tag{1}$$

where n represents the reflection order.

The condition for constructive interference of the scattered X-ray is that the path difference for waves reflected from two consecutive surfaces must be an integral number of wavelengths. Assuming that in a diffractometer, the X-ray wavelength λ which fixed a family of planes (hkl) produces a diffraction peak only at a specific angle 2θ. Therefore, we often consider that the position of the diffraction peaks is determined by the distance between parallel planes of atoms.

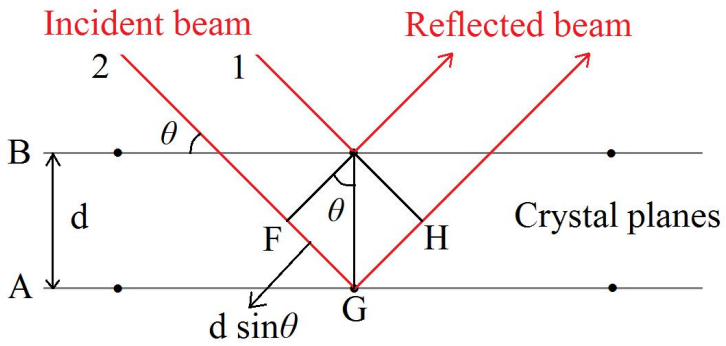

Fig. 2.9. Diagram for Bragg Reflection. FG + GH = nλ, FG = GH = dsinθ.

The relationship between the distance "d_{hkl}" and crystal lattice constant a, b, c, α, β and γ are summarized in Table. 2.3:

Table. 2.3. Distances "d_{hkl}" in different crystal lattice.

System	Equation
Cubic	$v = a^3$ $\frac{1}{d^2} = \frac{h^2 + k^2 + l^2}{a^2}$
Tetragonal	$v = a^2 c$ $\frac{1}{d^2} = \frac{h^2 + k^2}{a^2} + \frac{l^2}{c^2}$
Orthorhombic	$v = abc$ $\frac{1}{d^2} = \frac{h^2}{a^2} + \frac{k^2}{b^2} + \frac{l^2}{c^2}$
Trigonal	$v = a^3\sqrt{1 - 3\cos^2\alpha + 2\cos^3\alpha}$ $\frac{1}{d^2} = \frac{[(h^2 + k^2 + l^2)\sin^2\alpha + 2(hk + hl + kl)(\cos^2\alpha - \cos\alpha)]}{[a^2(1 + 2\cos^3\alpha - 3\cos^2\alpha)]}$
Hexagonal	$v = \frac{\sqrt{3}}{2}a^2 c$ $\frac{1}{d^2} = \frac{4}{3a^2}(h^2 + hk + k^2) + \frac{l^2}{c^2}$
Monoclinic	$v = abc\sin\beta$ $\frac{1}{d^2} = \frac{h^2/a^2 + l^2/c^2 - (2hl/ac)\cos\beta}{\sin^2\beta} + \frac{k^2}{b^2}$
Triclinic	$v = abc(1 + 2\cos\alpha\cos\beta\cos\gamma - \cos^2\alpha - \cos^2\beta - \cos^2\gamma)^{1/2}$ $\frac{1}{d^2} = \frac{1}{v^2}\begin{Bmatrix} h^2b^2c^2\sin^2\alpha + k^2c^2a^2\sin^2\beta + l^2a^2b^2\sin^2\gamma \\ + abc[kla(\cos\beta\cos\gamma - \cos\alpha)] \\ + lhb(\cos\gamma\cos\alpha - \cos\beta) \\ + hkc(\cos\alpha\cos\beta - \cos\gamma) \end{Bmatrix}$

Then the relations in Table. 2.3 show that from known unit cell parameters, we can predict the peak positions in the diffraction patterns or, in the opposite direction, from experimentally observed peak positions, we can determine unit cell parameters.

In this work the X-ray diffraction has been performed over polycrystalline materials, i.e millions of little crystals randomly oriented in the space. Every crystal diffracts according to the Bragg's law and the combination of all reflected beams is recorded by the detector, generating the diffraction pattern of the analyzed powder. Then the X-ray powder diffraction pattern is a plot of the intensity of X-ray scattered at different angles by a sample (Fig. 2.10).

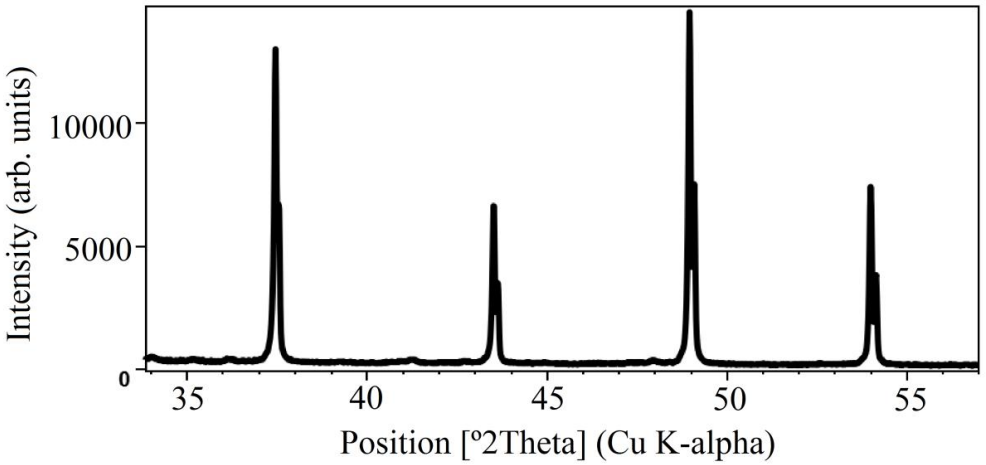

Fig. 2.10. X-ray diffraction pattern of a powder sample.

Whereas the interatomic distances determine the positions of the diffraction peaks, the diffraction peak intensities are related to the atom types and their arrangement in the sample. The intensity, *I* (hkl) (peak area) of each powder diffraction peak with miller indices, hkl, is directly related to the structure factor *F*:

$$I_{hkl} \propto |F_{hkl}|^2$$

where the structure factor F_{hkl} sums the result of scattering from all of the atoms in the unit cell to form a diffraction peak from the (hkl) planes of atoms, i.e.:

$$F_{hkl} = \sum_{j=1}^{m} N_j f_j \exp\left[2\pi i\left(hx_j + ky_j + lz_j\right)\right]$$

This expression shows that the amplitude of scattered light is determined by:

- The atom positions on the atomic planes expressed by the fractional coordinates x_j y_j z_j.
- The kind of atoms on the atomic planes from:
  - The scattering factor f_j that quantifies the efficiency of X-ray scattering at any angle by the group of electrons in each atom. The scattering factor is equal to the number of electrons around the atom at 0° θ, the scattering factor drops off as θ increases
  - N_j is the fraction of every equivalent position that is occupied by atom j.

For an ideal powder sample, factors related to the sample such as absorption, polarization, or thermal vibrations influenced the peak widths and shape [5]. Moreover, to extract the former information from the integrated intensities it must be taken into account that the profiles are the convolution of the one instrumental profile function and a sample function that contains information on the microstructure of the sample. Both factors influence the width and shape of the diffraction peaks. Instrumental line profiles arise from the distribution of wavelengths in the incident bean convoluted with several functions resulting from the geometry of the instrument such as beam divergence, finite width of the source and residual misalignment. The microstructure effects contribute to diffraction line broadening and can be related with the microcrystals size or internal stress distribution.

Both the width and shape of instrumental line profiles vary continuously with 2θ for conventional X-ray diffractometers. Commonly, the width of every peak is parametrized by FWHM, the full width at half maximum (Fig. 2.11) and the evolution versus the position θ by the Caglioti function $FWHM^2 = U\tan^2\theta + V\tan\theta + W$ being U, V, Wadjustable parameters from the experimental data.

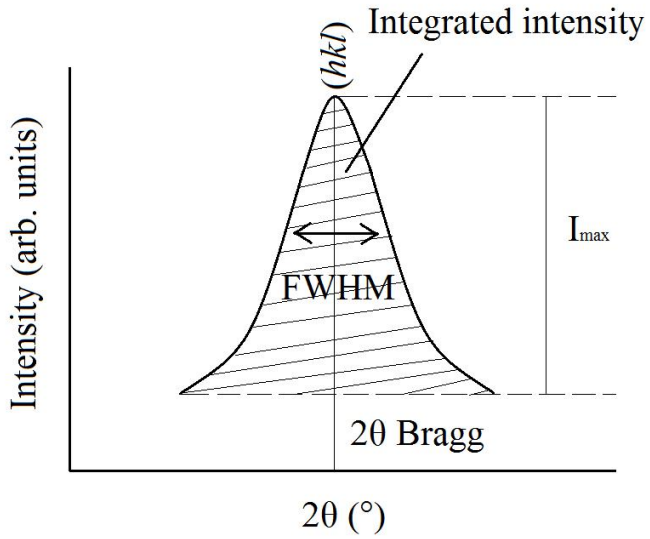

Fig. 2.11. Diffraction shape peak parameters.

The form of the profiles depends on the crystallite size distribution, resulting in a broad variety of line shapes. In X-ray diffraction the observed profiles usually range from the Gaussian to the Lorentzian and as a rule are modeled by a combination of the former profiles called pseudo Voight function $\Omega\ (2\theta) = \eta\ L + (1\text{-}\eta)\ G$, where η and $(1\text{-}\eta)$ are the fractions of Lorentzian (L) and Gaussian (G) shapes respectively.

2.6.3 Experimental system and sample preparation.

X-ray powder diffraction data were recorded by a vertically mounted INEL cylindrical position-sensitive detector (CPS-120), using Debye-Scherrer geometry.In this transmission geometry, Fig. 2.12, the source (monochromator) and detector are located on the surface of a circle with the sample at the center. The diffracted beam is collected by the detector at each 2θ, to give a plot of intensity versus 2θ. The CPS detector consists of 4096 channels which allow a simultaneous recording of a powder pattern over a 2θ range from 4 to 120º with an angular

step of 0.029º. This system requires a calibration procedure to determine the angular position of the detector channels that is performed by using the $Na_2Ca_2Al_2F_{14}$ compound.

Monochromatic CuKα1 radiation (λ = 1.5406 Å) is selected by means of the Ge (111) monochromator.

The system is equipped with a liquid nitrogen 700-series cryosystem cooler from Oxford Cryosystems (temperature accuracy of 0.1 K), which enabled isothermal measurement in the 100−500 K range.

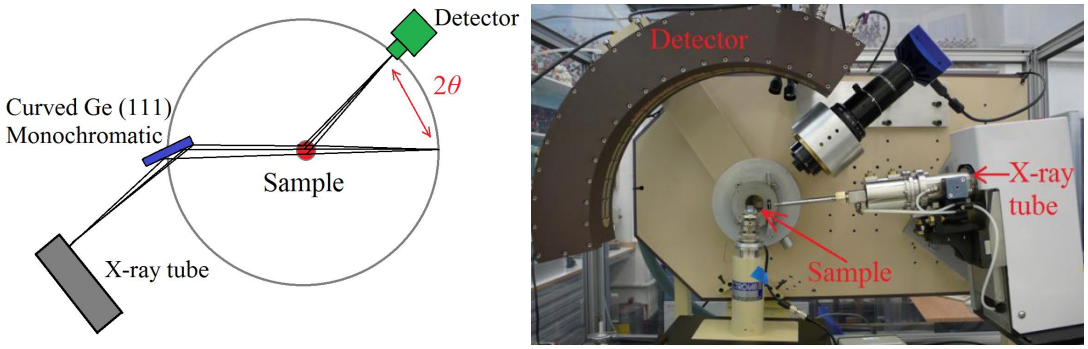

Fig. 2.12. Horizontally mounted INEL cylindrical position-sensitive detector (CPS-120) using Debye-Scherrer geometry.

The samples were introduced in Lindemann glass capillaries of 0.5 mm diameter (Fig. 2.13). These dimensions are adequate to obtain analyzable spectra at time intervals of a few hours. In order to obtain enough crystals statistically overall non-oriented and well packed in the capillary, the sample should be finely ground. To avoid grain effects sizes around 1 - 10 μm are suitable. The capillary situated perpendicularly to the X-ray beam is rotated during the experiment to minimize possible effects of preferred orientations.

These glass capillaries allow to work with very small sample amounts (micro gram or less) and can be easily sealed to avoid degradation or sublimation effects.

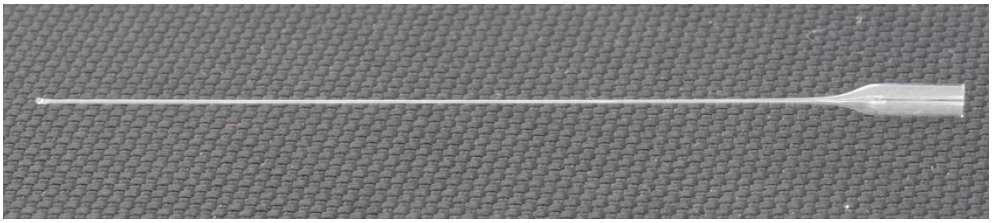

Fig. 2.13. Lindemann capillary tube.

2.6.4 Analysis of the Experimental Profiles.

In the analysis of the experimental profiles, the first step is the indexing of the diffraction pattern. This process is carried out through conventional auto indexing programs as ITO, TREOR or DICVOL[5]. The basis of these programs is the relation between the interplanar spacing d_{hkl} and the lattice parameters, as summarized in Table. 2.3. In a general form (triclinic lattice) the next relation can be obtained:

$$Q_{hkl} = \frac{1}{d^2_{hkl}} = h^2 A + k^2 B + l^2 C + hkD + klE + hlF$$

where the coefficients *A*, *B*, *C*, *D*, *E* and *F* are depending on the lattice symmetry (Table. 2.3).Then there is an equation for every reflection line on which the (*h k l*) index must be found. The search of indexing solutions is currently based on a limited number of lines, typically the first 20 lines in the pattern (or more than 20 lines if there is a dominant zone, i.e. one axis is significantly shorter than the other two). In fact, there is no absolute criterion to validate an indexing result, except for a subsequent successful structure determination from the powder diffraction data.

In this work, the used program has been DICVOL 91 [6,7]. This program uses the dichotomy method that is based on the variations of the lengths of cell edges and interaxial angles in direct space for finite ranges, which are progressively reduced by means of a dichotomy procedure if they contain a possible solution. It must be noted that the dichotomy strategy consists of searching the solution(s) with the smallest cell volume(s) according to the universal crystallographic convention, i.e. 'the smallest repeat unit for which its delineating

vectors are parallel to, or coincide with, important symmetry directions in the lattice'. The program allows checking different lattice symmetries between a range of volumes chosen by the user, using partitions of the volume space of 400 A^3. Additional advantages of the program are the calculation of a zero error and the possibility of discard spurious lines due to the presence, for example of a second (or more) crystalline phase.

The criterion for the physical plausibility of the solution is the figure of merit M_t introduced by Wolff [8] and defined as:

$$M_t = \frac{Q_t}{2\langle Q \rangle N_t}$$

Here the subscript t is the number of selected diffraction lines, N_t is the number of different calculated Q values up to Q_t which is the Q value for the tth observed and indexed line; $<Q>$ is the average discrepancy in Q for these t lines. Usually, the M figure is calculated for the 20 chosen lines being assumed that a value of $M_{20}>10$ guarantees that the indexing is substantially correct (or at least quite plausible).

Another figure of merit is the F_N index [9] defined by:

$$F_N = \frac{N}{\langle \Delta 2\theta \rangle N(\theta_g)}$$

where $N(\theta_g)$ is the number of different calculated Q values up to θ_g which is the θ value for a selected limit,$<\Delta 2\theta>$ is the average discrepancy in 2θ for the number of N observed lines below θ_g. This factor tests the accuracy of the observed angular positions.

Both figures of merit are displayed by the program for the indexed lines together with the cell parameters found and a possible space group. Although the program uses a finite number of lines for indexing, it allows introducing additional lines, making for all of them a first refinement.

From the unit cell and the selected space group, the position of the reflections can be adjusted and the cell parameters refined. To do that the intensity associated with each reflection can be determined by applying a whole-profile-fitting technique similar to that used

in a Rietveld refinement but with the intensities of the reflections rather than the structural parameters. This procedure, known as intensity extraction (Pattern Matching procedure) can be performed using either a least-squares method (Pawley) or an interactive approach (Le Bail). The application of this procedure over the complete pattern allows obtaining the refined cell parameters, the profile parameters and a list of integrated intensities. Given that several space groups can share the same systematic absences, the so-obtained list of integrated intensities allows a new check of the space group (CheckGroup in FullProf Suite).

The Rietveld method [10] consists in the refinement of the crystalline structure of a given material, minimizing the squared differences weighted between all the observed and calculated intensities:

$$\phi = \sum_{1}^{N} w_i \left[y_i - y_{ci} \right]^2$$

where N is the overall $2\theta_i$ profile positions, w_i is a weight attributed at each position, y_i the measured intensity at the $2\theta_i$ profile position and y_{ic} the calculated intensity at the $2\theta_i$ profile position [10]. By means of the minimization of the ϕ function, shape profile and structural parameters are refined.

In order to measure the process of convergence several agreement indices are used (Table. 2.4). The more frequently used of these are the *R* pattern (R_P) and the weighted-profile *R*-factor, (R_{wp}). Depending on the Rietveld codes the summation may be applied to all points, *i*, in the profile or only to those points where significant diffraction density is presented. The refinement result is considered to be reliable when R_{wp} reaches values about 10%.Another *R*-factor, known as the expected *R*-factor (R_E) (where *N* is the total number of observations, *i*, *P* is the number of parameters refined, and *C* is the number of constraints used in the refinement) is a measurement of data quality. The ratio of the above, two *R*-factors (R_{wp} and R_E) give the chi-squared value or goodness of fit (GoF). If the value is around 1.0 - 1.3, the refinement result is good [11].

Table. 2.4. Numerical criterion for the quality of results.

R-pattern	$R_P = \frac{\sum \lvert Y_i(obs) - Y_i(cal) \rvert}{\sum Y_i(obs)}$
R-weighted pattern	$R_{WP} = \left\{ \frac{\sum w_i \left[Y_i(obs) - Y_i(cal) \right]^2}{\sum w_i \left[Y_i(obs) \right]^2} \right\}^{1/2}$
R-expected	$R_E = \left[(N - P + C) / \sum_i^N w_i (Y_i(obs))^2 \right]^{1/2}$
Goodness-of-fit	$\chi^2 = \sum w_i \left[Y_i(obs) - Y_i(cal) \right]^2 / (N - P)$ $\chi^2 = R_{WP} / R_E$

Assuming that Rietveld procedure is a refining method then a starting model is necessary. In addition, the conventional treatment of atomic coordinates in crystal structure calculations may have to be restricted in several ways: a typical case is that of the structure determination of complex structures and also of simple structures involving orientational disorder. In these cases, the observations (the number of reflections is quite scarce) are not sufficient to fix unambiguously the structure. Then the asymmetric unit can be modeled by means of rigid bodies in which distances and angles between atoms in the body remain fixed during the analysis and consequently a lower number of parameters must be refined. The external orientation of the rigid body around the pivot point is typically defined by using Euler angles in an orthonormal coordinate system, which has been set by convention relative to basis vectors of the crystal lattice.The solvates of C_{60} with general expression C_{60}:n-solvent molecules with n≥1 contain a high number of atoms. In all cases the solvent molecule has been treated as a rigid body, obtaining intramolecular angles and distances from the bibliographic data from its solid phase structure. Depending on the degree of disorder present in the studied phase, the C_{60} molecule has been treated as a rigid body of 60 atoms or as a sphere of radius 3.5 Å (Spherical Harmonic Approximation)

The Fullprof software package [12] has been used for indexation (because it also contains the DICVOL program), Pattern-Matching and Rietveld Analysis by means of Spherical Harmonics. For the conventional Rietveld analysis by means of Rigid Bodies, the Materials

Studio [13] package has been used. The Rietveld analysis by means of the former suites, has been performed in collaboration with the doctors N. Qureshi (ILL, Grenoble) and P. Negrier (Université de Bordeaux), respectively.

2.7 References

[1] S. C. Mraw, Mathematical treatment of heat flow in differential scanning calorimetry and differential thermal analysis instruments, Review of Scientific Instruments, 53, 1982, 228.

[2] Y. Saito, K. Saito, T. Atake, Base line drawing for the determination of the enthalpy of transition in classical dta, power-compensated dsc and heat-flux dsc, Thermochimica Acta, 104, 1986, 275.

[3] G. D. Gatta, M. J. Richardson, S. M. Sarge, S. Stølen, Standards, calibration, and guidelines in microcalorimetry. Part 2. Calibration standards for differential scanning calorimetry* (IUPAC Technical Report), Pure and Applied Chemistry, 78, 2006, 7.

[4] P. M. Wolff, in International Tables for Crystallography, Kluwer:Boston, A. 9.3, 1996, 741.

[5] W. I. F. David, Structure Determination from Powder Diffraction Data. IUCr Monographs on Crystallography Oxford Science Publications 2002.

[6] A. Boultif, D. Louër, Powder pattern indexing with the dichotomy method, Journal of Applied Crystallography, 37, 2004, 724.

[7] A. Boultif, D. Louër, Indexing of powder diffraction patterns for low-symmetry lattices by the successive dichotomy method, Journal of Applied Crystallography, 24, 1991, 987.

[8] P. M. Wolff, A simplified criterion for the reliability of a powder pattern indexing, Journal of Applied Crystallography, 1, 1968, 108.

[9] G. S. Smith, R. L. Snyder, FN: A criterion for rating powder diffraction patterns and evaluating the reliability of powder-pattern indexing, Journal of Applied Crystallography, 12, 1979, 60.

[10] H. M Rietveld, A profile refinement method for nuclear and magnetic structures, Journal of applied Crystallography, 2, 1969, 65.

[11] R. A. Young, Introduction to the Rietveld method. In: The Rietveld Method, ed. by R.A. Young. IUCr Book series, Oxford University Press, Oxford, 1993, 51.

[12] J. Rodriguez-Carvajal, T. Roisnel, J. Gonzales-Platas, FullProf suite (2005 version). CEA-CNRS, CEN Saclay, France: Laboratoire Léon Brillouin, 2005.

[13] MS Modeling (Material Studio): http://www.accelrys.com/mstudio/ms_modeling.

3. The C_{60}:$CBr_2(CH_3)_2$ binary system

3.1 The solvent: 2,2-dibromo-propane

The solvent 2,2-dibromo-propane ($CBr_2(CH_3)_2$), density 1.782 g/mL, displays a molecule of tetrahedral shape with C_{2v} symmetry. The original sample was purchased from Aldrich with a purity of 95% and was fractionally distilled before using. The compound has a solid phase that transforms at 214 K to an orientationally disordered phase which melts at 256 K (Fig. 3.1). The enthalpy change for the former transformations measured in this work is 10.63 kJ/mol (52.63 J/g) and 1.91 kJ/mol (9.44 J/g), respectively. The former temperatures are in agreement with the literature data [1]. Only the symmetry of the high-temperature phase has been determined, it is rhombohedral with Z = 21 and V/Z = 165.22 $Å^3$/molecule at 223 K [2].

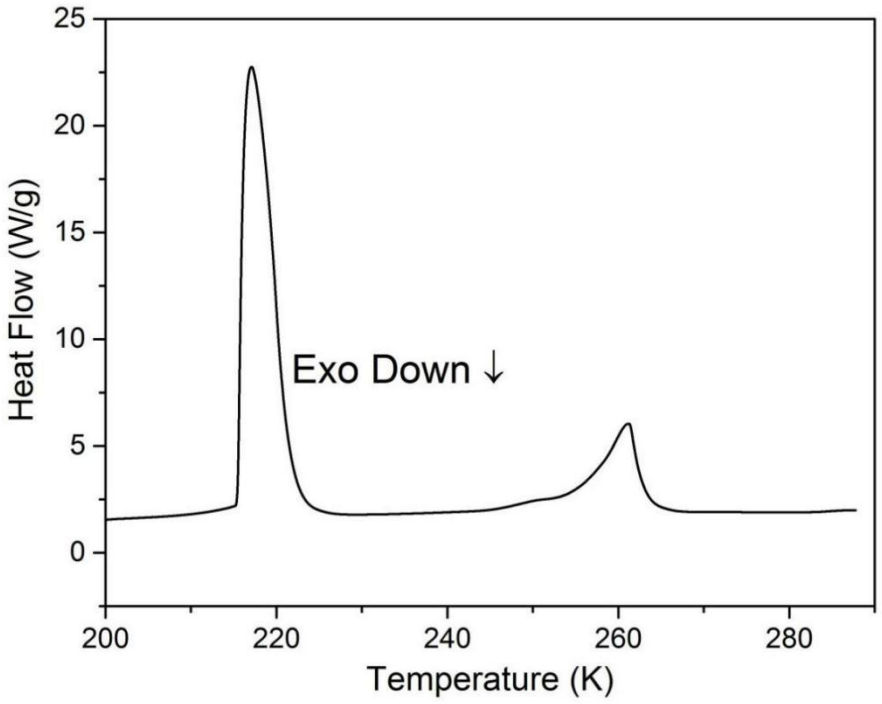

Fig. 3.1. Solid-solid transition and melting signals for the $CBr_2(CH_3)_2$ solvent by differential scanning calorimetry (DSC).

3.2 Study of the C_{60}:$CBr_2(CH_3)_2$ solvates

Solvate crystals were grown at room temperature from a heterogeneous mixture of FCC C_{60} in $CBr_2(CH_3)_2$ in screw-cap flasks, protected from light in the time span of several weeks and they were periodically monitored by optical microscopy. After several weeks the FCC C_{60} crystals started disappearing and new red colored crystals appeared. The morphology of the crystals was tested by means of scanning electron microscopy (Fig. 3.2). This cubic morphology was confirmed by X-ray diffraction.

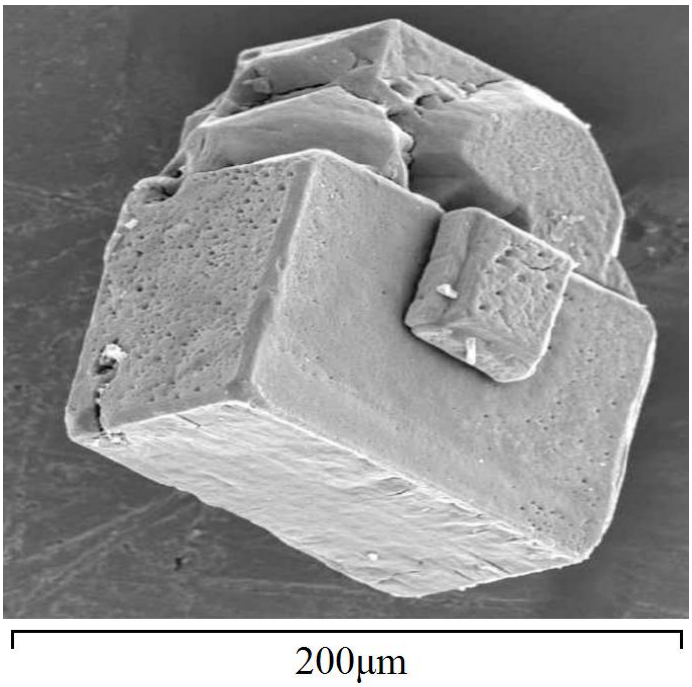

Fig. 3.2. Scanning electron microscopy photographs of the cubic $C_{60}\cdot 12CBr_2(CH_3)_2$ co-crystals (after TGA).

By X-ray diffraction, it was verified that the cubic solvate is not stable out the mother liquid and a quick evaporation of the liquid transforms the cubic solvate in the FCC C_{60} with

defects [3-6] (see later, Fig. 3.6 at 373 K). Then to study the behavior of this solvate, the crystals were maintained in contact with liquid or in saturated vapor conditions.

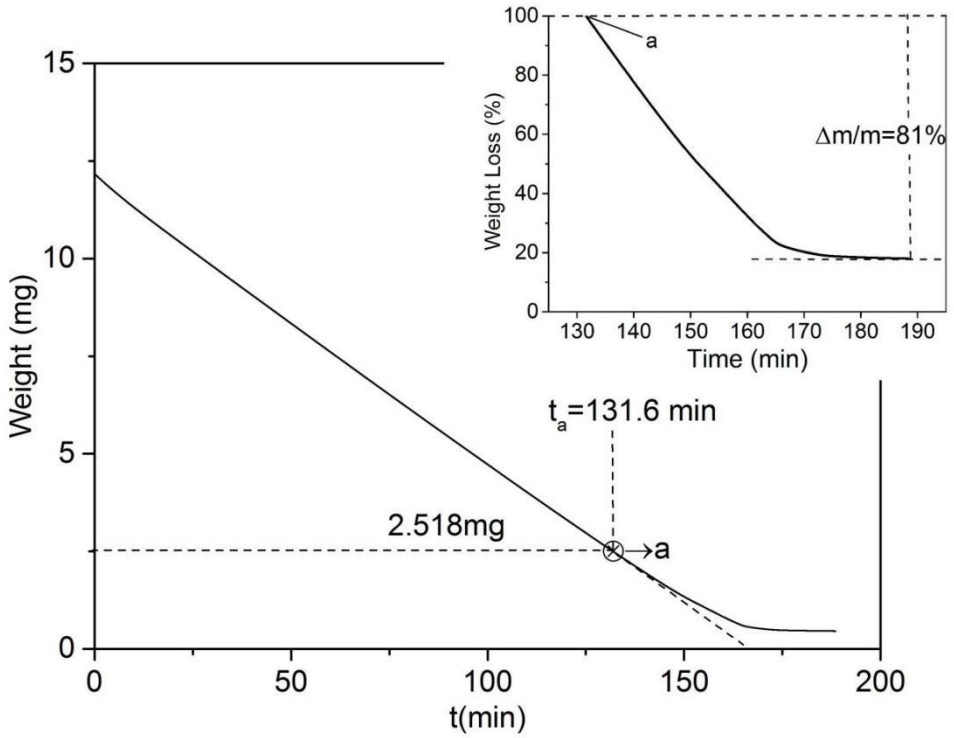

Fig. 3.3. Isothermal evaporation at 303 K of a sample consisting of cubic co-crystals and mother liquor. The initial segment up to point "a" corresponds to the evaporation of the mother liquor at a rate of 0.072 mg/min. Inset: Close-up of the graph starting at point "a", the initial mass of the cubic co-crystals alone. The mass loss is expressed in % of the initial mass of the co-crystals at t_a.

The stoichiometry of the cubic co-crystals was determined by measuring the mass loss as a function of time of the crystals in their mother liquor at 303 K. It can be seen in Fig. 3.3 that first the mother liquor evaporates followed by the desolvation of the cubic co-crystals. The

mass loss of the latter process equals 81% counting from point "**a**" as indicated in the inset of Fig. 3.3, at which point the mother liquor had fully evaporated. The observed percentage corresponds closely to a 1:12 (C_{60}: $CBr_2(CH_3)_2$) stoichiometry, which is equal to 77%.

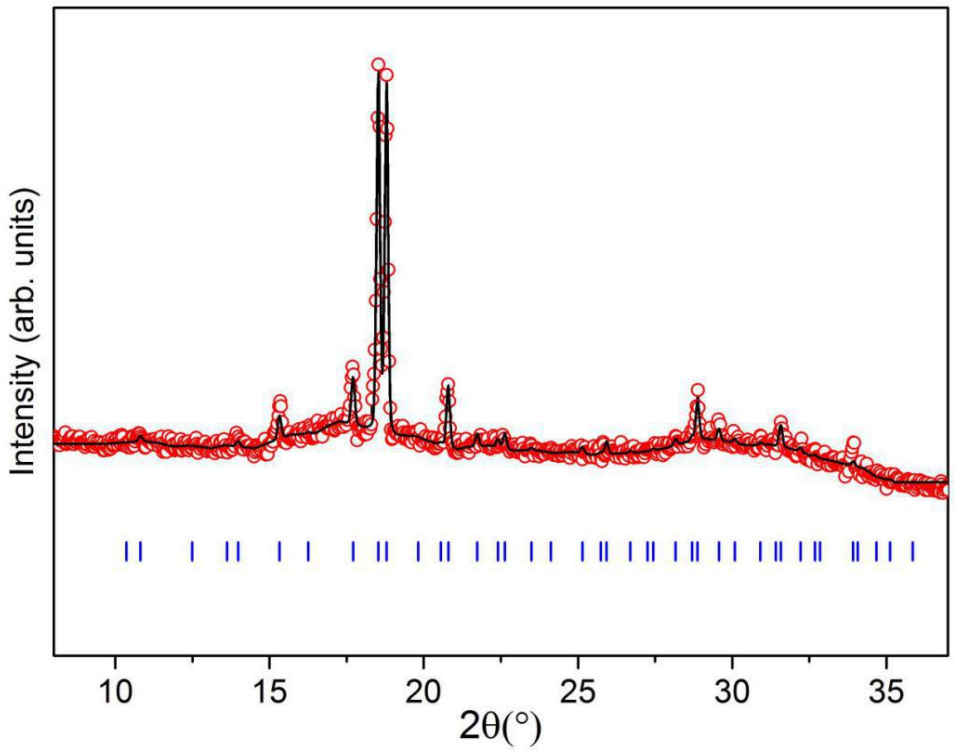

Fig. 3.4. X-ray diffraction profile at 300 K of the face-centered cubic solvate (C_{60}·12$CBr_2(CH_3)_2$) (after TGA) in equilibrium with the saturated liquid. Experimental (points) and calculated (lines) diffraction patterns along with the calculated Bragg peak positions (vertical bars) for the cubic C_{60}·12$CBr_2(CH_3)_2$ co-crystals.

X-ray diffraction measurements were performed in closed capillaries, with the crystals in equilibrium with the saturated liquid. The measured spectra, Fig. 3.4, only shown Bragg peaks of significant intensity at angles lower than 40°. This is a common trend in highly disordered

systems. Lattice parameters were determined using DICVOL resulting in a cubic lattice with systematic absences in agreement with an FCC symmetry. The refined parameter after a Pattern Matching procedure, assuming $Fm\bar{3}m$ group, was a = 28.282(3) Å, which, assuming Z = 8, gives rise to a lattice volume per molecular unit of V/Z = 2827.7 $Å^3$.

Similar volume values were obtained for the cubic co-crystals formed with solvents of tetrahedral molecular symmetry [7-9].

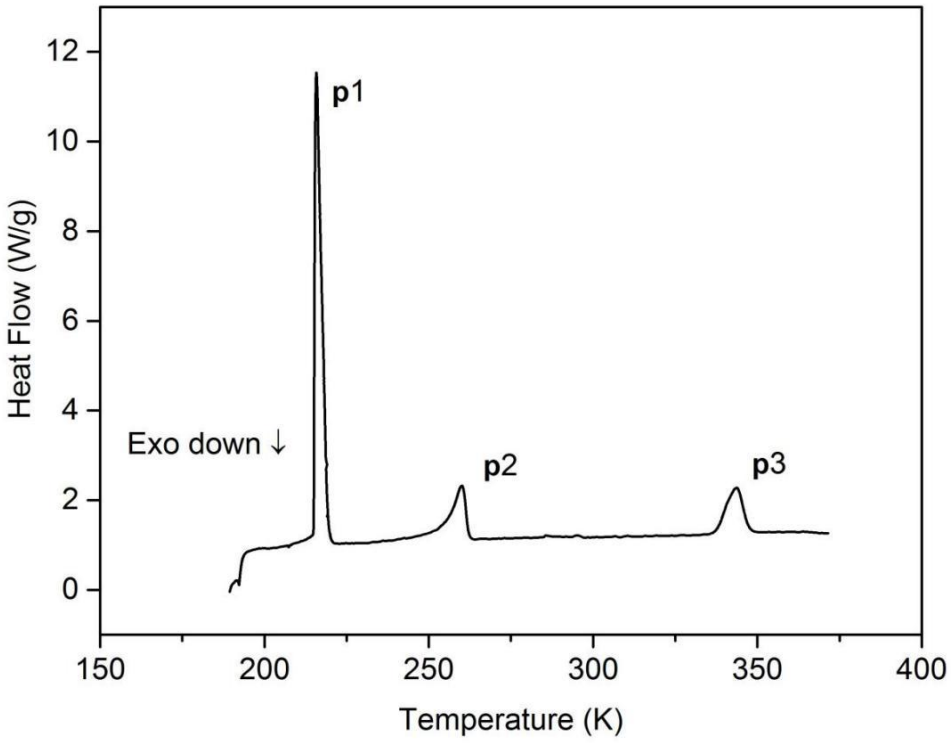

Fig. 3.5. DSC curve obtained in a sealed pan of the cubic solvate of $C_{60}\cdot 12CBr_2(CH_3)_2$ in the presence of mother liquor.

To verify if the cubic solvate shows some transition, aliquots of cubic crystals together with the mother liquor were put in stainless steel high-pressure pans for DSC studies. The result is shown in Fig. 3.5: The first two endothermic peaks corresponding to the degenerate solid-solid phase transition (214.7 K) and fusion (255.0 K) of pure $CBr_2(CH_3)_2$ (peaks **p1** and **p2**, respectively) and the additional endothermic peak at 338.2 K (**p3**) must be ascribed to the solvate.

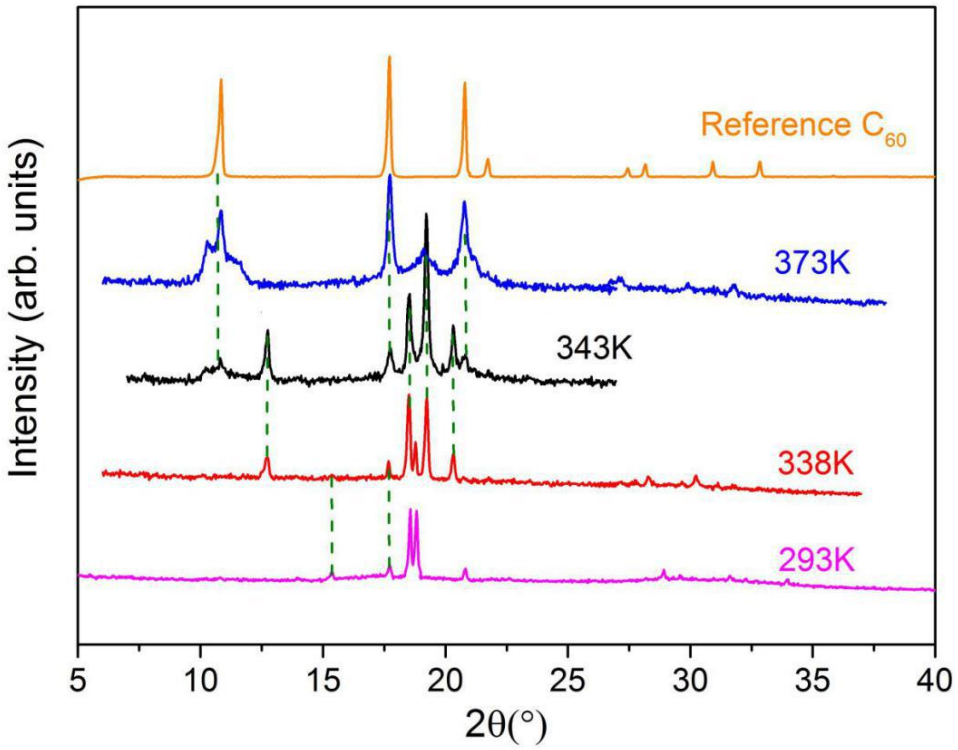

Fig. 3.6. X-ray diffraction patterns of the cubic solvate in mother liquor in a closed capillary as a function of temperature. The pattern on top is that of FCC C_{60} and is provided for reference.

To investigate the structural change associated with the latter endothermic peak (**p**3), X-

ray diffraction measurements over crystals with an excess of mother liquor in a closed capillary were carried out. Fig. 3.6 reveals that the cubic solvate transforms to a crystal with a different symmetry at around 338 K and that, at approximately 343 K, the latter crystals desolvate and thus become FCC C_{60}. Then the last thermal signal (**p**3) involves both transformations.

At this point, the question is to identify the nature of the thermal effect that starts at 338 K: Is it a phase transition of the C_{60}·12 $CBr_2(CH_3)_2$ solvate? Or is it related with a transformation to another solvate of lower stoichiometry?

Because of C_{60} cubic solvates have been observed together with poorly solvated C_{60} hexagonal solvates in C_{60}:CCl_4 and C_{60}:CCl_3Br [8,9] systems, two kinds of experiments were undertaken from samples of the cubic solvate with the excess of liquid:

1. Slow evaporation of the liquid in an open capillary at room temperature.
2. Heating of cubic co-crystals in stainless steel high-pressure pans to about 338 K and quick cooling to room temperature, allowing a quick evaporation of the liquid.
3. Slow evaporation of the liquid in a screw-cap tube at 338 K.

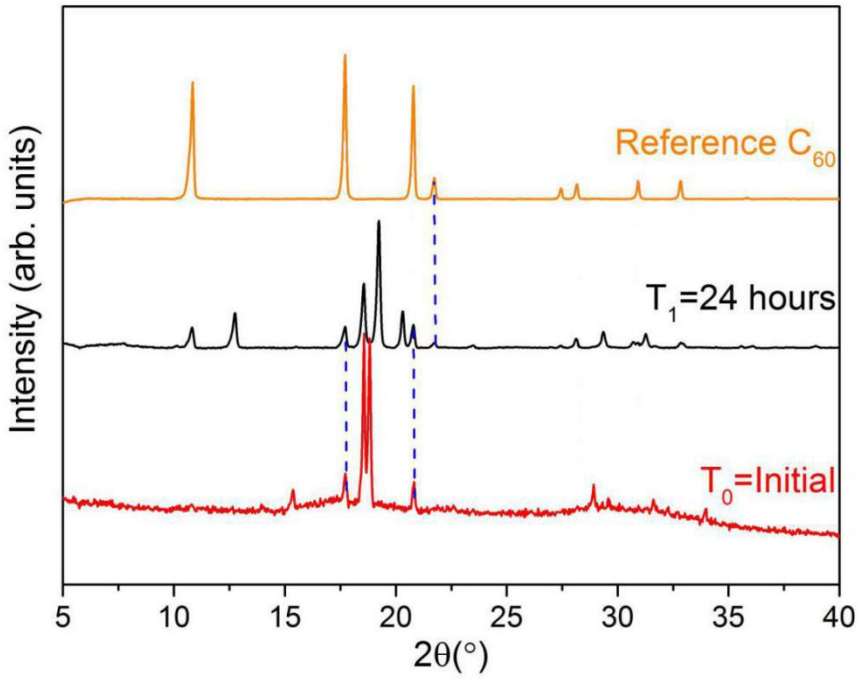

Fig. 3.7. X-ray diffraction patterns of the cubic co-crystals in mother liquor in an open capillary as a function of time.

The X-ray measurements performed in an open capillary show that after 24 hours together with the cubic co-crystal spectrum new Bragg reflections, appeared. These reflections are not related with the FCC C_{60} lattice, then assuming that the experience is performed at room temperature, the existence of a new co-crystal with different stoichiometry has been proved.

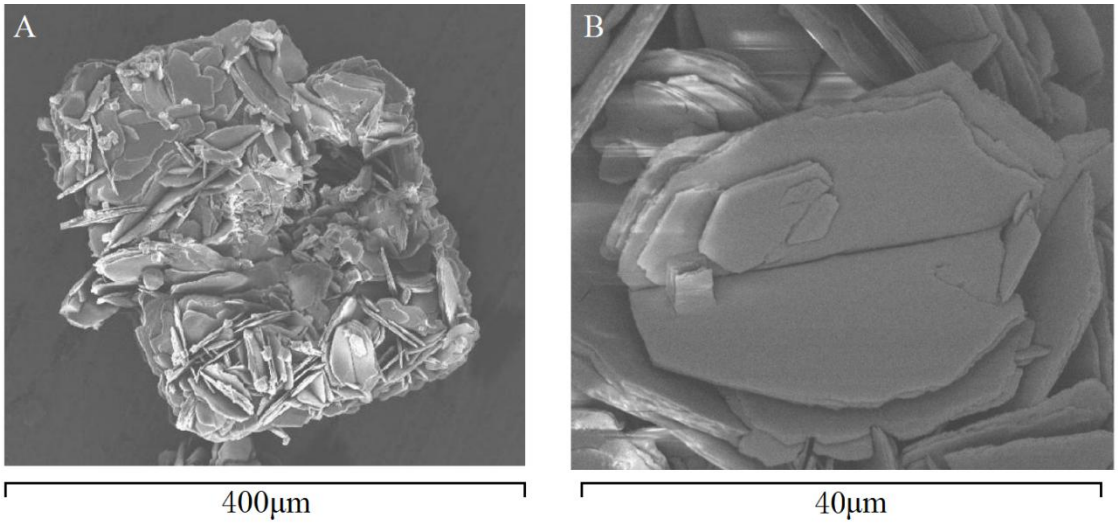

Fig. 3.8. Scanning electron microscopy photographs of the new co-crystal $C_{60}{\cdot}2CBr_2(CH_3)_2$ (after TGA): (A) Small hexagonal $C_{60}{\cdot}2CBr_2(CH_3)_2$ co-crystals grown by heating the cubic co-crystals. (B) Detail of photograph B showing the hexagonal plates of $C_{60}{\cdot}2CBr_2(CH_3)_2$.

The samples obtained after heating the cubic $C_{60}{\cdot}12CBr_2(CH_3)_2$ solvate to 338 K in stainless steel high-pressure pans were examined at 300 K. The SEM photograms Fig. 3.8, allow us to observe the growth of the hexagonal crystals from the cubic co-crystals.

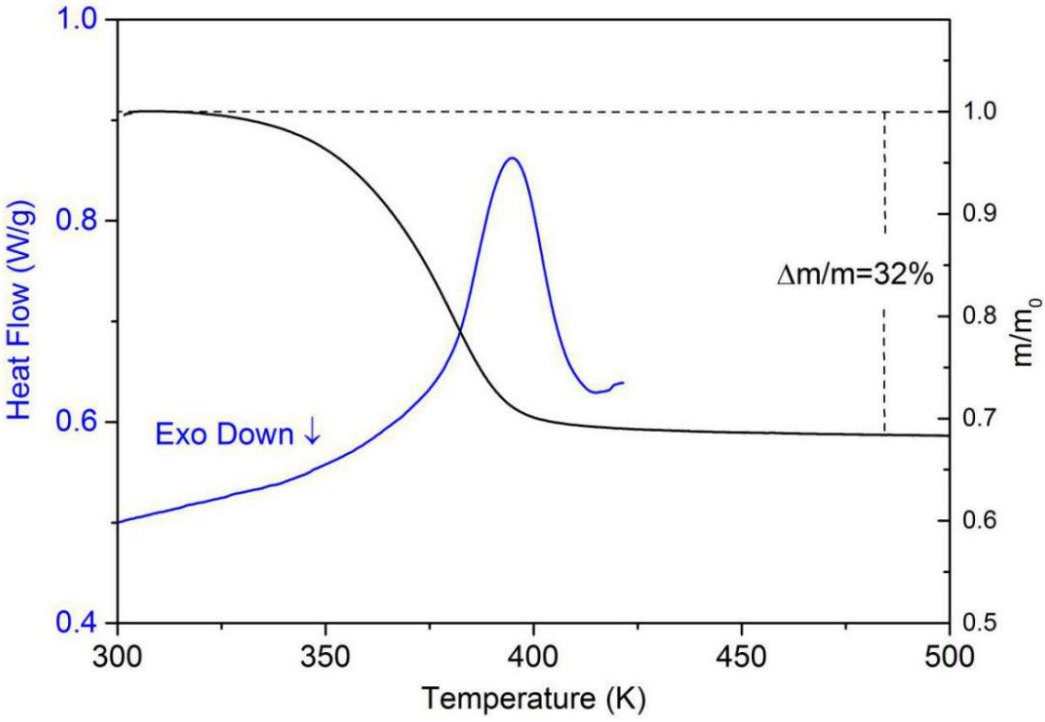

Fig. 3.9. TGA and DSC desolvation measurements of the hexagonal solvate $C_{60}\cdot 2CBr_2(CH_3)_2$.

The third procedure supply enough hexagonal-shaped crystals to perform TGA, DSC and X-ray analyses. The TGA and DSC measurements (Fig. 3.9) demonstrate that desolvation of the hexagonal crystals starts around 340 K and accounts for a mass loss of 32%, close to the expected 35.9% corresponding to a solvate with 2 molecules of solvent for each C_{60} molecule. The desolvation enthalpy is found to be 60.5 J/g of a solvate, i.e. 168 J/g of solvent (or 34 kJ/mol of solvent).

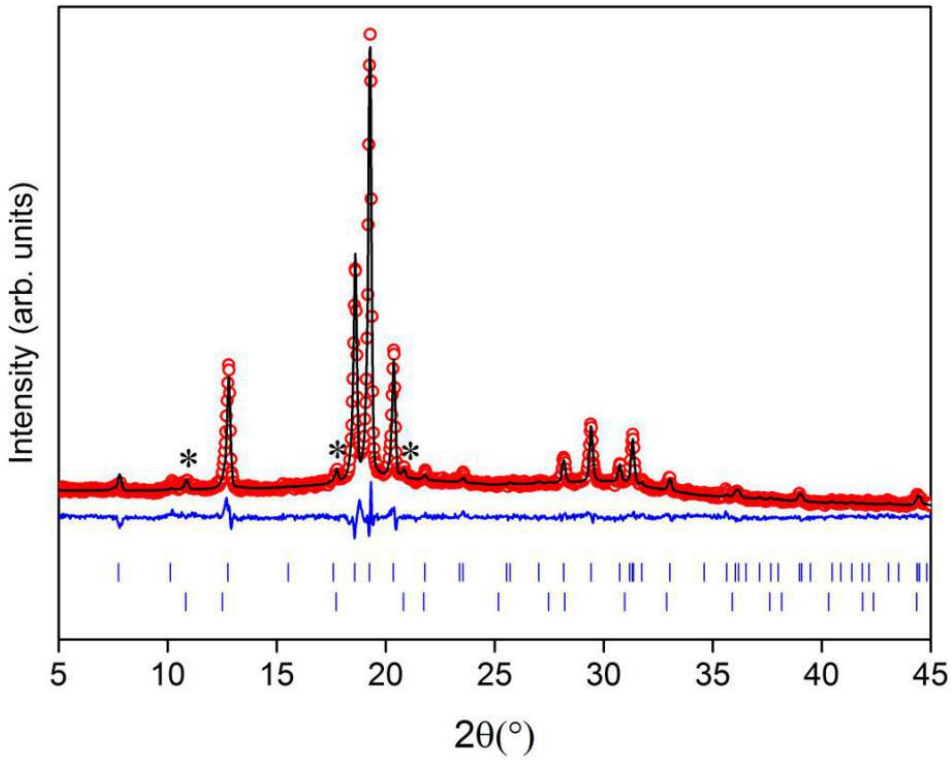

Fig. 3.10. X-ray diffraction profile at 300 K of the hexagonal $C_{60}{\cdot}2CBr_2(CH3)_2$ co-crystals, (* traces of cubic C_{60}). Experimental (points) and calculated (line) diffraction patterns along with the calculated Bragg peak positions (vertical bars). The calculated pattern is the result of a Rietveld refinement (see later) containing 2.9 % of FCC C_{60} indicated by blue vertical bars among the Bragg peak positions. The residuals between calculated and experimental patterns are plotted between the patterns and the Bragg peak positions. The range between 45 and 115° is not shown due to the absence of Bragg peaks with significant intensity, however, the Rietveld refinement included and reproduced the entire 2θ range.

The measured X-ray patterns (Fig. 3.10) were indexed by a hexagonal unit cell in agreement with the SEM results. Like in the cubic solvate only Bragg peaks with significant intensity appeared at low angles, then orientational disorder remains in the hexagonal solvate.

The pattern also contains a few Bragg peaks corresponding to FCC C_{60}, most likely due to the proximity of the peritectic equilibrium $C_{60}\cdot 2CBr_2(CH_3)_2$ + C_{60} + liquid. The presence of FCC C_{60} may also explain the difference between the experimental (32%) and the theoretical (35.9%) mass loss in the TGA measurements.

The refined lattice parameters by means Pattern Matching procedure for the hexagonal lattice were a = 10.072(2) Å and c = 11.333 (3) Å. Assuming Z = 1 results in a volume per molecular unit of V/Z = 995.6 $Å^3$, lower than the corresponding to the cubic solvate.

3.3 Discussion and structural characterization

The existence of two co-crystals $C_{60}\cdot 12CBr_2(CH_3)_2$ and $C_{60}\cdot 2CBr_2(CH_3)_2$ with cubic and hexagonal symmetries has been shown. The binary phase diagram, Fig. 3.11, is characterized by two peritectic invariants involving the equilibria $C_{60}\cdot 12CBr_2(CH_3)_2$ + $C_{60}\cdot 2CBr_2(CH_3)_2$ + liquid and $C_{60}\cdot 2CBr_2(CH_3)_2$ + liquid + (FCC) C_{60} at 338 K and 343 K respectively. These temperatures have been determined by X-ray since the proximity of the transformations makes impossible their resolution by means of DSC measurements.

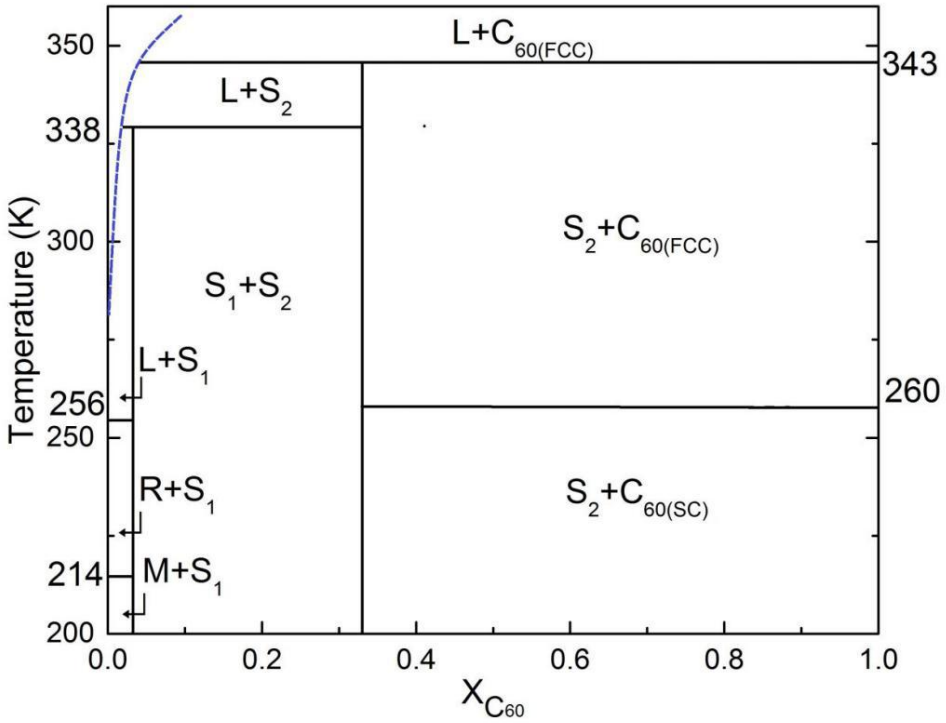

Fig. 3.11. Binary phase diagram $CBr_2(CH_3)_2$(1-X):C_{60}(X). S1 and S2 are the co-crystals $C_{60}\cdot 12CBr_2(CH_3)_2$ and $C_{60}\cdot 2CBr_2(CH_3)_2$, respectively.

The variation of the lattice parameters with temperature is shown in Fig. 3.12 A and B for $C_{60}\cdot 12CBr_2(CH3)_2$ and $C_{60}\cdot 2CBr_2(CH_3)_2$, respectively. The variation of the cubic parameter with the temperature is coherent with the DSC result, which evidences that any transition takes place in this solvate until the peritectic transformation to the hexagonal one.

The former figure shows that the thermal expansion of the cubic parameter is higher than that of the *a* or *c* hexagonal ones, resulting in a higher expansion of the V/Z lattice parameter in the cubic cell (Fig. 3.12 C). Then the interaction in the hexagonal solvate must be stronger than in the cubic one. However, in the hexagonal lattice, the variation of the *c* parameter is around 0.3 Å in front of 0.06 Å for the *a* parameter, which means that interactions are stronger in the (001) hexagonal planes.

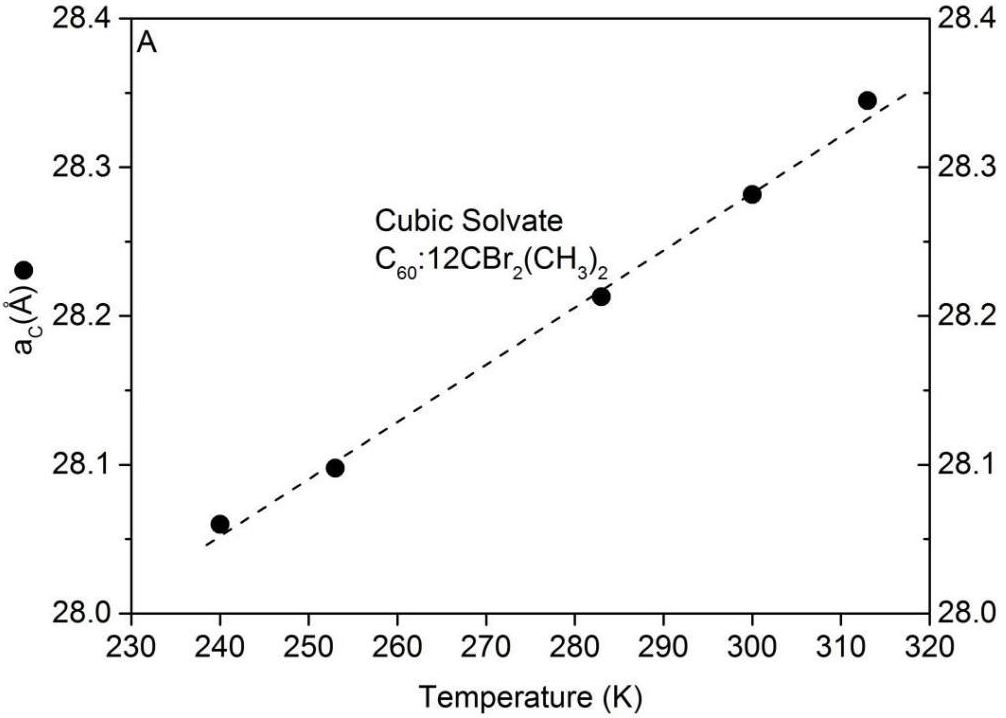
A
Cubic Solvate
C_{60}:12$CBr_2(CH_3)_2$
a_C(Å)
Temperature (K)
28.4
28.3
28.2
28.1
28.0
230
240
250
260
270
280
290
300
310
320

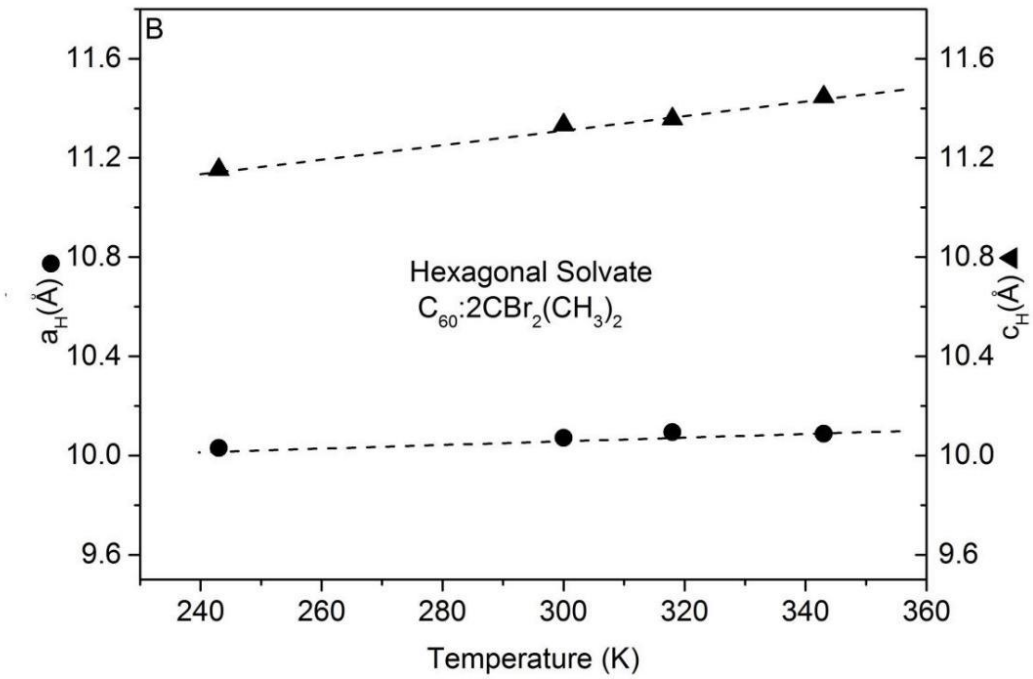
B
Hexagonal Solvate
C_{60}:2$CBr_2(CH_3)_2$
a_H(Å)
c_H(Å)
Temperature (K)
11.6
11.2
10.8
10.4
10.0
9.6
240
260
280
300
320
340
360

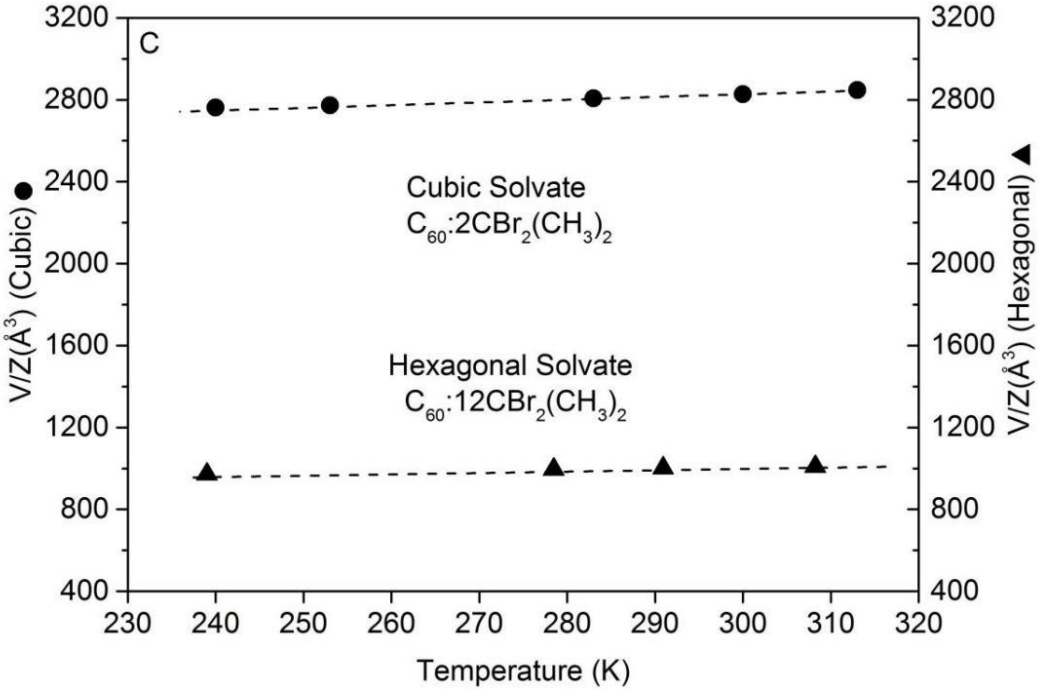

Fig. 3.12. Variation of the lattice parameters (A, B) and the volume of the unit cell (V/Z) (C) as a function of temperature for cubic solvate $C_{60}\cdot 12CBr_2(CH3)_2$ and hexagonal solvate $C_{60}\cdot 2CBr_2(CH3)_2$.

For the cubic solvate, no structural information beyond the lattice parameters (Fig. 3.4) could be obtained as a result of the extensive orientational disorder and the high number of molecules in the unit cell.

Only the structure of the hexagonal solvate has been analyzed using the FullProf Suite. The C_{60} molecule was modeled with spherical harmonics describing a homogeneous distribution of the 60 C-atoms positioned on a sphere with a radius of 3.59 Å. For the solvent molecule, assuming the lack of structural information, it was assumed a perfect tetrahedron with bond lengths C-Br = 1.95 Å and C-C = 1.53 Å [10]. The previous Le Bail analysis shows that the systematic absences were compatible with the spatial group P6/mmm, then the C_{60}

molecule was positioned at the origin of the unit cell (Wyckoff site 1a) and the solvent molecules were inserted into the interstices between C_{60} molecules (Wyckoff site 24 r).

In Fig. 3.10 the calculated pattern is the result of a Rietveld refinement containing 2.9% of FCC C_{60}. As a result of the former method, the position of the solvent molecules was refined at the position [0.358(4), 0.633(2), 0.519(2)]. The distance to the position [1/3, 2/3, 1/2] is 0.47 Å, which may be due to the fact that the center of mass of the molecule does not coincide with the central C-atom. The refined angles do not reveal any special orientation of the molecule with respect to the high symmetry directions of the unit cell resulting in a rather spherical distribution of the Br-atoms and methyl groups. The refined lattice parameters are a = 10.07(1) Å and c = 11.40(1) Å. The agreement factors are R = 11.3 and χ^2 =1.82.

The excess volume of a crystal is defined by $\Delta V/V = [(V/Z)^{exp} - (V/Z)^{cal}] / (V/Z)^{cal}$, where $(V/Z)^{exp}$ and $(V/Z)^{cal}$ are the experimental and calculated volumes of the crystal lattice per molecular unit, respectively. The $(V/Z)^{cal}$ values of the cubic and hexagonal solvates have been calculated using the molecular volumes from the literature for C_{60} (710 $Å^3$/molecule), and measured in the orientationally disordered phase of $CBr_2(CH_3)_2$ (165.2 $Å^3$/molecule) i.e (710 + 12 × 165.2) and (710 + 2 × 165.2), respectively. The excess volumes for the cubic solvate, which is not stable in the air, were found to be positive (+5%) similar to the positive excess volumes of cubic C_{60} solvates reported in previous studies [5,8,11,12]. On the contrary, a negative value of -4.3% is found for the hexagonal solvate. From a crystallographic point of view, these values are consistent with the observed stability.

3.4 Conclusions

Unstable-in-air cubic co-crystals $C_{60}\cdot 12CBr_2(CH_3)_2$ (a = 28.282(3) Å) were grown at room temperature in saturated solutions of FCC C_{60} and the $CBr_2(CH_3)_2$ solvent. These co-crystals transform into a hexagonal $C_{60}\cdot 2CBr_2(CH_3)_2$ co-crystal (a = 10.072(2) Å, c = 11.333(3) Å).

Whereas the cubic co-crystals form with a positive excess volumes (+5%) the stable hexagonal ones form with negative excess volumes (-4.3%). The excess volumes correlate with the relative stabilities of the co-crystals.

3.5 References

[1] A. Würflinger, L.C. Pardo, Thermodynamic Measurements on CH_3CCl_3, $(CH_3)_2CBr_2$, and on $nC_{20}H_{42}$ at High Pressures, Zeitschrift für Naturforschung, A Journal of physical sciences, 57, 2002, 177.

[2] J. Ye, M. Barrio, R. Céolin, N. Qureshi, I. B. Rietveld, J. Ll. Tamarit, Van-der-Waals based solvates of C_{60} with CBr_2Cl_2 and $CBr_2(CH_3)_2$. Chemical Physics, 477, 2016, 39.

[3] S. Toscani, H. Allouchi, J. Ll. Tamarit, D. O. López, M. Barrio, V. Agafonov, A. Rassat, H. Szwarc and R. Céolin, Decagonal C_{60} crystals grown from n-hexane solutions: solid-state and aging studies, Chemical Physics Letters, 330, 2000, 491.

[4] P. Espeau, M. Barrio, D. O. López, J. Ll. Tamarit, R. Céolin, H. Allouchi, V. Agafonov, F. Masin, H. Szwarc, Phase Equilibria in the C_{60} + Ferrocene System and Solid-State Studies of the C_{60}:2Ferrocene Solvate, Chemistry of Materials, 14, 2002, 321.

[5] M. Barrio, D. O. López, J. Ll. Tamarit, P. Espeau, R. Céolin, Solid-State Studies of C_{60} Solvates Formed in the C_{60}-$BrCCl_3$ System, Chemistry of Materials, 15, 2003, 288.

[6] G. B. M. Vaughan, Y. Chabre, D. Dubois, Effect of stacking disorder on the orientational ordering transition of solid C_{60}, Europhysics Letters, 31, 1995, 525.

[7] R. Céolin, V. Agafonov, D. Andre, A. Dworkin, H. Szwarc, J. Dugue, Fullerene C_{60}·2 CCl_4 solvate: a solid-state study. Chemical Physics Letters, 208, 1993, 259.

[8] M. Barrio, D. O. Lopez, J. Ll. Tamarit, H. Szwarc, S. Toscani, R. Céolin, C_{60}-CCl_4 phase diagram: polythermal behaviour of solvates C_{60}·12 CCl_4 and C_{60}·2 CCl_4. Chemical Physics Letters, 260, 1996, 78.

[9] M. Barrio, D. O. López, J. Ll Tamarit, P. Espeau, R. Céolin, Solid state studies of C_{60} solvates formed in the C_{60}-$BrCCl_3$ system, Chemistry of Materials, 15, 2003, 288.

[10] Ph. Negrier, M. Barrio, J. Ll. Tamarit, N. Veglio, D. Mondieig, Structure of Phase III and Polymorphism of $(CH_3)_3CBr$. Crystal Growth & Design, 10, 2010, 2793.

[11] B. Keita, L. Nadjo, R. Céolin, V. Agafonov, D. Andre, H. Szwarc, J. Dugue, C. Fabre, A. Rassat, Atomic-Force Microscopy Characterization of Stable Faces in Cubic C-60 and Hexagonal C-60, 2CCl_4 Single-Crystals, Chemical physics, 179, 1994, 595.

[12] R. Céolin, J. Ll Tamarit, M. Barrio, D. O. López, P. Espeau, H. Allouchi, R. J. Papoular, Solid state studies of the C_{60}·2$(CH_3)CCl_3$ solvate, Carbon, 43, 2005, 417.

4. The C_{60}:CBr_2Cl_2binary system

4.1 The solvent: Dibromodichloromethane

Solvent dibromo-dichloro-methane CBr_2Cl_2, purchased from Across with a purity of 98% was used without further purification. The polymorphism and thermal behavior of this material were studied by means a set of experimental techniques as a function of the temperature and pressure in the past [1]. At normal pressure the low-temperature phase is monoclinic with V/Z= 148.52 $Å^3$/molecule at 255 K. This phase transforms on heating to an FCC cubic phase with V/Z = 162.03 $Å^3$/molecule at 290 K. The temperature and enthalpy changes determined in this work for the solid-solid transition are 258 K and 5.22 kJ/mol (21.51J/g). As for the melting, 293 K and 2.3 kJ/mol (9.5 J/g) were determined. Those values match up the published values [1]. The liquid remains until the boiling point at 393 K [2].

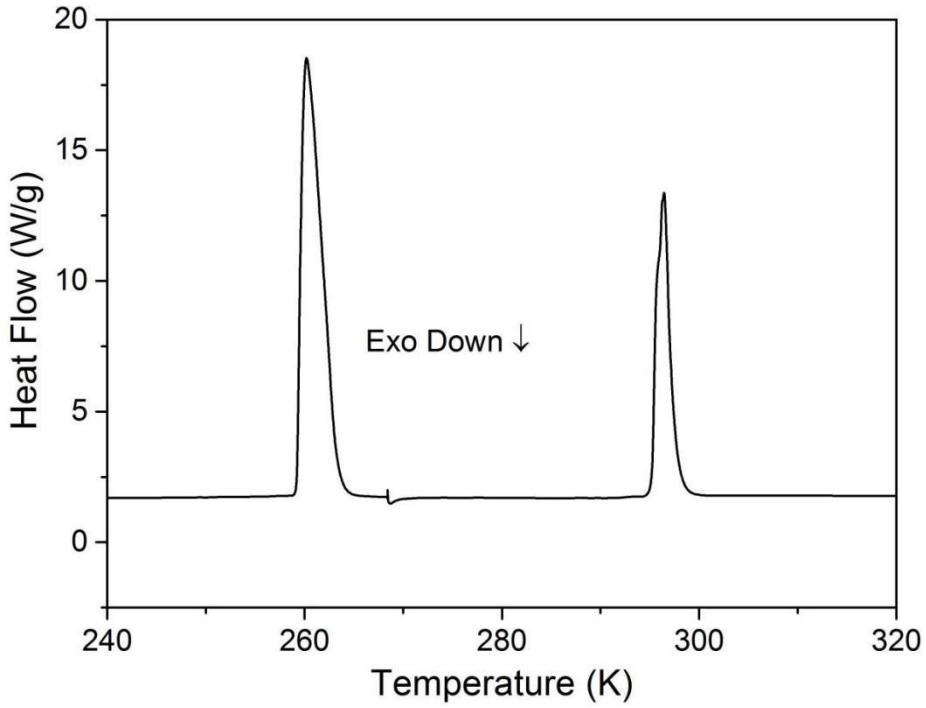

Fig. 4.1. Solid-solid transition and melting signals for the CBr_2Cl_2 solvent by differential scanning calorimetry (DSC).

4.2 Study of the C_{60}:CBr_2Cl_2 solvates

As usual, the FCC C_{60} crystals were mixed with the CBr_2Cl_2 solvent in screw-cap tubes. After a few hours, it was observed that the liquid acquired a purple color. After a couple of weeks, some crystal was removed from the solution and analyzed by scanning electron microscopy (SEM). A cubic morphology is clearly seen from the SEM measurements. (Fig. 4.2)

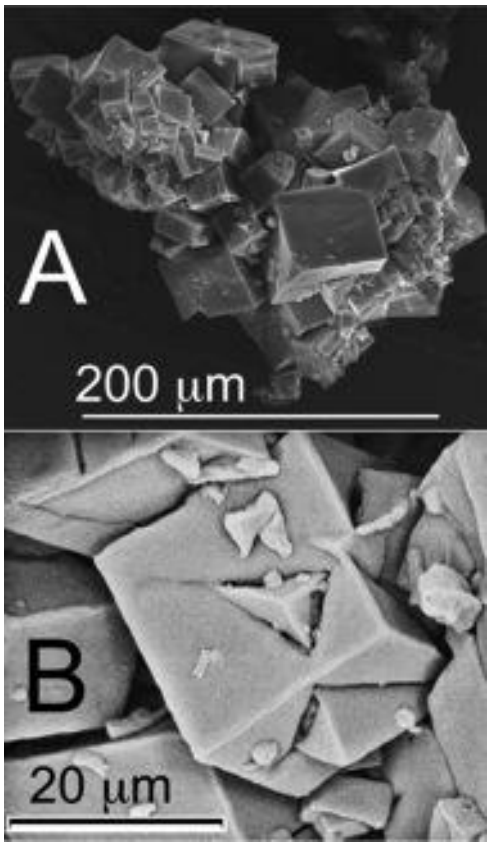

Fig. 4.2. Scanning electron microscopy photographs of crystals formed by the C_{60}:CBr_2Cl_2 system: (A) Cubic crystals of C_{60}:CBr_2Cl_2 directly obtained from the mother liquor, (B) Enlargement of the center of (A), showing intercalated twinning of the fluorite type with two cubes rotated about [111].

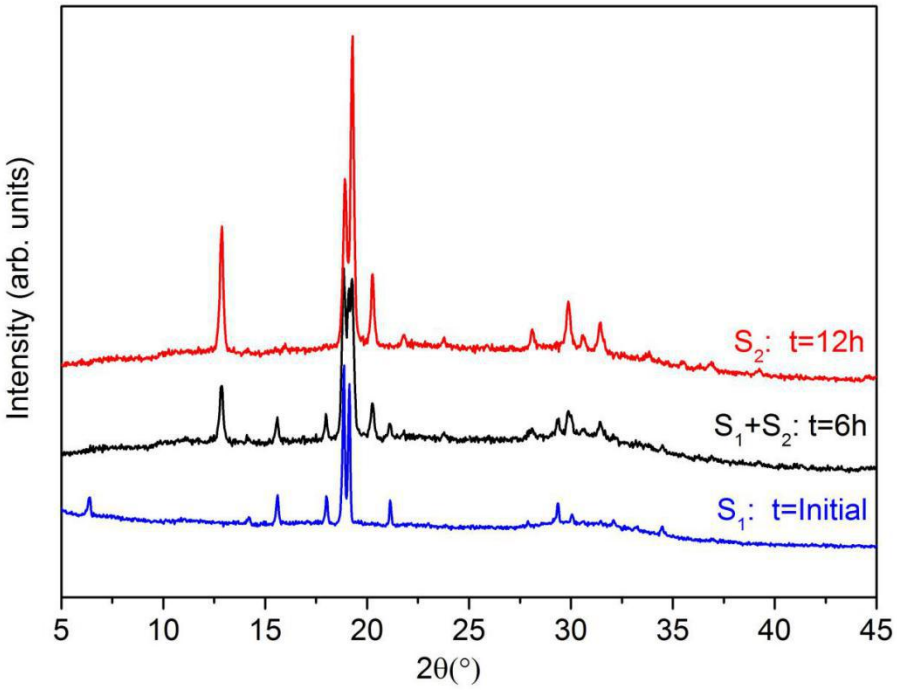

Fig. 4.3. The transformation from S_1 to the S_2 solvate by X-ray at room temperature.

To ascertain the stability of this cubic solvate, samples of the solvate together with mother liquor were extracted from the solution and quickly introduced into Lindeman capillaries. Then the capillary was partially obstructed with quartz wool in order to allow a slow evaporation of the liquid. In all cases the appearance of new Bragg peaks takes place in a time range between some hours and couples of days, depending on the amount of the mother liquor initially introduced.

The coexistence of both phases can remain until the disappearance of the cubic phase. As an example, the former evolution is shown in Fig. 4.3. The original pattern corresponding to the cubic solvate, named S_1, shows after 6 hours new reflections belonging to the final pattern, named S_2, that was obtained after 12 hours. Both profiles S_1 and S_2 keep similarities with those obtained for the cubic and hexagonal solvates in the C_{60}:$CBr_2(CH_3)_2$ system. In contrast to the former system in which a very slow evaporation of the liquid allows us to obtain the

hexagonal solvate, but always with traces of C_{60}, in this case, it seems that the formation of the new solvate is preferred over the desolvation of the cubic solvate.

The crystal symmetry and lattice parameters were tested by means the DICVOL program for both solvates. For the cubic solvate S_1, an FCC solution with lattice parameter a = 27.914(7) Å was obtained. The solution for the S_2 profile was a hexagonal lattice with lattice parameters a = 10.110(4) Å and c = 11.106(6) Å. The systematic absences are compatible with the space groups $Fm\bar{3}m$ and P6/mmm, respectively.

Mixtures of cubic crystals in mother liquor were introduced in pierced pans and maintained isothermally at 303 K within the thermogravimetric analyzer for determining the stoichiometry of the solvate. Immediately after the mother liquor had evaporated, the sample was heated to 525 K with a heating rate of 2 K/min.

The measured mass loss is presented in Fig. 4.4 and it exhibits two steps over an extensive temperature interval. The final mass loss is about 78%, very near the expected value of 80% for the desolvation process $C_{60}\cdot 12CBr_2Cl_2$ (solid) → C_{60} (solid) + $12CBr_2Cl_2$ (vapor). As for the first step, the mass loss of 68% agrees very well with the decomposition from $C_{60}\cdot 12CBr_2Cl_2$ (solid) → $C_{60}\cdot 2CBr_2Cl_2$ (solid) + $10CBr_2Cl_2$ (vapor), i.e., the transformation from cubic to hexagonal co-crystals, with an expected mass loss of 67%.

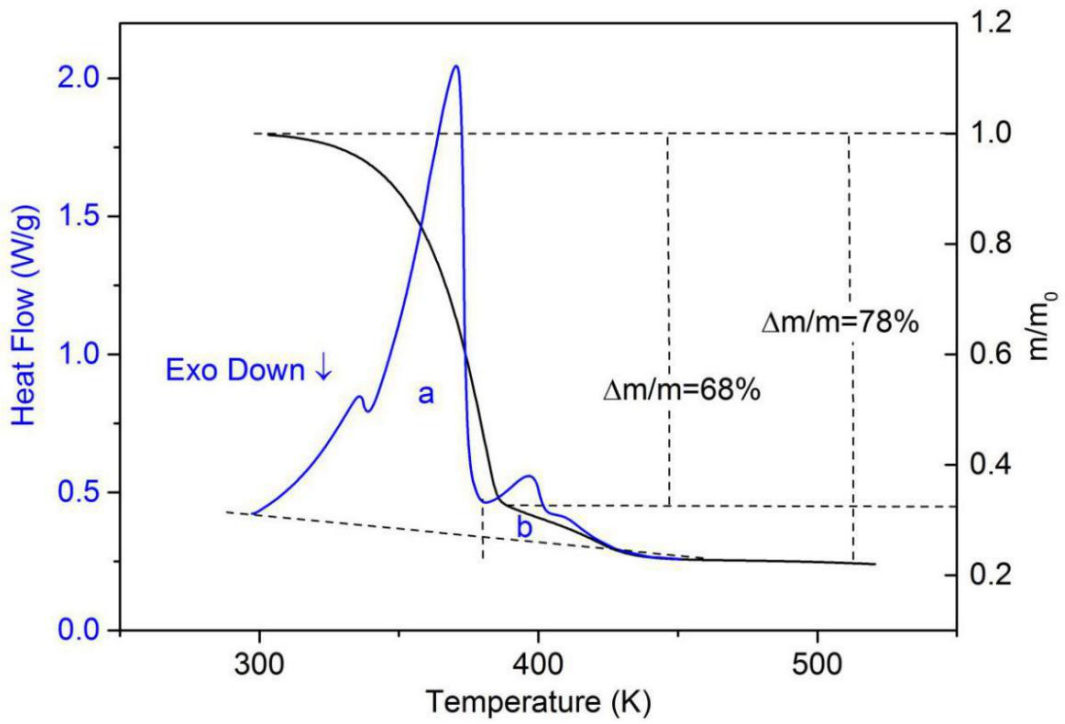

Fig. 4.4. Thermogravimetric (black line) and DSC (blue line) curves for the cubic solvate of $C_{60}\cdot 12CBr_2Cl_2$ in an open pan after the mother liquor had evaporated.

DSC measurements in pierced pans enable us to account for the related enthalpy change for the aforementioned desolvation process. The total enthalpy change for the desolvation of the cubic co-crystals (peaks **a** and **b**) gives a desolvation enthalpy of 124 - 148 J/g of $C_{60}\cdot 12CBr_2Cl_2$ (38 - 45 kJ/mole of solvent). As for the desolvation of the $C_{60}\cdot 2CBr_2Cl_2$ hexagonal solvate (peak **b**), the desolvation enthalpy is determined to be 36 - 49 J/g of solvate (i.e., 22 - 29 kJ/mol of solvent).

To obtain a more accurate value for the desolvation enthalpy of the $C_{60}\cdot 2CBr_2Cl_2$, some hexagonal-shaped crystals were subjected to TGA and DSC analyses. The results are shown in Fig. 4.5. The final mass loss is about 33%, very near the expected value of 32% for the

desolvation process $C_{60}{\cdot}2CBr_2Cl_2$ (solid) → C_{60} (solid) + $2CBr_2Cl_2$ (vapor). The desolvation enthalpy around 46 J/g of solvate matches up the previous values.

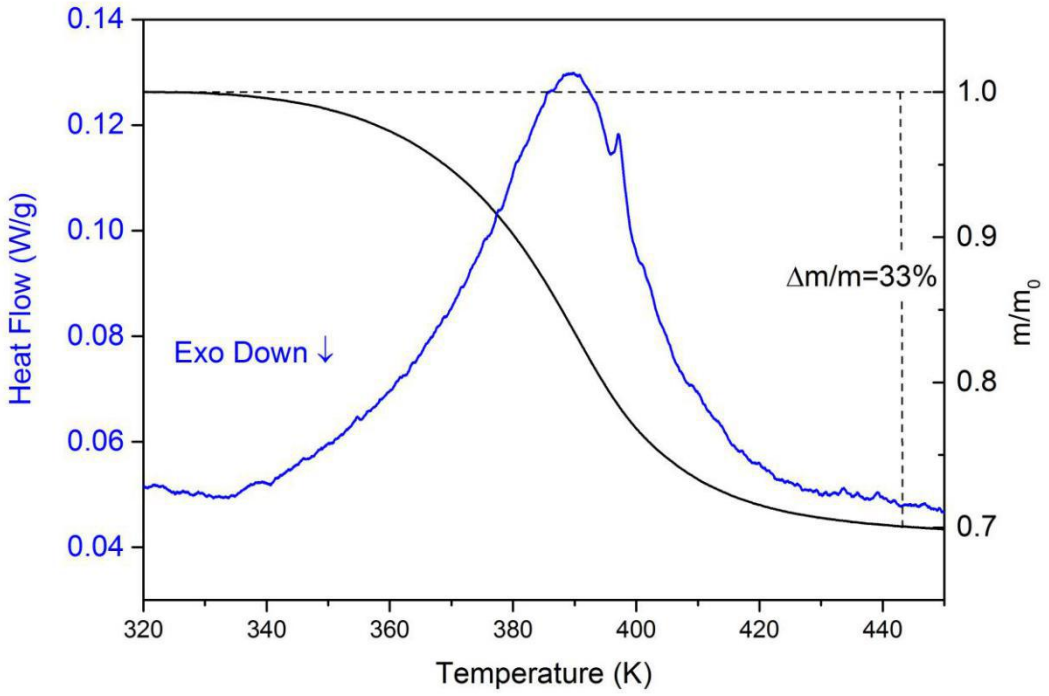

Fig. 4.5. TGA and DSC measurements of the desolvation of the hexagonal solvate: $C_{60}{\cdot}2CBr_2Cl_2$.

Because of the instability of the cubic solvate, mixtures of the crystals in their mother liquor were placed in stainless steel high-pressure pans for DSC studies. The resulting DSC curve can be seen in Fig. 4.6. The endothermic peaks **p**1at 259 K and **p**2 at 294 K corresponding to the solid-solid phase transition and fusion of pure solvent CBr_2Cl_2. The onset temperatures are virtually the same as those of pure CBr_2Cl_2; hence, the transitions correspond to degenerated invariant equilibria in the C_{60}:CBr_2Cl_2 binary system: M + FCC + $C_{60}{\cdot}12CBr_2Cl_2$ and Liquid + FCC + $C_{60}{\cdot}12CBr_2Cl_2$.

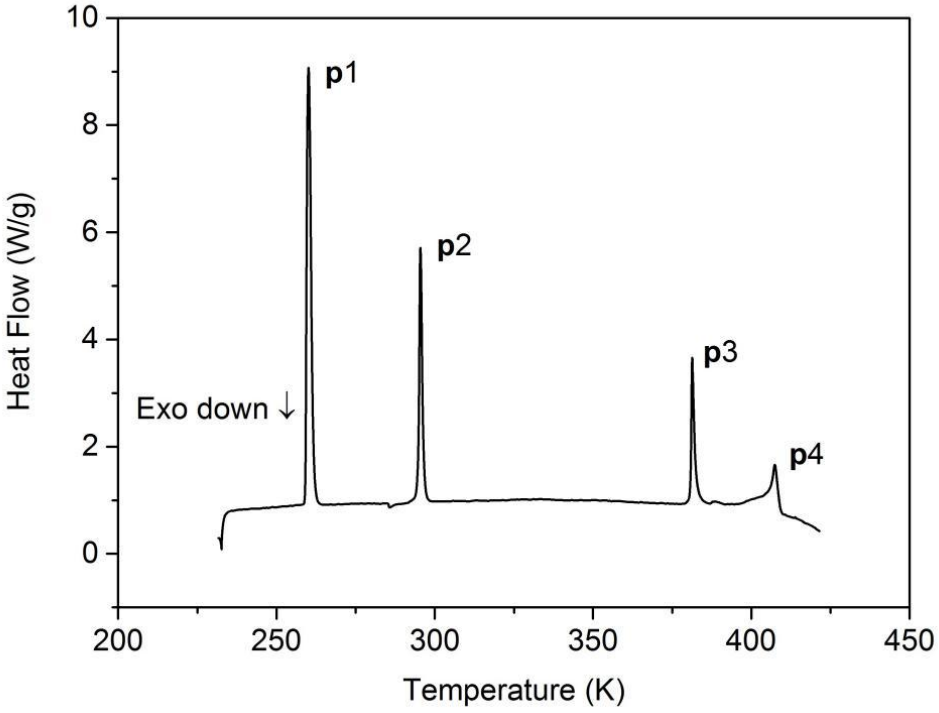

Fig. 4.6. DSC curve for the cubic crystals with an excess of mother liquid in a closed pan.

Peaks **p**3 at 382.4 K and **p**4 at 405K in Fig. 4.6 correspond, as demonstrated by the next X-ray measurement, to the peritectic invariants (C_{60}·12CBr_2Cl_2 + C_{60}·2CBr_2Cl_2 + liquid) and (C_{60}·2CBr_2Cl_2 + liquid + FCC C_{60}), respectively.

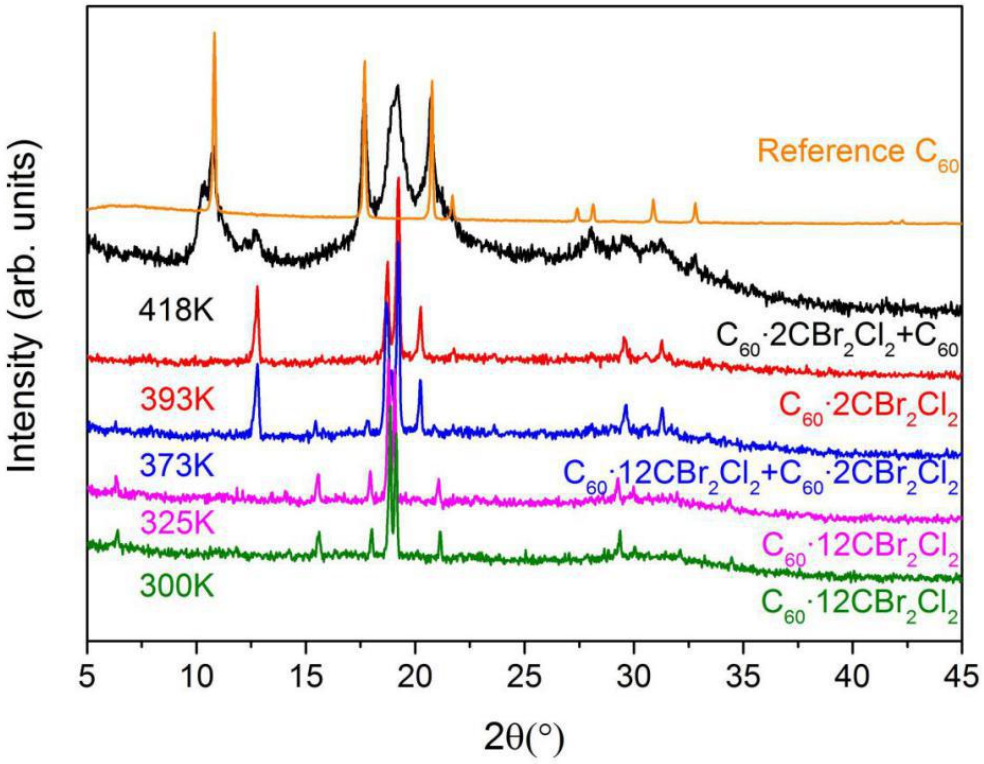

Fig. 4.7. Patterns as a function of temperature from cubic solvate in an excess of mother liquor in a sealed capillary. The range between 45 and 115° is not shown due to the absence of Bragg peaks with significant intensity.

To verify the previous assignment, X-ray diffraction of cubic crystals with mother liquor in a closed capillary was carried out as a function of temperature (see Fig. 4.7). The profile at 373K shows the co-existence of both solvates, and that at 418 K the coexistence of the hexagonal one with FCC C_{60} with stacking-faults [3-6].The diffraction patterns as a function of temperature confirm the assignment of the different invariants observed in the DSC measurements (Fig. 4.6).

4.3 Discussion and structural characterization

Using the experimental stoichiometries and the DSC thermal events, the binary phase diagram between C_{60} and CBr_2Cl_2 has be constructed (Fig. 4.8). It shows the stability domain of both co-crystals at mole fractions of X = 1/13 ($C_{60}\cdot 12CBr_2Cl_2$) and X = 1/3 ($C_{60}\cdot 2CBr_2Cl_2$), which, as determined above, possess FCC and hexagonal symmetries, respectively.

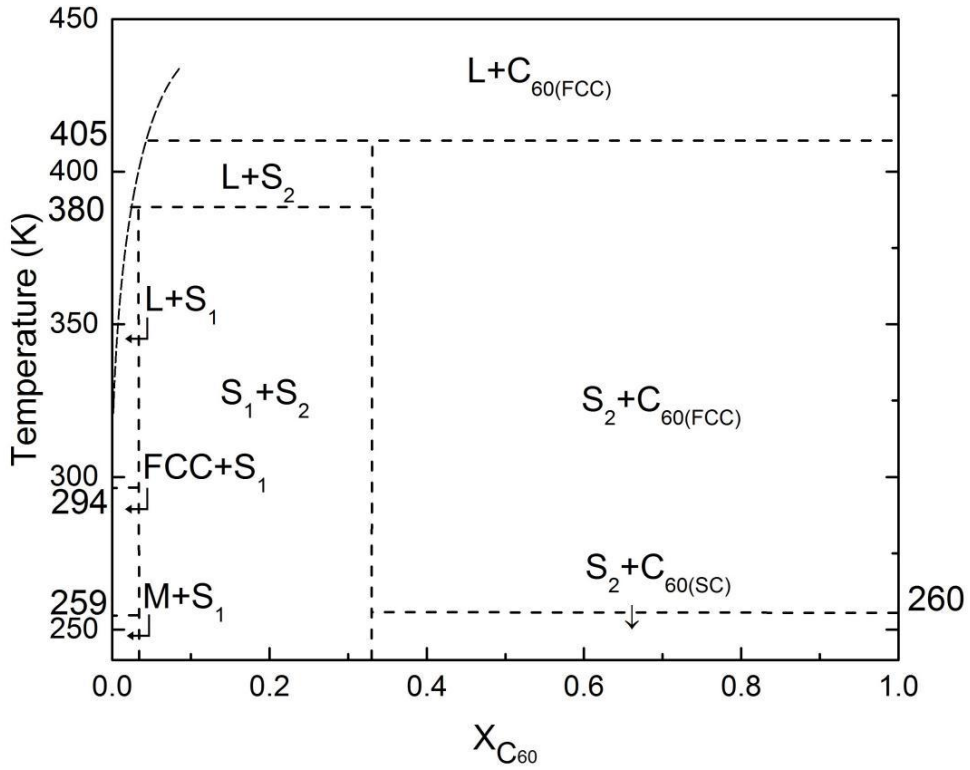

Fig. 4.8. C_{60}:CBr_2Cl_2 phase diagram. S1 and S2 are the respective co-crystals $C_{60}\cdot 12CBr_2Cl_2$ and $C_{60}\cdot 2CBr_2Cl_2$, and M and FCC are the ordered and disordered phases of the solvent.

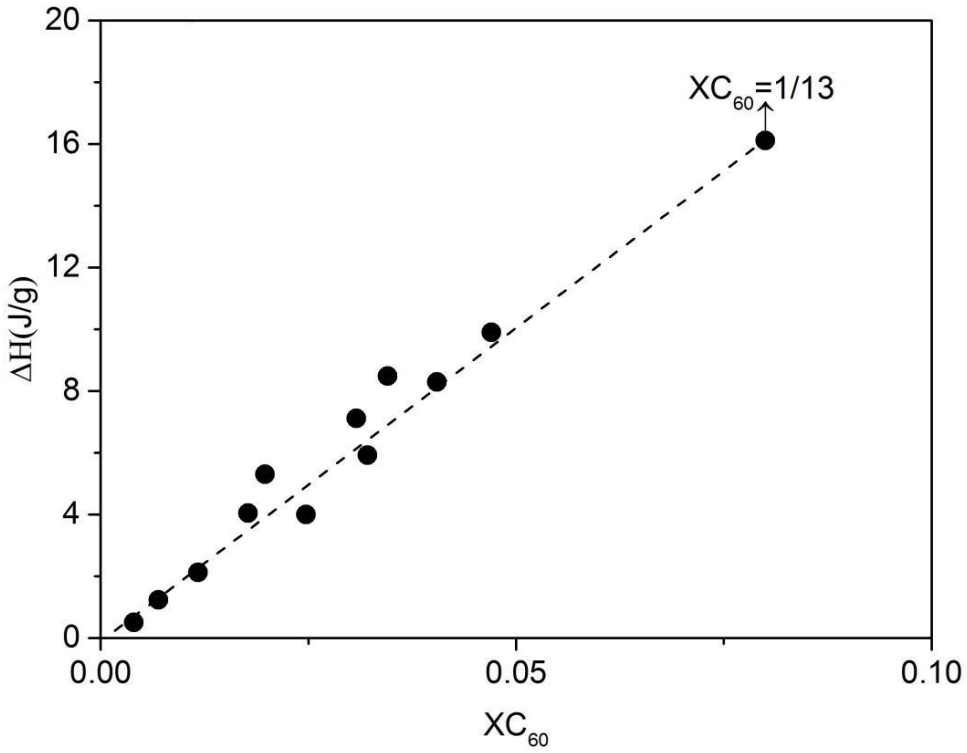

Fig. 4.9. Tammann diagram for the $C_{60}\cdot 12CBr_2Cl_2$ + $C_{60}\cdot 2CBr_2Cl_2$ + liquid peritectic equilibrium.

The enthalpy of the peritectic invariant $C_{60}\cdot 12CBr_2Cl_2$ + $C_{60}\cdot 2CBr_2Cl_2$ + liquid was determined by DSC by means the DSC measurements of several samples with compositions between X = 0 (CBr_2Cl_2) and X = 1/13 (~0.08, i.e. the $C_{60}\cdot 12CBr_2Cl_2$ co-crystal composition). The enthalpy associated with the peritectic transition at T = 382.4 K was found to be 17 J/g of cubic co-crystal (see Fig. 4.9).

Taking as staring point the symmetry and lattice parameters obtained by means of DICVOL, the cubic solvate profile (in Fig. 4.10) was refined by a Pattern Matching procedure assuming a $Fm\bar{3}m$ group: a=27.884(5) Å, V/Z=2710.1(8) $Å^3$ and Z=8. For the cubic solvate,

no structural information beyond the lattice parameters could be obtained as a result of the extensive orientational disorder and the high number of molecules in the unit cell.

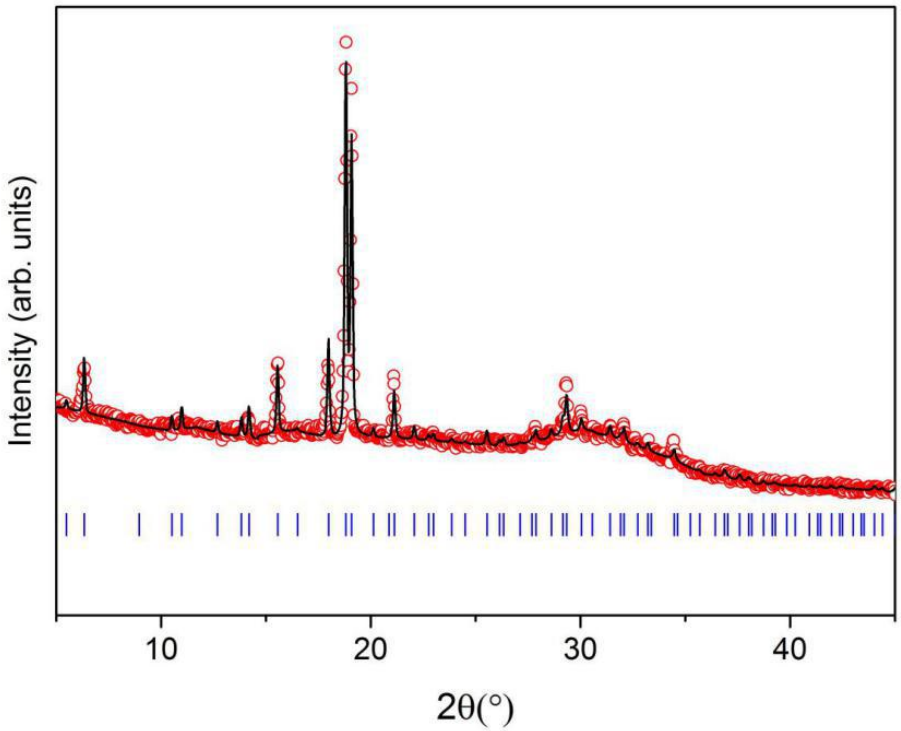

Fig. 4.10. Experimental (points) and calculated (lines) diffraction patterns along with the calculated Bragg peak positions (vertical bars) for the cubic $C_{60}\cdot 12CBr_2Cl_2$.

Similarly to as was done with the cubic solvate, starting from the results obtained with DICVOL, for the hexagonal $C_{60}\cdot 2CBr_2Cl_2$solvate the lattice parameters were refined by means of the Pattern Matching procedure, assuming a P6/mmm group: a = 10.1101(8) Å, c = 11.022(9) Å with V = 982.7(1) $Å^3$.

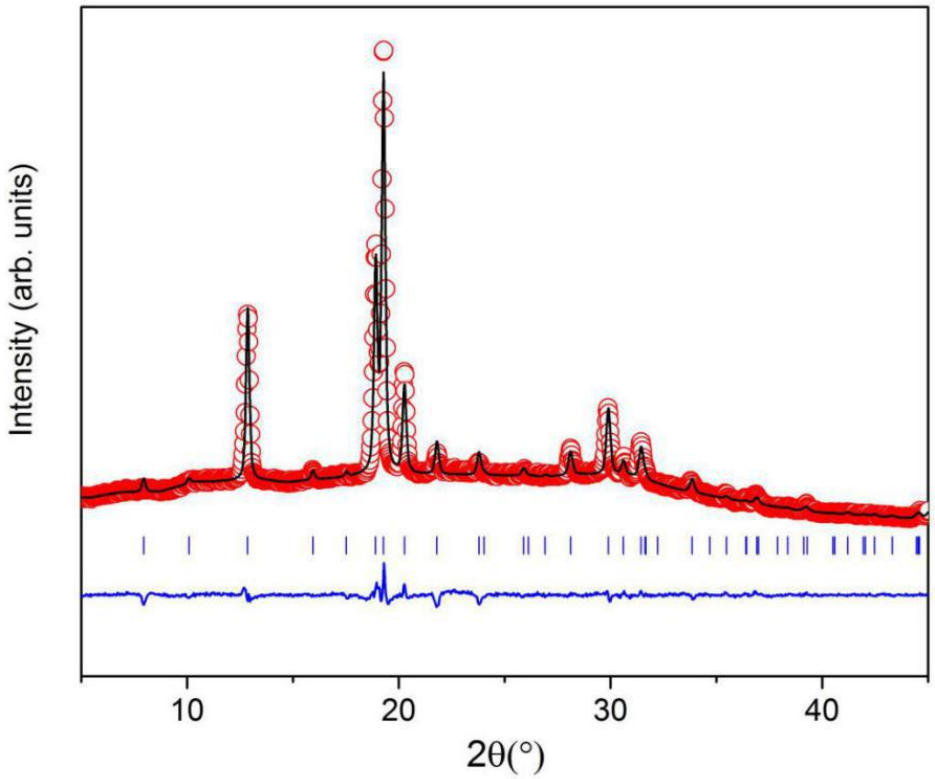

Fig. 4.11. Experimental (points) and calculated (lines) diffraction patterns along with the calculated Bragg peak positions (vertical bars) for the hexagonal $C_{60}{\cdot}2CBr_2Cl_2$ solvate. The calculated pattern is the result of a Rietveld refinement (the residuals are plotted below the Bragg peak positions).

The Rietveld analysis of the hexagonal co-crystal has been performed using the FullProf Suite. The C_{60} molecule on Wyckoff site 1a of space group P6/mmm has been modeled with spherical harmonics describing a homogeneous distribution of 60 C-atoms positioned on a sphere with a radius of 3.59 Å. The CBr_2Cl_2 molecule has been described as a rigid body with the C-atom at the center of the molecule, two Cl-atoms at a distance of 1.77 Å and two Br-atoms at a distance of 1.93 Å [1]. For simplicity, the angle between the ligands has been set to that of a perfect tetrahedron. The variable structural parameters within the Rietveld refinement

process were the lattice constants, the position of the CBr_2Cl_2 molecule and its orientation. An overall isotropic temperature factor has been refined for all involved atoms and the background has been described by a linear interpolation. No symmetry constraint has been assumed for the position of the molecule (Wyckoff site 24r).

The result of the refinement (Fig. 4.11 for X-ray patterns, and Fig. 4.12 for the structure) demonstrates that the central C atom of the CBr_2Cl_2 molecule is situated approximately at the prismatic hexagonal void with the refined position of [0.377(4), 0.689(4), 0.507(4)]. The distance to the position (1/3, 2/3, 1/2) is 0.5 Å, which may be due to the fact that the center of mass of the molecule does not coincide with the central C-atom.

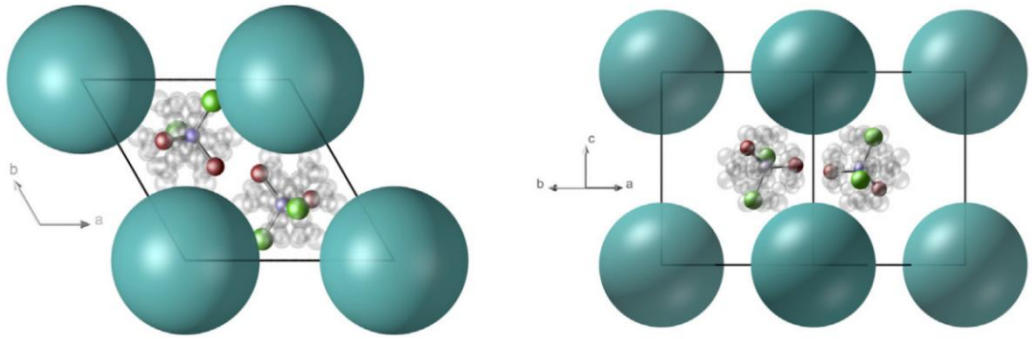

Fig. 4.12. Structure of the $C_{60}\cdot 2CBr_2Cl_2$ hexagonal solvate along [001] (left) and [110] (right) directions. The orientational disorder of the CBr_2Cl_2 molecules at the prismatic positions is highlighted by several compatible orientations in grey.

The refined angles do not reveal any special orientation of the molecule with respect to the high symmetry directions of the unit cell resulting in a rather spherical distribution of the Br- and Cl-atoms, when the dynamic disorder is taken into account. The starting orientation did not have an influence on the result of the Rietveld refinement, i.e. the final orientations were always symmetry equivalent which corroborates the validity of our result. The refined

lattice constants are a = 10.09(1) Å and c = 11.10(1) Å. The agreement factors are R = 14.9 and χ^2 = 1.55.

The excess volume of a crystal defined by $\Delta V/V = [(V/Z)^{exp} - (V/Z)^{cal}] / (V/Z)^{cal}$, where $(V/Z)^{exp}$ and $(V/Z)^{cal}$ are the experimental and calculated volumes, respectively, of the crystal lattice per molecular unit were calculated for both co-crystals. The $(V/Z)^{cal}$ values have been calculated using the molecular volumes from the literature for C_{60} (VC_{60} = 710 $Å^3$/molecule) and CBr_2Cl_2 ($V_{CBr2Cl2}$ = 162.03 $Å^3$/molecule for the high-temperature FCC phase [1]). The excess volume for the cubic solvate, which is not stable in air, was found to be positive, +2%, whereas a negative value, -5%, was found for the hexagonal solvate. Then the excess volumes correlate with the relative stabilities of the solvates. Positive and negative values of the excess volumes for the metastable and stable solvates have been obtained in the $CBr_2(CH_3)_2$ system and have been reported for other C_{60} solvates [6-8].

4.4 Conclusions

Cubic co-crystals of $C_{60}\cdot 12CBr_2Cl_2$ (a = 27.884(5) Å) were grown at room temperature in saturated solutions of FCC C_{60}. This co-crystal is unstable in the air and transforms spontaneously into the hexagonal co-crystal $C_{60}\cdot 2CBr_2Cl_2$ with unit-cell parameters a = 10.1101(8) Å and c = 11.022(9) Å. Whereas the cubic co-crystals have positive excess volumes (+2%), the stable hexagonal crystals possess negative excess volumes (-5%). The excess volumes correlate then with the relative stabilities of the solvates.

4.5 References

[1] M. Barrio, J. Ll.Tamarit, P. Negrier, L. C. Pardo, N. Veglio, D. Mondieig, Polymorphism of CBr_2Cl_2, New Journal of Chemistry, 32, 2008, 232.

[2] A. P. Kudchadker, S. A. Kudchadker, R. P. Shukla, P. R. Patnaik, Vapor pressures and boiling points of selected halomethanes, Journal of Physical and Chemical Reference Data, 8, 1979, 499.

[3] G. B. M. Vaughan, Y. Chabre, D. Dubois, Effect of Stacking Disorder on the Orientational Ordering Transition of Solid C_{60}, Europhysics Letters, 31, 1995, 525.

[4] S. Toscani, H. Allouchi, J. Ll. Tamarit, D. O. López, M. Barrio, V.Agafonov, A. Rassat, H. Szwarc, R. Céolin, Decagonal C_{60} crystals grown from n-hexane solutions: solid-state and aging studies, Chemical Physics Letters, 330, 2000, 491.

[5] P. Espeau, M. Barrio, D. O. López, J. Ll. Tamarit, R. Céolin, H. Allouchi, V. Agafonov, F. Masin, H. Szwarc, Phase Equilibria in the C_{60} + Ferrocene System and Solid-State Studies of the C_{60}·2Ferrocene Solvate, Chemistry of Materials, 14, 2002, 321.

[6] M. Barrio, D. O. López, J. Ll. Tamarit, P. Espeau, R. Céolin, Solid-State Studies of C_{60} Solvates Formed in the C_{60}-$BrCCl_3$ System, Chemistry of Materials, 15, 2003, 288.

[7] L. A. Solovyov, N. V. Bulina, G. N. Churilov, Crystal structures of chloroform solvates of fullerenes, Russian Chemical Bulletin, 50, 2001, 78.

[8] B. Keita, L. Nadjo, R. Céolin, V. Agafonov, D. Andre, H. Szwarc, J. Dugue, C. Fabre, A. Rassat, Atomic force microscopy characterization of stable faces in cubic C_{60} and hexagonal C_{60}, $2CCl_4$ single crystals, Chemical Physics Letters, 179, 1994, 595.

5. The C_{60}:CBr_2H_2 binary system

5.1 The solvent: Dibromomethane

The liquid dibromomethane (CBr_2H_2), density 2.50 g/mL, was purchased from Aldrich with a purity higher than 99%. At normal pressure, the liquid crystallizes in a monoclinic structure with space group C2/c [1-3]. The temperature and enthalpy change for the melting determined in this work (Fig. 5.1) are 219.0 K and 9.08 kJ/mol (52.16 J/g) respectively. These values are in agreement with the literature data [4]. The liquid phase remains until the boiling point at 370 K, being the vaporization enthalpy of 37 kJ/mol [5].

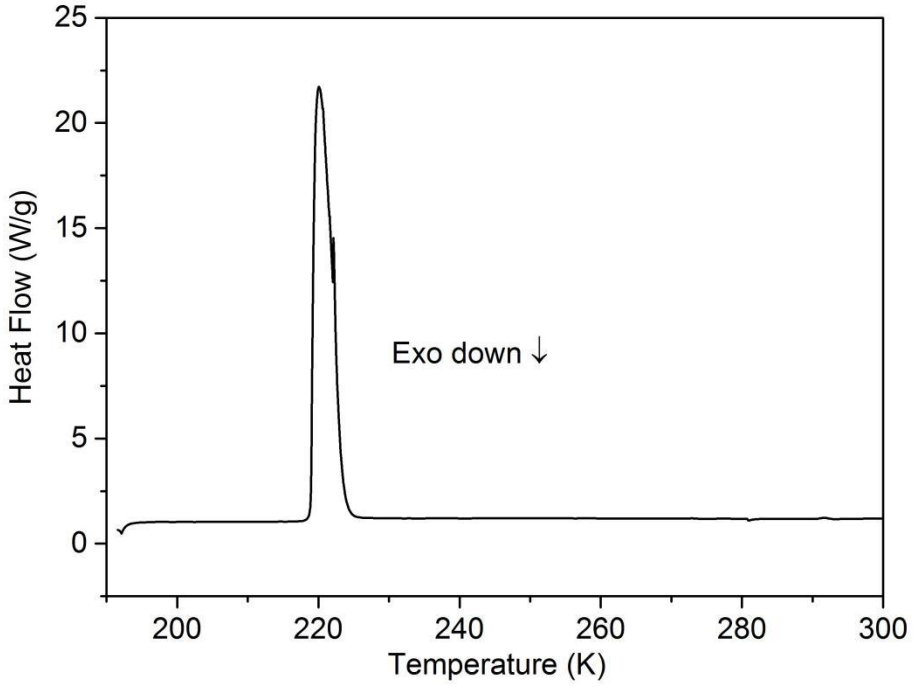

Fig. 5.1. Melting of solvent CBr_2H_2 by differential scanning calorimetry (DSC).

5.2 Study of the C_{60}:CBr_2H_2 solvates

Solid C_{60} was dissolved in solvent CBr_2H_2 at room temperature in screw-cap tubes that were subsequently stored for several months in the dark. Unlike other solvates, black and bright crystals were formed at the surface of the colorless solution. The morphology of the crystals (Fig. 5.2) was examined by means of scanning electron microscopy (SEM).

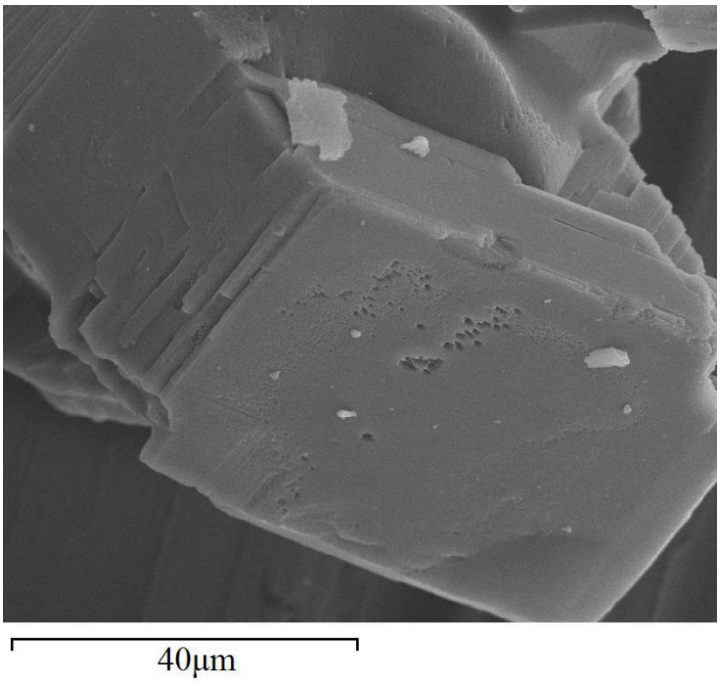

Fig. 5.2. Scanning electron microscopy (SEM) photograph of C_{60}·$2CBr_2H_2$ crystals(after TGA)

To study the stability of the solvate the evolution of the X-ray diffraction pattern was checked as a function of the time (see Fig. 5.3) at room temperature. After several days in contact with the air there were no significant changes indicating that the solvate is stable in the air.

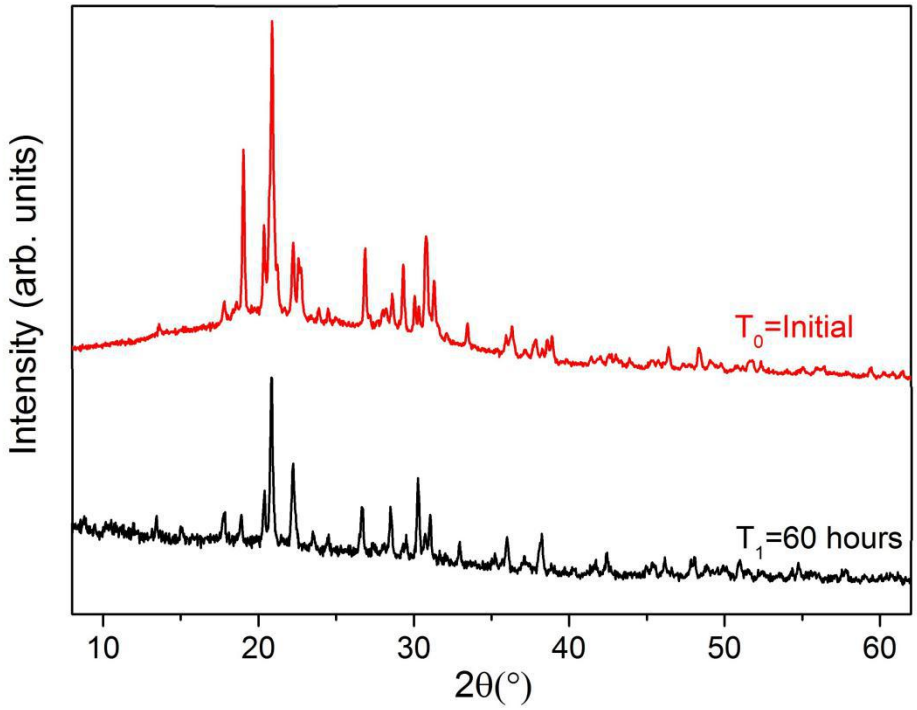

Fig. 5.3. X-ray diffraction patterns of the C_{60}:CBr_2H_2 co-crystals in mother liquor in an open capillary as a function of time.

The experimental profile was indexed by the DICVOL program. The best figures of merit were obtained for a monoclinic lattice with parameters a = 10.112 Å, b = 17.451 Å, c = 9.904 Å, β = 102.814º, V = 1704.19 Å^3.

A few crystals together with a small quantity of mother liquor were subjected to thermogravimetric analyses. After the recorded mass reached a constant value at room temperature, the sample was assumed to be mother liquor-free. It was subsequently heated to 550 K (Fig. 5.4) with a constant heating rate of 2 K/min. The experimental mass loss was found to be ca. 32%, i.e. very close to the expected value of 33% (= 2×173.8/1067.7) for the C_{60}:CBr_2H_2 = 1:2 molar ratio. The TG curve in Fig. 5.4 clearly demonstrates that the desolvation process takes place in two overlapping steps. It could indicate the formation of a

solvate with a lower stoichiometry or the existence of a desorption process following the desolvation of the 1:2 solvate.

The same procedure as for the TG measurements was followed for the DSC measurements (Fig. 5.4). Again, it can be observed that two thermal effects are convoluted as the endothermic signal (T_{onset} = 326 K) clearly consists of two overlapping peaks. In fact, the derivative of the mass loss with respect to the temperature (red curve in Fig. 5.4, which results from the TG measurements) mimics the DSC signal even if a small shift in temperature exists.

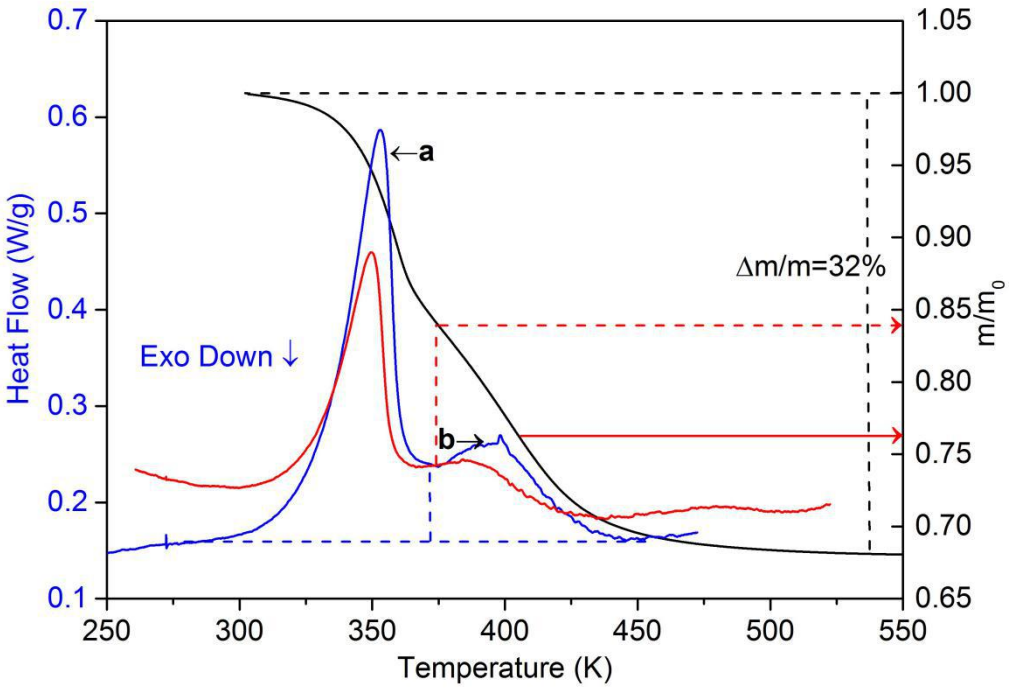

Fig. 5.4. Differential scanning calorimetry curve (blue, left axis) and thermogravimetry curve (black, right axis) as a function of the temperature for the $C_{60}{\cdot}2CBr_2H_2$ solvate. Red curve corresponds to the derivative of the weight loss with respect to the temperature. The dashed red arrow indicates the mass loss at the minimum of the derivative (see text).

To investigate the two convoluted peaks in the desolvation process more closely, aliquots of crystals together with the mother liquor were put in stainless steel high-pressure pans for DSC studies, and X-ray diffraction measurements were carried out on crystals in a closed capillary as a function of the temperature.

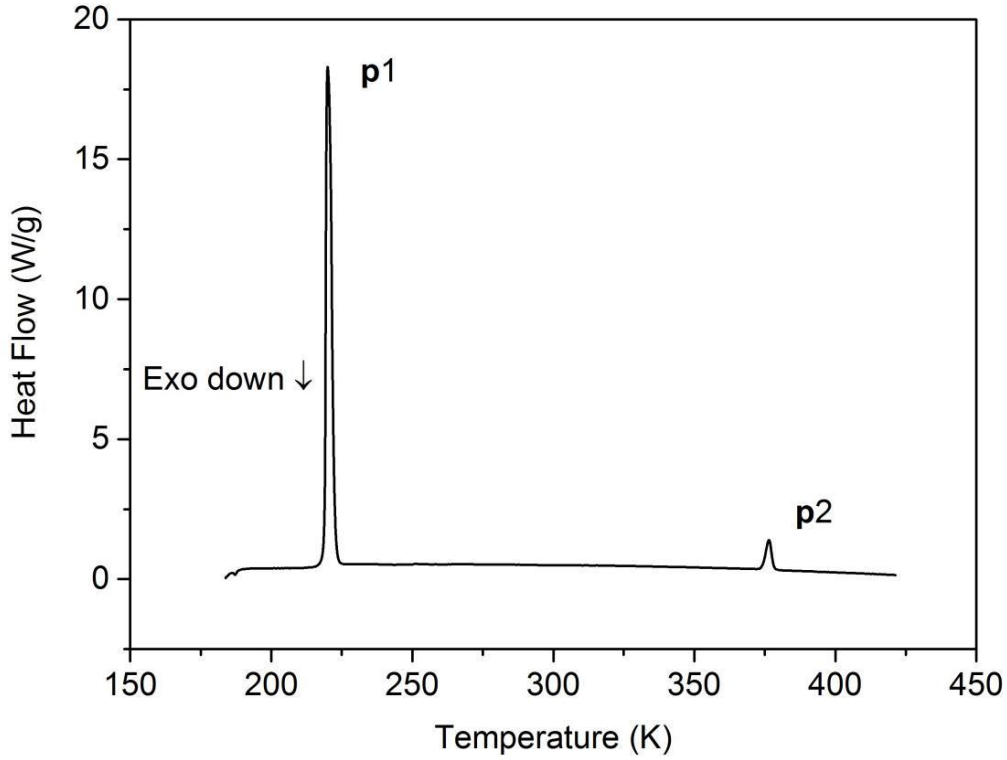

Fig. 5.5. DSC curve of a heterogeneous sample made of cubic $C_{60}{\cdot}2CBr_2H_2$ powder and excess of the mother liquor.

The DSC result is shown in Fig. 5.5: The first endothermic peak corresponds to the melting (219.0 K) of pure CBr_2H_2 (peaks **p**1), whereas the single endothermic peak at 373 K (**p**2) must be ascribed to the solvate. As the existence of two effects on the signal cannot be

ruled out, the evolution of the co-crystal spectra as a function of the temperature was tested by means X-ray measurements.

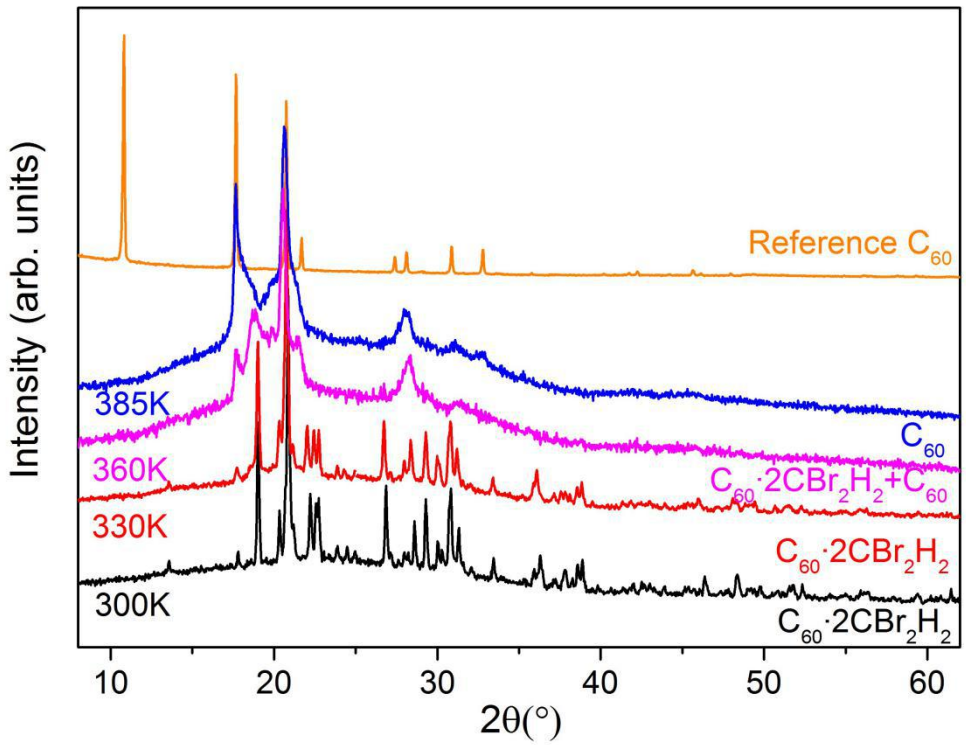

Fig. 5.6. X-ray patterns of the $C_{60}{\cdot}2CBr_2H_2$ solvate as a function of the temperature. The pattern of pure FCC C_{60} is shown at the top for reference purposes.

Fig. 5.6. shows several patterns between room temperature and 385 K, which is near the end of the second endothermic process **p**2. Patterns at temperatures between 300 and 385 K reveal that the Bragg peaks of the monoclinic solvate remain. The diffraction pattern at 385 K shows the desolvated C_{60}, i.e., partially amorphized by crystal defects and stacking faults as commonly observed after desolvation of C_{60} solvates [6-9]. It indicates that the existence of a second solvate with a smaller stoichiometry is not likely. The X-ray results are in agreement

with the DSC ones: The existence of a solvate that does not suffer any phase transition before the peritectic transformation:

$$C_{60}{:}2CBr_2H_2(s) \rightarrow C_{60}(s) + 2CBr_2H_2 \text{ (liquid)}$$

5.3 Discussion and structural characterization

The preliminary results show that only one solvate with stoichiometry 1:2 ($C_{60}{\cdot}2CBr_2H_2$), is formed between C_{60} and CBr_2H_2. This solvate is stable in the air until the desolvation temperature at around 350 K. For its structural analysis by means Materials Studio Program, the DICVOL solution was used as a starting point being the systematic absences compatible with the centered monoclinic space group C2/m. To determine the structure of the solvate, atom coordinates of the individual molecules C_{60} and CBr_2H_2 were used from the literature [1] and fitted in the obtained diffraction patterns. For the Rietveld refinement, a rigid-body constraint was used for CBr_2H_2. The position and orientation of the molecules were refined with a single overall isotropic displacement parameter and preferred orientation using the March-Dollase formula [10]. The refinement results are depicted in Fig. 5.7, together with the experimental pattern and the difference between the refined pattern and the experimental one. The values of the final Rietveld refinement are summarized in Table. 5.1.

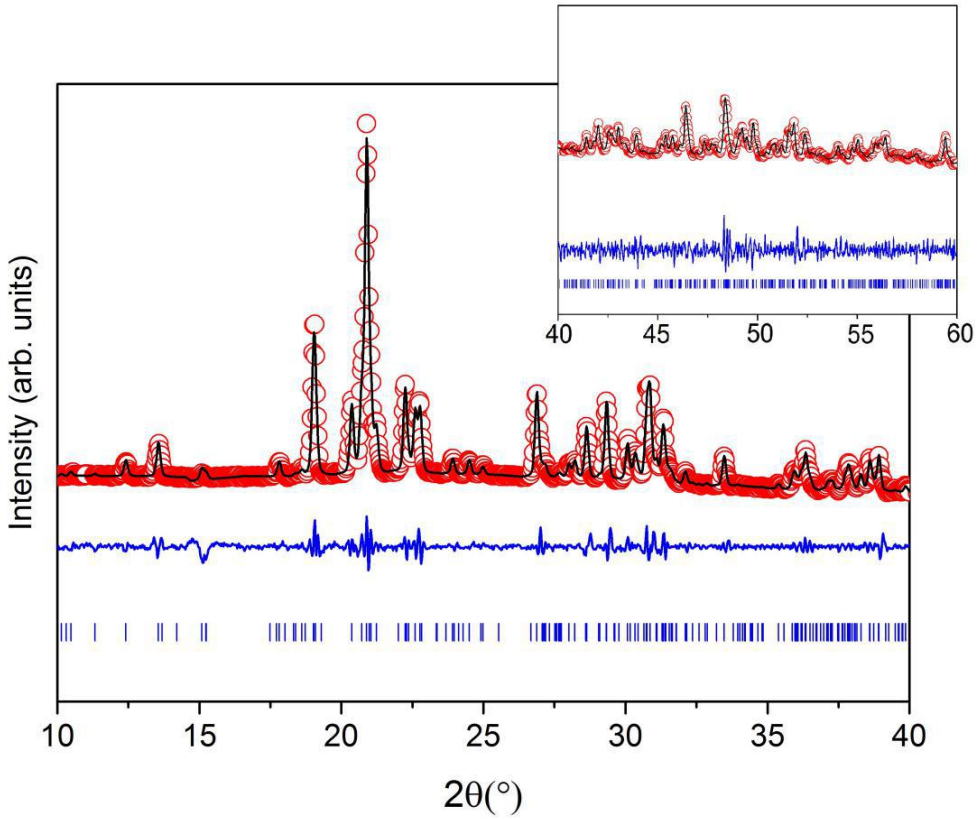

Fig. 5.7. Experimental (circles) and calculated (line) diffraction patterns along with the difference profile (blue line) and Bragg reflections (vertical bars) of the monoclinic C2/m space-group of the $C_{60}{\cdot}2CBr_2H_2$ solvate at room temperature. The inset corresponds to the scale for the data between 40 and 60° of 2θ.

Table. 5.1. Crystal structure information and Materials Studio results of the Rietveld refinement for the $C_{60}\cdot 2CBr_2H_2$ solvate.

Chemical Formula	$C_{60}\cdot 2CBr_2H_2$
M /g·mol^{-1}	1068.31
2θ - Angular Range	7 – 80^{o}
Space group	*C*2/*m*
a /Å *b* / Å *c* / Å α / ^{o} β / ^{o} γ / ^{o}	9.9001(4) 17.446(1) 10.1013(4) 90 102.769(2) 90
V / Å^3	1701.5(4)
Z	2
Temperature	293 K
D_x / g·cm^{-3}	2.085(1)
Wavelength (Cu Kα1)	λ = 1.5406 Å
2θ - shift (zero correction)	0.0264 (12)
Profile Parameters	
Na	0.509 (15)
Reliability Parameters	
R_{wp}	6.08%
R_p	4.24%
Peak width parameters	
U *V* *W*	0.124(17) -0.037(10) 0.0175(16)
Overall isotropic temperature factor, *U* / Å^2	0.0332 (6)
Asymmetry Correction (Finger-Cox-Jephcoat)	
H/*L* *S*/*L*	0.0280 (3) 0.0280 (3)
Preferred Orientation (March-Dollase)	
*a**	0.517(30)
*b**	0.838 (19)
*c**	0.189 (36)
R_0	1.055 (7)

Surprisingly, the C_{60} molecules appeared to be orientationally ordered in the current solvate. For confirmation, an independent Rietveld refinement of the structural model was carried out with the FullProf program. In a first step, the C_{60} molecule was modeled as a spherical shell with the scattering density of 60 carbon atoms homogeneously distributed on a sphere with a radius of 3.59 Å, which represents a freely rotating molecule. The CBr_2H_2 molecule was modeled as a rigid body with the atom coordinates taken from Podsiadło et al. [1]. The local coordinate system was set with the 2-fold rotation axis of the CBr_2H_2 molecule pointing along the local *z* axis (the local coordinate system is defined by $x \parallel a$, $y \parallel b$ and $z \parallel (a \times b)$ with $\theta = \phi = \chi = 0$, which therefore permits to rotate the molecule around its 2-fold rotation axis by the angle χ independently of its orientation in the unit cell. A first refinement clearly shows that the CBr_2H_2 molecule is oriented with its 2-fold rotation axis parallel to the monoclinic *b* axis, i. e. $\theta = \phi = 90$ degrees.

In a second step, the C_{60} molecule was modeled as a rigid body with its 2-fold rotation axis along the local *z* axis. A clear improvement of the refinement is apparent between the spherical-shell model with the agreement factor, R_F, equal to 8.0 and the rigid-body model with $R_F = 4.2$, which strongly suggests that the C_{60} molecule is not freely rotating. The resulting orientation is such that its 2-fold rotation axis is aligned with the monoclinic *b* axis just like the CBr_2H_2 molecule (i.e. $\theta = \phi = 90$ degrees).

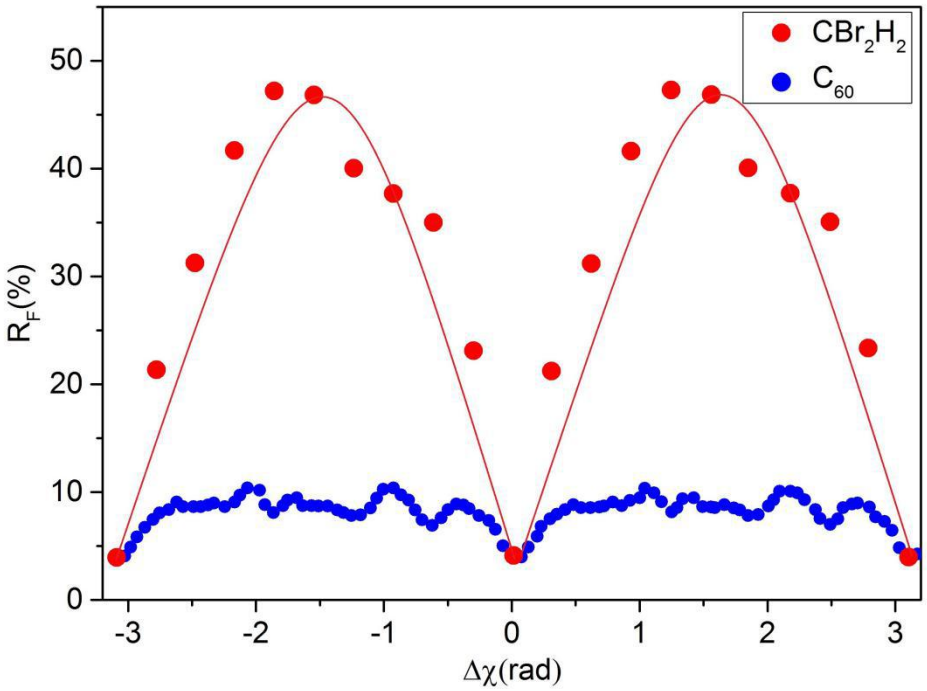

Fig. 5.8. The crystallographic agreement factor, R_F, as a function of the rotation angle around the 2-fold rotation axis of C_{60} (blue dots) and of CBr_2H_2 (red dots). A clear optimal orientation can be observed around the 2-fold rotation axes, which is more strongly pronounced for CBr_2H_2. The angular dependence exhibits the expected pi-periodicity, however, due to the more complex structure of C_{60} and its 3-fold and 5-fold rotation axes, additional local minima are present.

Rotating the two molecules each around their individual 2-fold rotation axes corresponding to the angle χ for both molecules exhibits a strong influence on the agreement factor, in particular for dibromomethane, however also C_{60} has a clear single minimum within one π periodicity (see Fig. 5.8). The results confirm the orientational order of dibromomethane with the same alignment of its rotation axis in relation to the monoclinic cell. A dynamic rotation of the CBr_2H_2 molecule around its 2-fold axis can be ruled out due to the very strong dependence of the angle χ on R_F (see Fig. 5.8), which demonstrates that the molecule must

have a fixed orientation, i.e. with the Br ligands pointing towards the longer diagonal of the *a*-*c* plane (see Fig. 5.9). The final structural parameters obtained from the last refinement were virtually the same as those obtained by means of the Materials Studio package. In the case of C_{60} the results are not as clear-cut as for CBr_2H_2, but the difference between the global minimum and the local minima is convincing enough to expect C_{60} to be mainly stuck in a single orientation, even if a stepwise arrested rotation cannot be excluded due to the many local minima.

Both Rietveld refinements reveal that the C_{60} and CBr_2H_2 molecules are orientationally ordered in the solvate structure. This structure is characterized by alternating planes consisting of either C_{60} or guest molecules stacked along the *c* axis (Fig. 5.9). The CBr_2H_2 molecule is located at [0, 0.2710(2), 0.5] in the unit cell, while the position [0, 1/3, 1/2] corresponds to the prismatic void [1/3, 2/3, 1/2] of the hexagonal parent structure of C_{60} with space group P6/mmm. In fact, the monoclinic *b* axis in the C-centered cell is approximately $2\cdot\cos(30^\circ)$ times the hexagonal *a* axis. Therefore, due to the identical packing and void filling, the structure of $C_{60}\cdot 2CBr_2H_2$ can be regarded as a distorted hexagonal one.

This is quite unusual, because in general in solvates with small halogen-methane or -ethane derivatives, the C_{60} molecules, and often the solvent molecules too, are found to exhibit an orientational disorder. For example, in the previous chapters solvent molecules possessing C_{2v} symmetry, such as CBr_2Cl_2 or $CBr_2(CH_3)_2$, were found to be orientationally disordered in solvates with a hexagonal structure.

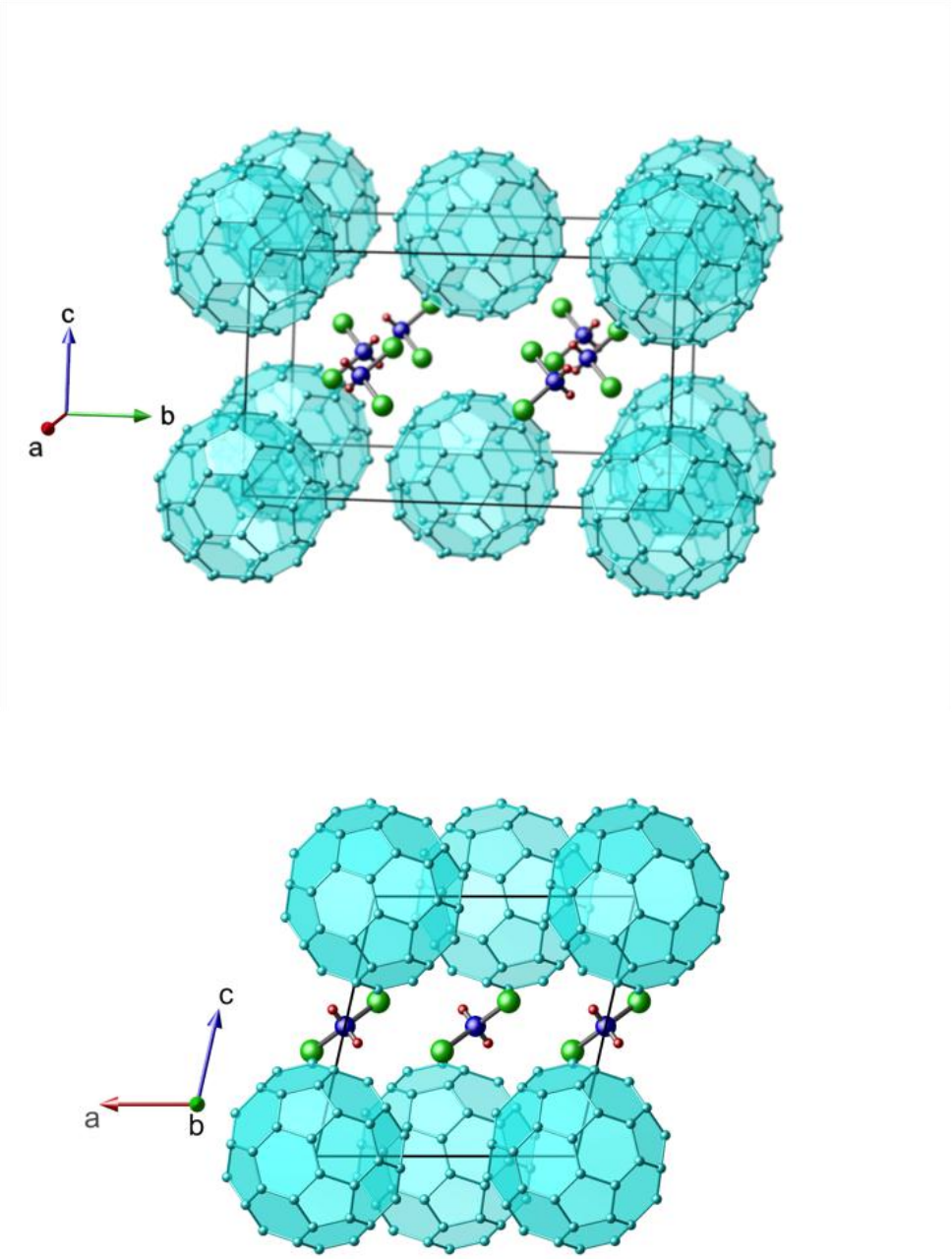

Fig. 5.9. The molecular positions in the crystal structure of $C_{60}{\cdot}2CBr_2H_2$ approximately along the [100] direction (left panel) and along the [010] direction (right panel)

The overall orientational order in the CBr_2H_2 solvate cannot be explained by the dipole moment of the solvent of 1.51 D, because $CBr_2(CH_3)_2$ possesses a similar value of 1.64 D in contrast to that of Br_2CCl_2 of 0.2 D, which both exhibit orientational disorder in their respective solvates. To take a closer look at the host-guest interactions, excess volumes can be studied. Such volumes are defined as the difference between the measured volume of a solvate (defined as $V_{unit\ cell}/Z$, i.e. 1701.5/2 = 850.75 Å^3) and the sum of the molecular volumes of the C_{60} and solvent molecules from their respective pure structures. For C_{60}, the molecular volume is 710 Å^3 from its FCC structure and the molecular volume of CBr_2H_2 was determined as 95.175 Å^3 from the structure by Kawaguchi et al. [2]. Accordingly, the excess volume is found to be negative: 850.75 - (710 ＋ 2 × 95.175) = -49.6 Å^3, which is relatively high and demonstrates the strong interaction between the C_{60} and solvent molecules.

From a crystallographic standpoint, a high negative excess volume is consistent with the solvate's stability. From a thermodynamic standpoint, this stability must be correlated with a high desolvation enthalpy. The desolvation process, which can be written as:

$$C_{60}\cdot 2CBr_2H_2\ (s) \rightarrow C_{60}\ (s) + 2CBr_2H_2\ (g) \qquad (1)$$

Occurs in two steps as demonstrated by DSC as well as thermogravimetry by peaks **a** and **b** in Fig. 5.4. The enthalpy change of the process is found to be 103 J/g of the solvate (110.0 kJ/mol of solvate) or 316 J/g of solvent (54.9 kJ/mol of solvent) by summing over peaks **a** and **b** as a whole. The total enthalpy is higher than the sublimation enthalpy of CBr_2H_2 of 46.2 kJ/mol (obtained by adding the melting enthalpy, 9.2 kJ/mol, and the vaporization enthalpy, 37 kJ/mol [5]). It implies that CBr_2H_2 and C_{60} attract each other relatively strongly in the $C_{60}\cdot 2CBr_2H_2$ solvate. The TG-curve indicates that the first peak is accompanied by a weight loss of 16.3 % of the initial mass. This corresponds to the loss of about one of the two moles of CBr_2H_2 from the solvate $C_{60}\cdot 2CBr_2H_2$ as 0.163 × 1068.31 g/mol = 174.1 g/mol, which is very close to the molar mass of the solvent of 173.8 g/mol.

The bimodal thermal effect associated with the desolvation process was not caused by the formation of a second solvate as demonstrated by the X-ray experiments as a function of the temperature in Fig. 5.6, because impure FCC C_{60} is observed in the temperature range related

to peak **b** and no additional peaks of a possible new solvate have been observed. Because the desolvation process must occur first, the second step will be vaporization of the released solvent. Thus, after the desolvation process, CBr_2H_2 may first liquefy and remain temporarily adsorbed to the C_{60} followed by evaporation. This can be summarized in the following two steps:

$$C_{60}\cdot 2CBr_2H_2\,(s) \rightarrow C_{60}\,(FCC) + 2CBr_2H_2\,(l,\ adsorbed) \quad (2)$$

$$C_{60}\,(FCC) + 2\ CBr_2H_2\,(l,\ adsorbed) \rightarrow C_{60}\,(FCC) + 2CBr_2H_2\,(g) \quad (3)$$

Peak **a**, which has an enthalpy change of 73.9 J/g (78.95 kJ/mol) of initial solvate, consists of the complete destruction of the solvate network, step (2), and the evaporation of about 1 mol of solvent, half the step (3). Thus, the enthalpy change related to step (2) is found by subtracting the vaporization enthalpy of one mole of solvent (i.e. step 3) from 78.95 kJ/mol of initial solvate. This leads to $\Delta H(2) = 41.95$ kJ/mol of initial solvate. The enthalpy change related to peak **b** (29.1 J/g of initial solvate) belongs to 83.7 % of the remaining sample, which coincidentally has a 1:1 mol ratio (one mole of solvent per mole of C_{60}). The enthalpy can, therefore, be expressed as 34.77 J/g of remaining sample or as 31 kJ/mol of desorbing and evaporating solvent. This value is of the same order as the enthalpy needed to desorb similar organic solvents from graphitized thermal carbon [11].

5.4 Conclusions

The monoclinic solvate $C_{60}\cdot 2CBr_2H_2$, which is stable in air, has been structurally and thermodynamically characterized. The C_{60} molecules possess a hexagonal base structure, which is deformed and become monoclinic due to the presence of solvent molecules. Notwithstanding the similarity of CBr_2H_2 with other solvent molecules that form C_{60} hexagonal solvates, in particular, those with the same C_{2v} molecular symmetry as CBr_2Cl_2 and $CBr_2(CH_3)_2$, the CBr_2H_2 solvate exhibits overall orientational order for both the C_{60} and the CBr_2H_2 molecules, rarely seen in the other solvates. The orientational order is consistent with the solvate's stability, which has a high negative excess volume and a high desolvation

enthalpy. All these physical properties demonstrate the strong host-guest interactions. Although the correct space group symmetry of the solvate is monoclinic (C2/m), the overall packing is very similar to the hexagonal packing found in many other solvates.

5.5 References

[1] M. Podsiadlo, K. Dziubek, M. Szafranski and A. Katrusiak, Molecular interactions in crystalline dibromomethane and diiodomethane, and the stabilities of their high-pressure and low-temperature phases, Acta Crystallographica Section B, 62, 2006, 1090.

[2] T. Kawaguchi, M. Hijikigawa, Y. Hayafuji, M. Ikeda, R. Fukushima, and Y. Tomiie, The Crystal Structures of Methyl Bromide and Methyl Iodide, Bulletin of the Chemical Society of Japan, 46,1973, 53.

[3] B. H. Torrie, O. S. Binbrek, I. P. Swainson, and B. M. Powell, Crystal structures of dibromochloromethane and bromodichloromethane, Molecular Physics, 97, 1997, 581.

[4] C. L. Yaws, Thermophysical Properties of Chemicals and Hydrocarbons, 2nd Edition, 2014, 638.

[5] W. Acree. Jr, J. S. Chickos, Phase Transition Enthalpy Measurements of Organic and Organometallic Compounds. Sublimation, Vaporization and Fusion Enthalpies From 1880 to 2010, Journal of Physical and Chemical Reference Data, 39, 2010, 043101.

[6] S. Toscani, H. Allouchi, J. Ll. Tamarit, D. O. López, M. Barrio, V. Agafonov, A. Rassat, H. Szwarc, R. Céolin, Decagonal C_{60} crystals grown from n-hexane solutions: solid-state and aging studies, Chemical Physics Letters, 330, 2000, 491.

[7] P. Espeau, M. Barrio, D. O. López, J. Ll. Tamarit, R. Céolin, H. Allouchi, V. Agafonov, F. Masin, H. Szwarc, Phase Equilibria in the C_{60}+Ferrocene System and Solid-State Studies of the C_{60}:2Ferrocene Solvate, Chemistry of Materials, 14, 2002, 321.

[8] M. Barrio, D. O. López, J. Ll. Tamarit, P. Espeau, R. Céolin, Solid-State Studies of C_{60} Solvates Formed in the C_{60}-$BrCCl_3$ System, Chemistry of Materials, 15, 2003, 288.

[9] G. B. M. Vaughan, Y. Chabre, D. Dubois, Effect of stacking disorder on the orientational ordering transition of solid C_{60}, Europhysics Letters, 31, 1995, 525.

[10] W. A. Dollase, Correction of intensities for preferred orientation in powder diffractometry: application of the March model, Journal of Applied Crystallography, 19, 1986, 267.

[11] N. N. Avgul, A. V. Kiselev, in Chemistry and Physics of Carbon, edited by P. L. Walker, Jr. (Dekker, New York) 6, 1970, 39.

6. The C_{60}:$CBrCl_2H$ binary system

6.1 The solvent: Bromodichloromethane

Bromodichloromethane ($CBrCl_2H$) is a colorless halogenated hydrocarbon with density 1.98 g/mL at room temperature. The sample was purchased from Aldrich, with 98% of purity and used without further purification. The liquid crystallizes in a triclinic structure with P $\bar{1}$ symmetry [1,2] with a volume of 112.11 $Å^3$ per molecular unit at 200K. The compound melts (Fig. 6.1), at 215.9 K, with an enthalpy change of ΔH = 9.5 kJ/mol (57.8 J/g). The liquid phase remains until the boiling point at 363.15 K, being the variation of enthalpy associated with this transformation ΔH = 30.9 kJ/mol, (188.4 J/g) [3].

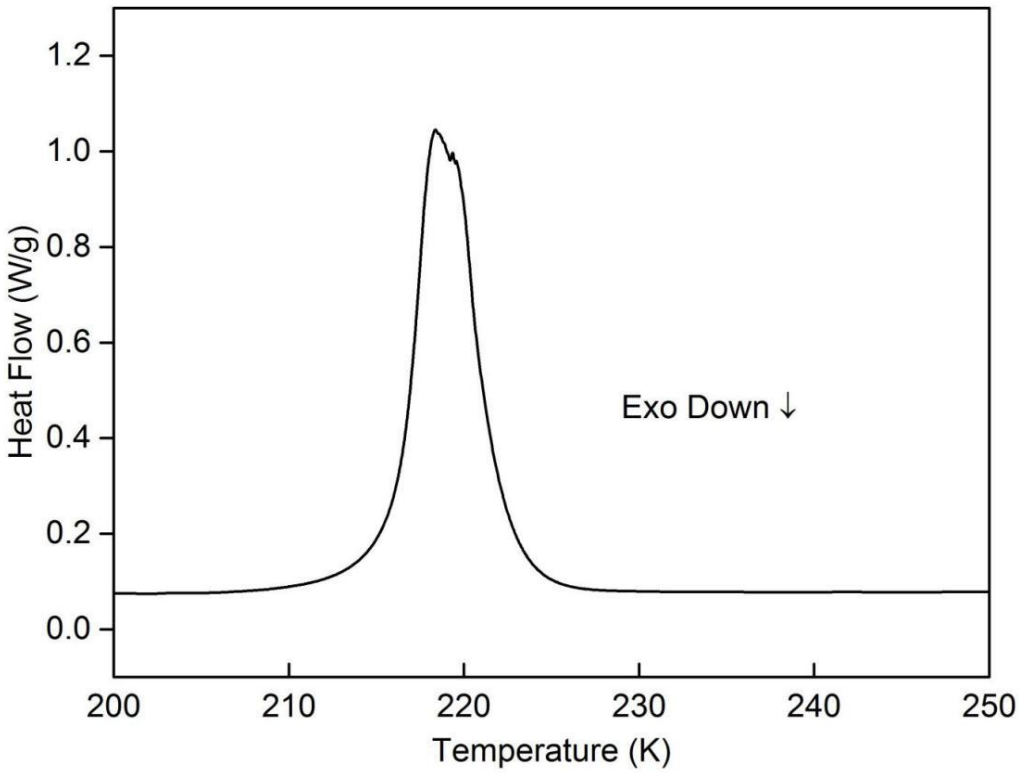

Fig. 6.1. DSC curve showing the melting of solvent $CBrCl_2H$.

6.2 Study of the C_{60}:$CBrCl_2H$ solvates

As usual FCC C_{60} and the solvent were mixed in screw cap tubes. In a short time, a couple of days, the solution gets a grey color, and the solvate crystals could be observed on the surface of the liquid.

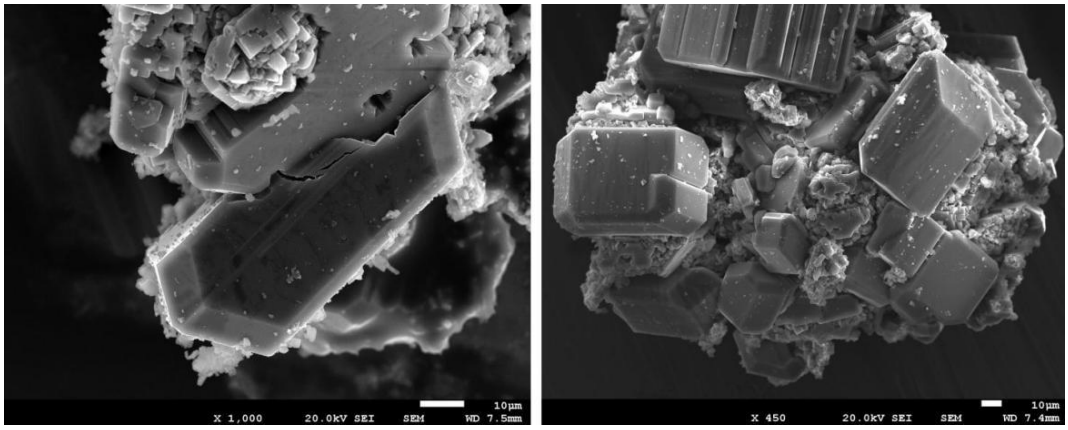

Fig. 6.2. Scanning electron microscopy (SEM) photograph of C_{60}:$CBrCl_2H$ crystals.

The morphology of the crystals was examined by means of scanning electron microscopy at room temperature. The photograph of the crystals (Fig. 6.2) shows crystallized hierarchical architecture composed of irregular microprisms. The crystals no longer exhibited the usual morphologies of FCC C_{60} crystals, and only hexagonal-shaped crystals were observed.

The hexagonal crystals were picked as soon as extracted from the mother liquor, and introduced into a Lindemann capillary, that remained open allowing a slow evaporation of the liquid. The so-obtained crystals were maintained at room temperature and the evolution of the profile was recorded as a function of time (Fig. 6.3). Despite the slight degeneration of the original spectrum, some widening of the bases of the peaks occurs, the characteristic spectrum of degenerate FCC C_{60} not appeared, so indicating that the solvate can remain stable out of the liquid.

The experimental profile was indexed by the DICVOL program. The best figure of merit was obtained for a hexagonal lattice with parameters a = 10.131 Å, c = 10.141 Å, V = 901.33 $Å^3$.

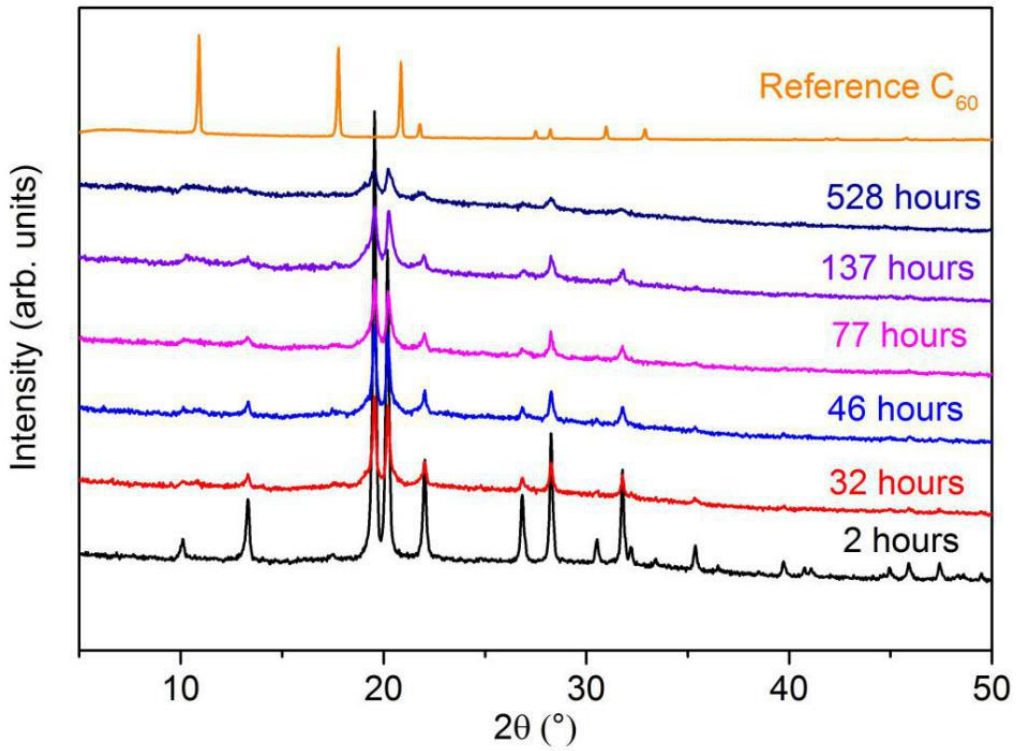

Fig. 6.3. X-ray diffraction profiles recovered at room temperature after 2 hours, 32 hours, 46 hours, 77 hours, 137 hours and 528 hours. The range between 50 and 115° is not shown due to the absence of Bragg peaks with significant intensity. Acquisition times of 7000 s were used for all the measurements. In addition, the pattern of FCC C_{60} is provided on top as a reference.

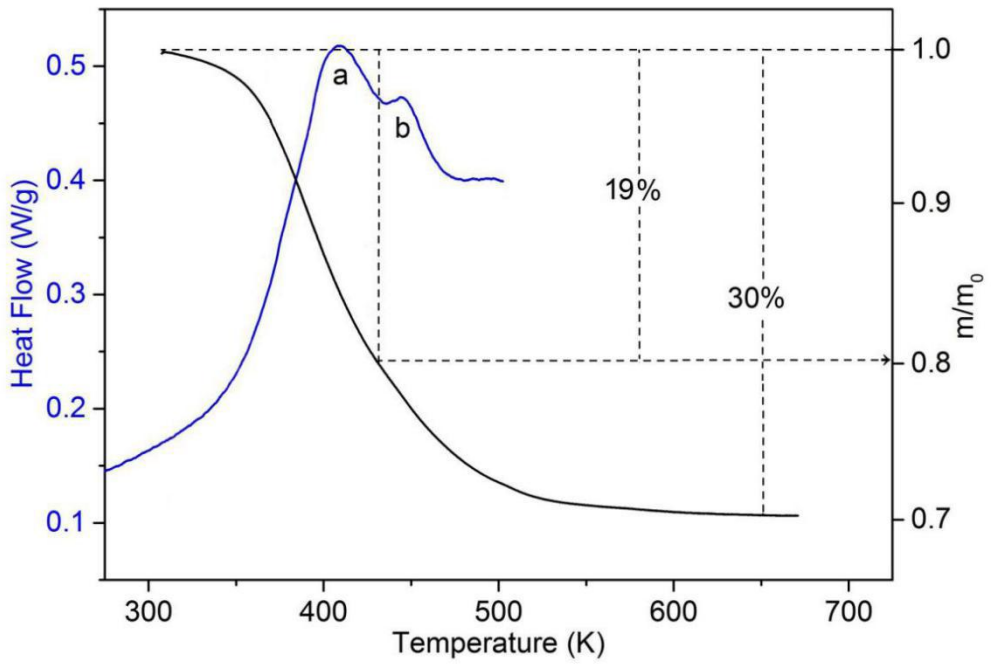

Fig. 6.4. Thermogravimetric (right axis) and DSC (left axis) curves for the C_{60}·2$CBrCl_2H$ solvate, in an open pan after the mother liquor has evaporated. The dashed black arrow indicates the mass loss for the first peak.

The stoichiometry of the solvate was determined by measuring the mass loss of the crystals, as extracted from the mother liquor, after complete evaporation of the excess of mother liquor. At this point, the sample is assumed to be free of mother liquid and was heated in the temperature range of 323 to 670 K in the TGA device (Fig. 6.4). The measured mass loss exhibits two steps over the whole temperature interval. The final mass loss around 30% is closed to the theoretical value 31% for the desolvation process C_{60}·2$CBrCl_2H$ (solid) → C_{60} (solid) + 2$CBrCl_2H$ (vapor).

For the whole measurements performed, the TGA curves show a weak inflection with a loss of mass around 19%. This value is slightly higher than the 16% that would correspond to the transformation C_{60}·2$CBrCl_2H$ (solid) → C_{60}·$CBrCl_2H$ (solid) + $CBrCl_2H$ (vapor). On the

other hand, the inflexion could be related to a phenomenon of desorption as it happened in the case of the $C_{60}\cdot 2CBr_2H_2$ (ChapterV). Anyway, the DSC measurements (Fig. 6.5) performed in open pans following the same procedure that the TGA measurements reveal two thermal effects convoluted as an endothermic peak at 350 K.

The desolvation enthalpy from DSC measurements in open pans is found to be ΔH = 68.27 J/g of the hexagonal solvate, i.e. 218.3 J/g of solvent or 35.8 kJ/mol of solvent. It follows that the desolvation enthalpy is slightly smaller than the sublimation enthalpy of $CBrCl_2H$, 40.4 kJ/mol (by adding the melting enthalpy, 9.5 kJ/mol, and the vaporization enthalpy, 30.9 kJ/mol). This indicates that solvation occurs with no apparent extra-interaction between the C_{60} and solvent molecules in the solvate lattice [4,5].

To investigate the two convoluted peaks in the desolvation process more closely, aliquots of crystals together with the mother liquor were put in stainless steel high-pressure pans for DSC studies. The heating ramps were performed from 200 K to 450 K, but after peak **p**2 (see Fig. 6.5) the base line was plenty of spurious signals probably related with the vaporization of the mother liquor.

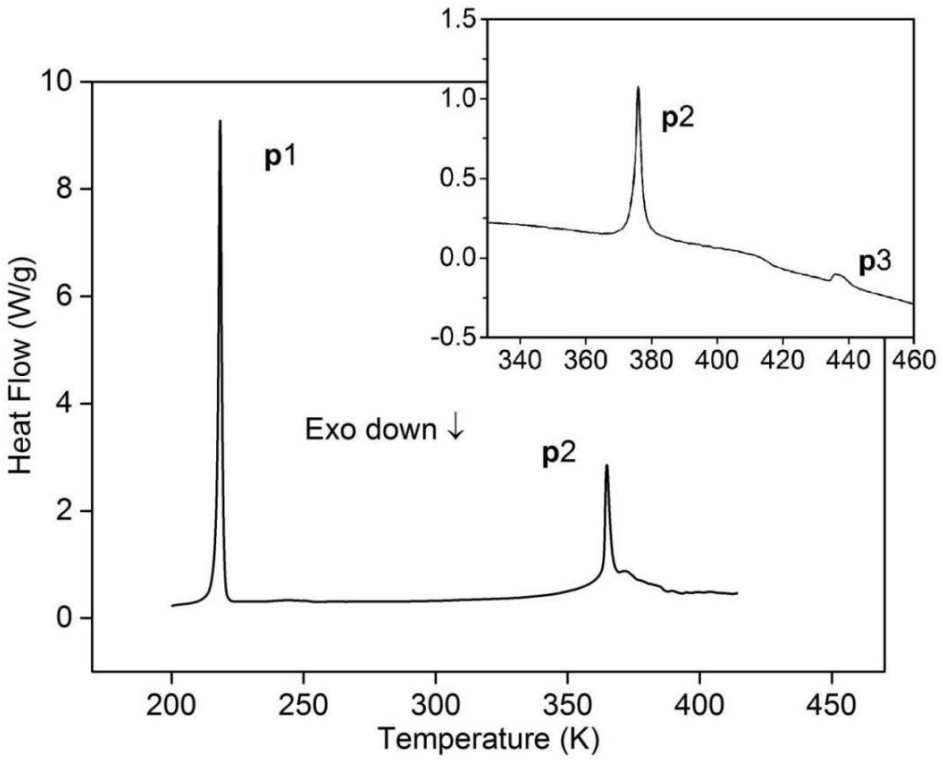

Fig. 6.5. DSC curves obtained in a sealed pan of C_{60}·2$CBrCl_2H$ solvate with an excess of mother liquid.

To elucidate if the signals were related with the liquid, samples without liquid were heated from 300 K to 460 K (inset Fig. 6.5). This signal reveals that the thermal effect that starts at 372 K is not finished until 410 K, the temperature at which the base line is recovered. At higher temperature, around 430 K, a new signal emerges.

Therefore the first endothermic effects **p**1 observed in Fig. 6.5 at 216 K corresponding to the melting of the crystalline $CBrCl_2H$, whereas peaks **p**2 at 373 K and **p**3 at 430 K correspond, as demonstrated by the next X-ray and TGA measurement, to the peritectic invariants (C_{60}·2$CBrCl_2H$ + C_{60}·$CBrCl_2H$ + liquid) and (C_{60}·$CBrCl_2H$ + liquid + C_{60}), respectively.

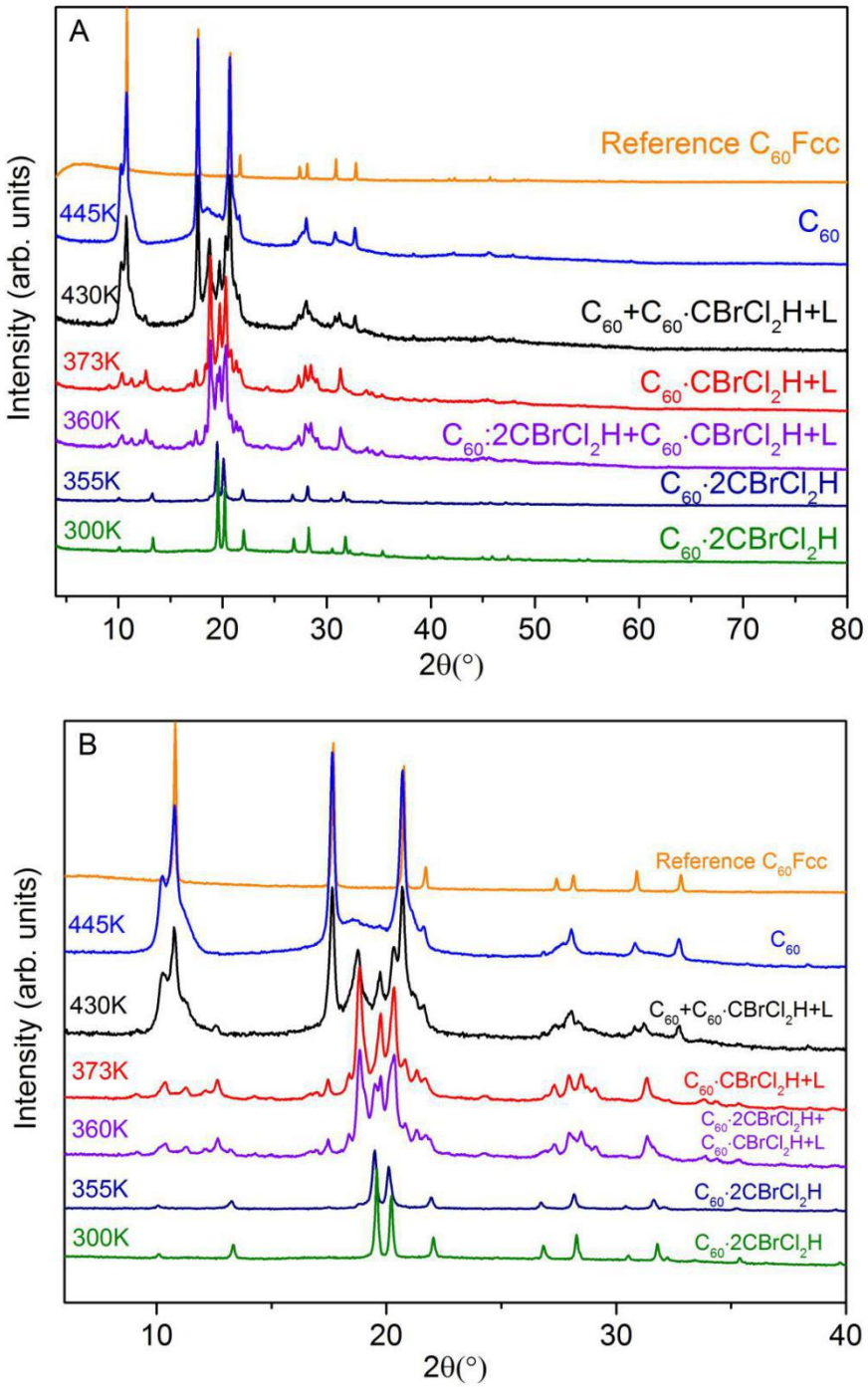

Fig. 6.6. Series of X-ray profiles of the C_{60}·$2CBrCl_2H$ solvate in mother liquor in a closed capillary as a function of the temperature (A).The experimental profile of C_{60} FCC phase has

been represented on top for comparison. B: Enlargements of low angle parts of the XRPD profiles.

Fig. 6.6 shows several X-ray patterns of co-crystals C_{60}·2$CBrCl_2H$ between 300-445 K. The profile evolution reveals that in the temperature range from room temperature to 360 K the pattern is the one corresponding to the hexagonal solvate C_{60}·2$CBrCl_2H$. At 360 K new reflections coexist with those corresponding to the hexagonal solvate that is the only ones remaining at 373 K. The new spectrum remains up to 430 K at which the FCC C_{60} reflections appeared. Then the DSC signals **p**2 and **p**3 in Fig. 6.5 must be related to these changes. To establish if the change at 360 K is related with a solid-solid transition in the hexagonal solvate or if it is related with a transformation to another solvate, samples of the hexagonal co-crystal without liquid were heated up to 400 K and subsequently cooled to room temperature. The recovered spectrum was the same as that obtained at high temperature. The corresponding lattice parameters and symmetry will be introduced in the next section. This result allows concluding the existence of another solvate of lower stoichiometry.

To obtain with a better accuracy the stoichiometry of the new solvate, samples previously heated up to 400 K were submitted at TGA and DSC measurements in open pans. The results are shown in the Fig. 6.7.

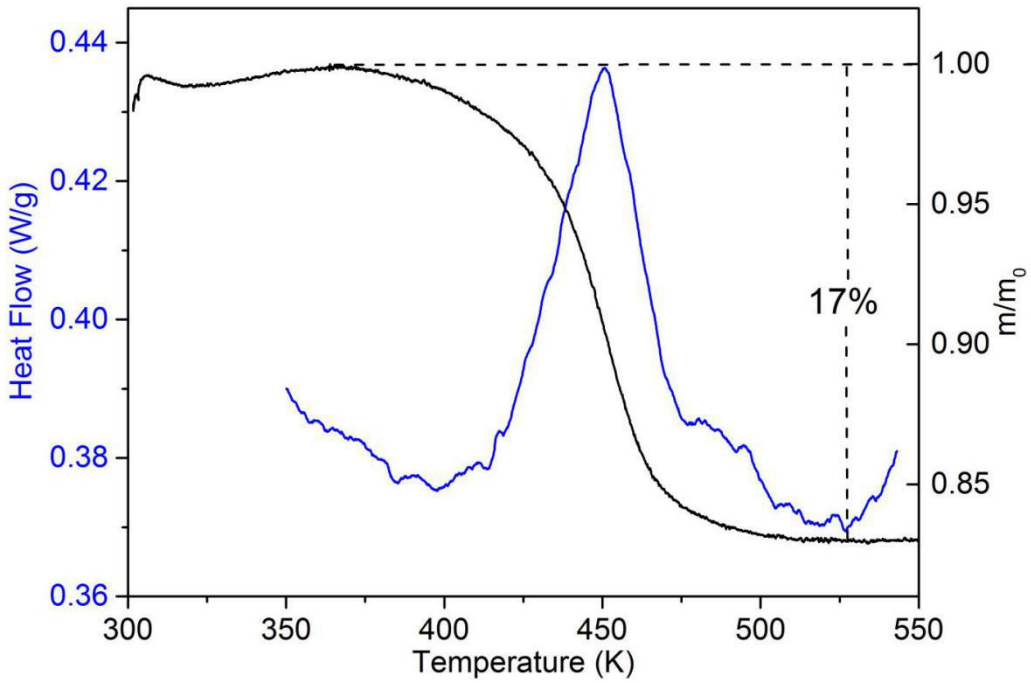

Fig. 6.7. Thermogravimetry and Differential scanning calorimetry curves as a function of temperature for the C_{60}·$CBrCl_2H$ solvate.

The mass loss is found to be 17% i.e very close to the expected value of 18.6% for the C_{60}:$CBrCl_2H$ (1:1) molar ratio. By Comparing the DSC signal with that shown in Fig. 6.4, it can be observed that the new one appears in the same temperature range that the peak **b**. The better determination of the new signal allows obtaining a more accurate value for the desolvation enthalpy of the C_{60}·$CBrCl_2H$ solvate. This value is found to be 21.2 J/g of solvate i.e 114.4 J/g of solvent or 18.74 kJ/mol of the solvent. This value is lower that the sublimation enthalpy of $CBrCl_2H$ (40.4 kJ/mol).

6.3 Discussion and structural characterization

From the previous results, the existence of two solvates between C_{60} and the $CBrCl_2H$ solvate has been proved. The hexagonal solvate $C_{60}{\cdot}2CBrCl_2H$ was grown at room temperature in a saturated solution of FCC C_{60} whereas that the $C_{60}{\cdot}CBrCl_2H$ was obtained by heating to 400 K of the hexagonal solvate. Although both solvates can remain in the air, a greater trend to form the cubic C_{60} has been observed in the $C_{60}{\cdot}CBrCl_2H$ solvate. This fact is consistent with the difference between the desolvation enthalpies, 35.8 and 18.74 kJ/mol of solvent obtained for $C_{60}{\cdot}2CBrCl_2H$ and $C_{60}{\cdot}CBrCl_2H$, respectively. Moreover, the desolvation enthalpy of the $C_{60}{\cdot}CBrCl_2H$ solvate is lower than the sublimation enthalpy of the solvent (40.4 kJ/mol), a fact that would imply weak attraction between C_{60} and $CBrCl_2H$ molecules.

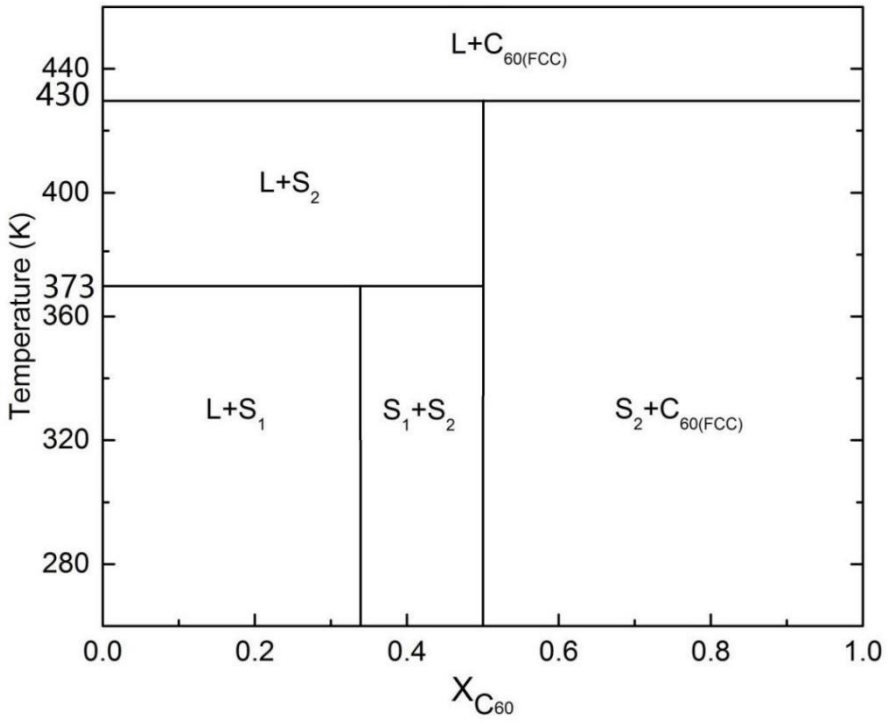

Fig. 6.8. C_{60}:$CBrCl_2H$ phase diagram. S_1 and S_2 are co-crystals $C_{60}{\cdot}2CBrCl_2H$ and $C_{60}{\cdot}CBrCl_2H$, respectively.

From the DSC and X-ray results, the transformations involving every solvate have been established, which allows to build up the binary phase diagram in Fig. 6.8. This illustrates the existence of the two co-crystals at mole fractions X = 0.33 (S_1 = C_{60}·2$CBrCl_2H$) and X = 0.5 (S_2 = C_{60}·$CBrCl_2H$) and accordingly two peritectic invariants. The invariant (C_{60}·2$CBrCl_2H$ + C_{60}·$CBrCl_2H$ + liquid) at 370.3 K (**p**2 signal in Fig. 6.5) with an enthalpy value at the peritectic point of 19.13 J/g of the hexagonal solvate. The invariant (C_{60}·$CBrCl_2H$ + liquid + C_{60}), at around 430 K correspond to the peritectic melting of C_{60}·$CBrCl_2H$.

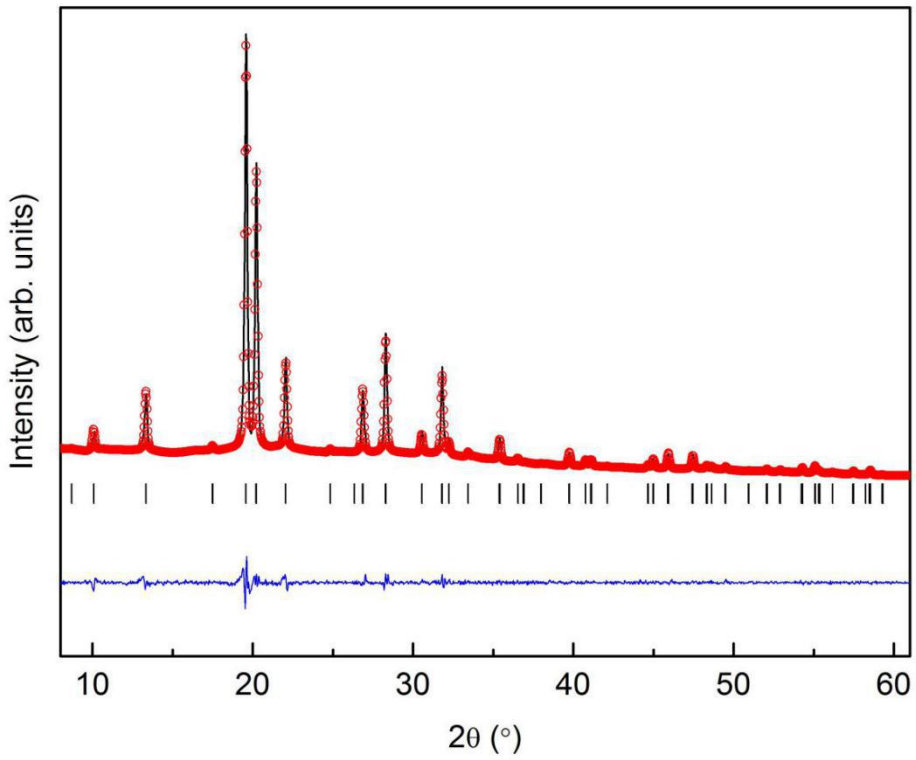

Fig. 6.9. Experimental (points) and simulated (line) X-ray diffraction Patterns together with the difference profile (bottom line) and Bragg reflections (vertical sticks) of P6/mmm hexagonal solvate.

The experimental X-ray pattern of $C_{60}\cdot 2CBrCl_2H$ measured at room temperature is depicted in Fig. 6.9. A Pattern Matching procedure allows us to refine the hexagonal parameters that were used as a starting point for a Rietveld refinement performed by means the Full Prof suite.

The C_{60} molecule was modeled with spherical harmonics describing a homogeneous distribution of 60 C-atoms positioned on a sphere with an overall radius of 3.59 Å. The solvent molecule $CBrCl_2H$ has been described as a rigid body assuming halogen disorder with every site occupied on average by 2/3Cl:1/3Br.This kind of disorder leads to the average C_{3v} symmetry of the $CBrCl_2H$ molecule. The distances and angles involved in the molecule were taken from reference [6]. An overall isotropic temperature factor has been refined for all involved atoms and the background has been described by a linear interpolation. The result of the refinement provides agreement factors of $\chi^2 = 2.09$. The final refined results yielded: Hexagonal, P6/mmm, a = 10.131(2) Å, c = 10.135(2) Å, V = 900.7(6) $Å^3$. The C-atom of a solvent molecule is located in a general position with refined position (0.349(4),0.719(3),0.483(6)) near to the prismatic hexagonal void (1/3,2/3,1/2). The refinement results are depicted in Fig. 6.9, together with the experimental pattern and the difference between the refined pattern and the experimental one. The values of the final Rietveld refinement are summarized in Table. 6.1.

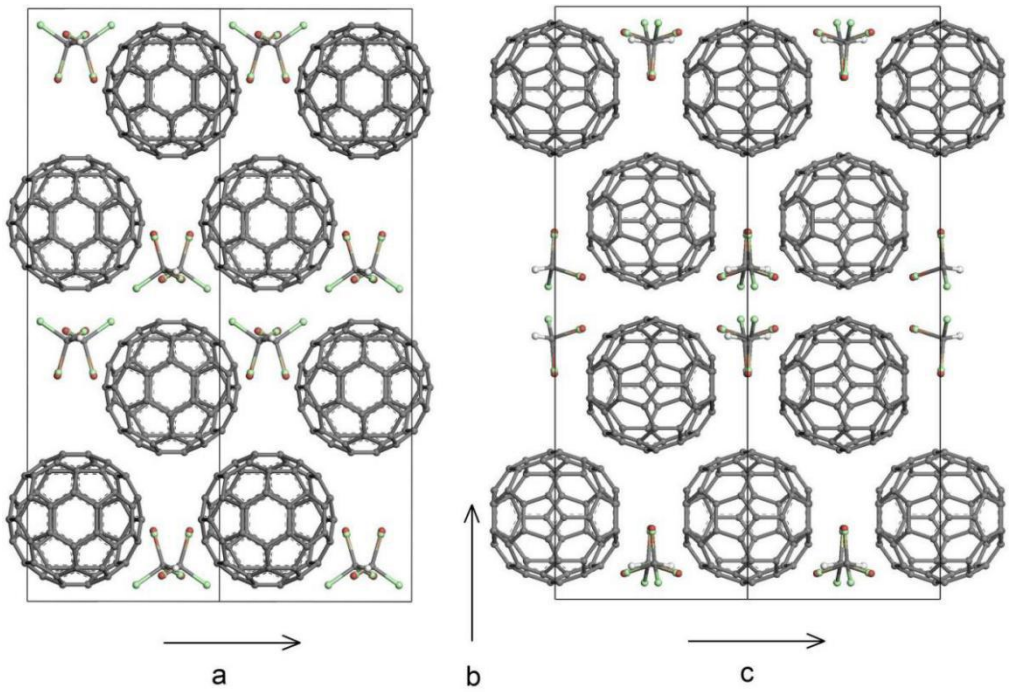

Fig. 6.10. Crystal structure of C_{60}·$CBrCl_2H$ in (001) plane (left panel) and (100) plane (right panel).

For the C_{60}·$CBrCl_2H$ solvate, several monoclinic solutions with lattice volumes around 1500 and 3500 Å were obtained from DICVOL. Assuming the density values obtained for another solvate the corresponding Z values for the former lattices would be 2 and 4, respectively. The similarity between the pattern obtained for this solvate and that corresponding to the co-crystal C_{60}:1,1,2 Trichoroethane [7] decided us for the higher volume option.

Systematic absences for the space group assessment were compatible with the centered monoclinic space group C2/c. The Rietveld refinement was performed with the Materials Studio Program. For the structure determination, atoms coordinates of the C_{60} molecule and $CBrCl_2H$ were taken from the literature and fitted in the obtained diffraction pattern. The C_{60} molecules are orientationally ordered whereas that for the $CBrCl_2H$ are disordered, resulting in average Cs molecular symmetry with site occupancies for the halogen atoms, 1/2 Cl:1/2 Br,

1/2 Cl:1/2 Br, 1 Cl. For the center of mass of C_{60} located in the 4e site (Wyckoff notation) the refined position was (0, 0.13823(25), 0.25). The $CBrCl_2H$ molecule was located in an 8f symmetry point (Wyckoff notation), that implies that the asymmetric unit must be a half-molecule by density requirements. The final refined position for the central carbon atom is (0.483(2), 0.001(4), 0.708(2)). In both kind of molecules, a single overall isotropic displacement parameter was refined and the preferred orientation was modeled using the March-Dollarse function [8]. The molecular arrangement of the motifs is shown Fig. 6.10, and the Rietveld refinement results are depicted in Fig. 6.11, together with the experimental pattern and the difference between the refined pattern and the experimental one. The values of the final refinements are summarized in Table. 6.1.

Table. 6.1. Structure information and Rietveld refinement results for the $C_{60}\cdot 2CBrCl_2H$ and $C_{60}\cdot CBrCl_2H$ solvates

Chemical Formula	$C_{60}\cdot 2CBrClH_2$ (LT)	$C_{60}\cdot 2CBrClH_2$ (HT)
M /g·mol^{-1}	1048	884
2 -Angular Range	5-65°	5-65°
Space group	P 6/mmm	C2/c
a/Å	10.131(2)	10.140(3)
b/Å	10.131(2)	31.233(9)
c/Å	10.135(2)	10.122(3)
α/º	90	90
β/º	120	90.214(2)
γ/º	90	90
V/Å^3	900.7(6)	3205.6(4)
Z	1	4
Temperature	300 K	300 K
Wavelength (CuKα1)	λ = 1.5406 Å	
2 -shift (zero correction)	- 0.025(5)	0.028(6)
Reliability Parameters		
R_{wp}	3.72%	4.80%
R_p	5.07%	3.74%
Peak width parameters	U = 0.153 V = -0.100 W = 0.047	U = 12.407 V = -5.777 W = 0.707

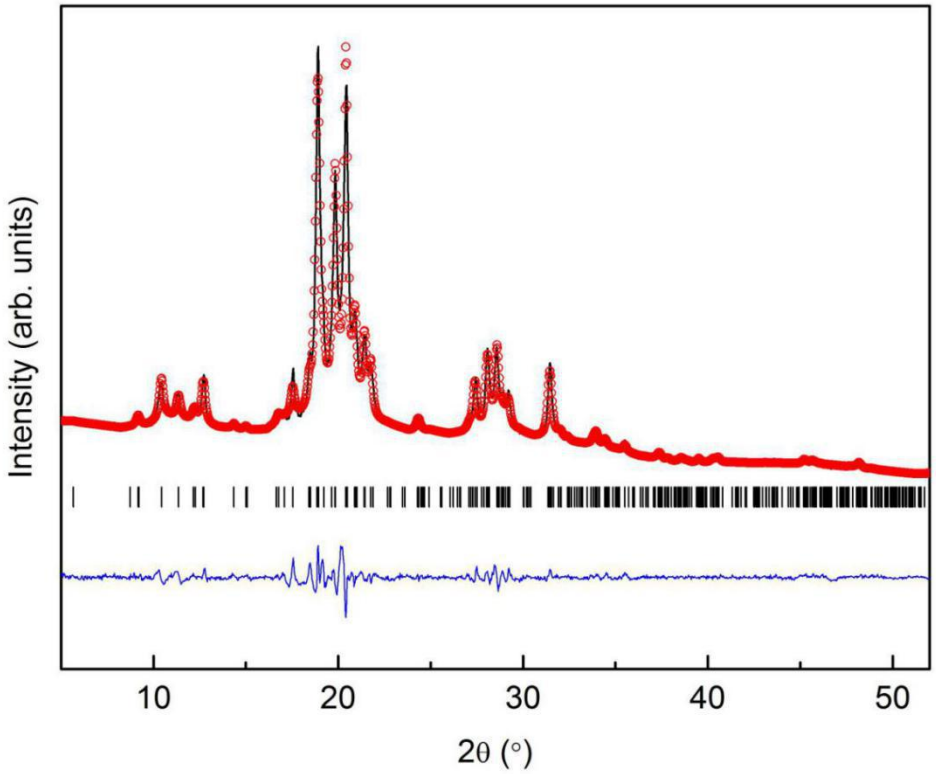

Fig. 6.11: Experimental (**points**) and simulated (**line**) X-ray diffraction Patterns together with the difference profile (**bottom line**) and Bragg reflections (**vertical sticks**) of the monoclinicC2/c space-group of C_{60}·$CBrCl_2H$ solvate.

To compare the intermolecular interaction in both solvates the excess volumes were calculated. The volume available for one molecule in the hexagonal and monoclinic solvates, V/Z = 900.7 Å^3/molecule and 801.4 Å^3/molecule, are quite similar. Considering the value of 710 Å^3/molecule from the FCC phase of C_{60} and the value of 112.11 Å^3/molecule from the triclinic phase of $CBrCl_2H$ at 200 K [1], the resulting excess volumes were -33.5 and -20.7 Å^3/molecule for the hexagonal and monoclinic solvates, respectively. Negative excess volumes have usually been observed in stable solvates [9, 10] revealing strong interactions between C_{60} and the solvents molecules.

From a thermodynamic point of view, the desolvation enthalpy accounts for the interaction between the solvent molecules and C_{60}. Similarly, the sublimation enthalpy of the pure solvent accounts for the intermolecular interactions in its solid phase. Then, it would be expected desolvation enthalpy values higher than sublimation enthalpy ones when stable solvates are formed, and even more when excess volumes are clear negatives.

6.5 Conclusions

The solvate $C_{60}\cdot 2CBrCl_2H$, which is stable in open air, has been thermodynamically and structurally characterized. As revealed by X-ray diffraction the solvate possesses the Hexagonal symmetry, space group P6/mmm, and is formed with a negative excess volume (-3.7%). This solvate undergoes a transformation to another solvate of lower stoichiometry $C_{60}\cdot CBrCl_2H$ at around 373 K. The new solvate has a monoclinic (C2/c) structure and is also formed with a negative excess volume (-2.6%). The negative excess volumes suggest the existence of strong interactions between C_{60} and the solvents. Paradoxically the measured desolvation enthalpies for both $C_{60}\cdot 2CBrCl_2H$ and $C_{60}\cdot CBrCl_2H$ do not exceed the sublimation enthalpy of pure $CBrCl_2H$.

6.6 References

[1] K. Dziubek, M. Podsiadło, A. Katrusiak, Molecular Symmetry and Isostructural Relations in Crystal Phases of Trihalomethanes $CHCl_3$, $CHBrCl_2$, $CHBr_2Cl$, and $CHBr_3$, The Journal of Physical Chemistry B, 113, 2009, 13195.

[2] B. H. Torrie, O. S. Binbrek, I. P. Swainson, B. M. Powell, Crystal structures of dibromochloromethane and bromodichloromethane, 97, 1999, 581.

[3] C. L. Yaws, Thermophysical Properties of Chemicals and Hydrocarbons, 2nd Edition, 2014, 497.

[4] A. Bondi, Heat of Siblimation of Molecular Crystals: A Catalog of Molecular Structure Increments, Journal of Chemical & Engineering Data, 8, 1963, 371.

[5] R. Céolin, F. Michaud, S. Toscani, V. Agafonov, J. Ll. Tamarit, A. Dworkin, H. Szwarc, Crystals of C_{60} solvates. Recent advances in the chemistry and physics of fullerenes and related materials, The Electrochemical Society, Vol 5, 1997, 373.

[6] B. H. Torrie, O. S. Binbrek, I. P. Swainson, B. M. Powell, Crystal structures of dibromochloromethane and bromodichloromethane, 97, 1999, 581.

[7] E. Mitsari, M. Romanini, N. Qureshi, J. Ll. Tamarit, M. Barrio, R. Macovez, C_{60} Solvate with (1,1,2)-Trichloroethane: Dynamic Statistical Disorder and Mixed Conformation, 120, 2016, 12831.

[8] H. Toraya, F. Marumo, Preferred orientation correction in powder pattern-fitting, Mineralogical Journal, 10, 1980, 211.

[9] M. Barrio, D. O. López, J. Ll. Tamarit, P. Espeau, R. Céolin, Solid-State Studies of C_{60} Solvates Formed in the C_{60}-$BrCCl_3$ System, Chemistry of Materials, 15, 2003, 288.

[10] R. Céolin, J. Ll. Tamarit, M. Barrio, D. O. López, P. Espeau, H. Allouchi, R. J. Papoular, Solid state studies of the $C_{60}{\cdot}2(CH_3)CCl_3$ solvate, Carbon, 43, 2005, 417.

7. The C_{60}:$CBrClH_2$ binary system

7.1 The solvent: Bromochloromethane

The solvent Bromochloromethane ($CBrClH_2$), density 1.93 g/mL, crystallizes in a monoclinic phase, C2/c with V/Z = 91.16 $Å^3$/molecule at 170 K [1]. The melting point, determined in this work, is 184.4 K (see Fig. 7.1), with a change of enthalpy of ΔH = 7.38 kJ/mol (57.02 J/g). The liquid phase remains until the boiling point at 341.2 K being the enthalpy associated with this transformation ΔH = 31.12 kJ/mol (240.3 J/g) [2].

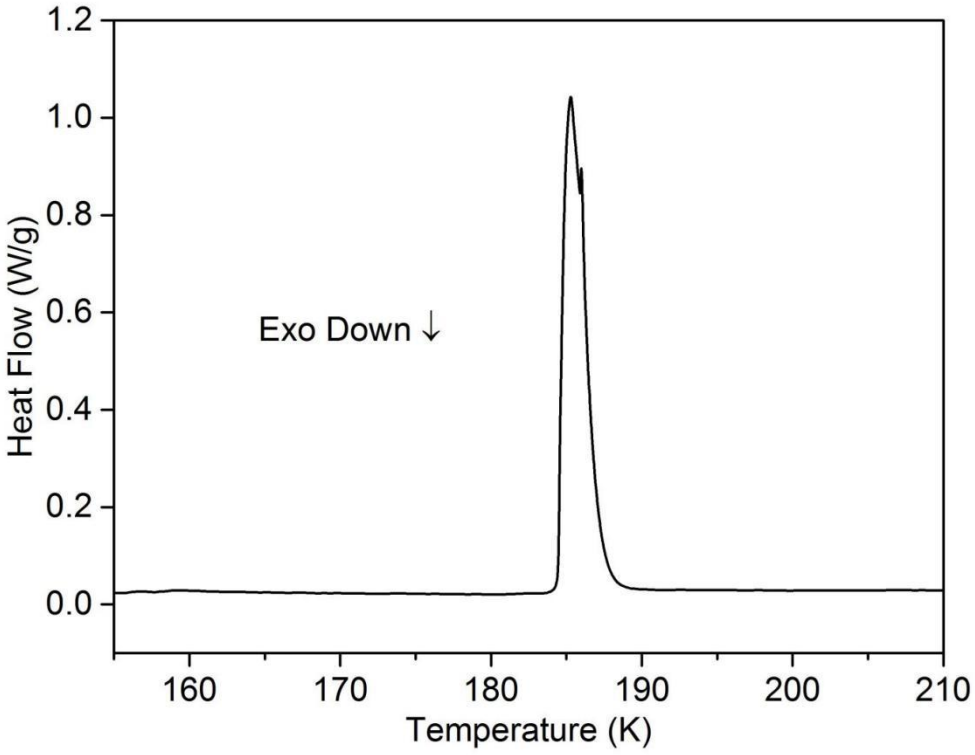

Fig. 7.1. DSC curve showing the melting of solvent $CBrClH_2$.

7.2 Study of the C_{60}:$CBrClH_2$ solvates

FCC C_{60} and Bromochloromethane solvent mixed in screw-cap tubes at room temperature in the absence of light were periodically monitored by optical microscopy. After several months, when the mixture no more exhibited the FCC C_{60} morphology, the characterization measurements were undertaken.

The stability of the mixture was tested by X-ray diffraction: The co-crystals were picked gently, extracted together with a solution and quickly introduced into a Lindemann capillary. The capillary was partially obstructed to slow solvent evaporation, by collecting the X-ray profiles as a function of time at room temperature. In Fig. 7.2 the first profile collected after 2 hours is shown. After 4 hours the original profile can be retained but some broadening of the Bragg reflections appeared. The degeneration of the spectrum can be clearly observed after 5 hours, new reflections belonging to the FCC phase (vertical dash lines) of C_{60} appear. The decrease of intensities with increasing time and peak broadening can be due to a continuous decrease of the crystallite size. From the former evolution, it must be assumed that this co-crystal is not air stable and spontaneously loses its crystallization solvent.

Taking into account the above, closed capillaries retaining a small quantity of liquid were submitted to X-ray measurements. The whole of the Bragg peaks were indexed in the monoclinic system by means the program DICVOL. The systematic absences are compatible with the space group C2/m and assuming this group a first refinement of the lattice parameters was undertaken by means Pattern Matching procedure. The resulting parameters were a = 9.924(6) Å, b = 17.422(6) Å, c = 10.066(1) Å, β = 101.96(2)º, V = 1702.6(5) $Å^3$. The $C_{60}·2CBr_2H_2$ (Chapter V) solvate crystallizes in the same lattice (monoclinic C/2m) with similar lattice parameters then both solvates are isostructural and thus the same stoichiometry would be expected for this solvate.

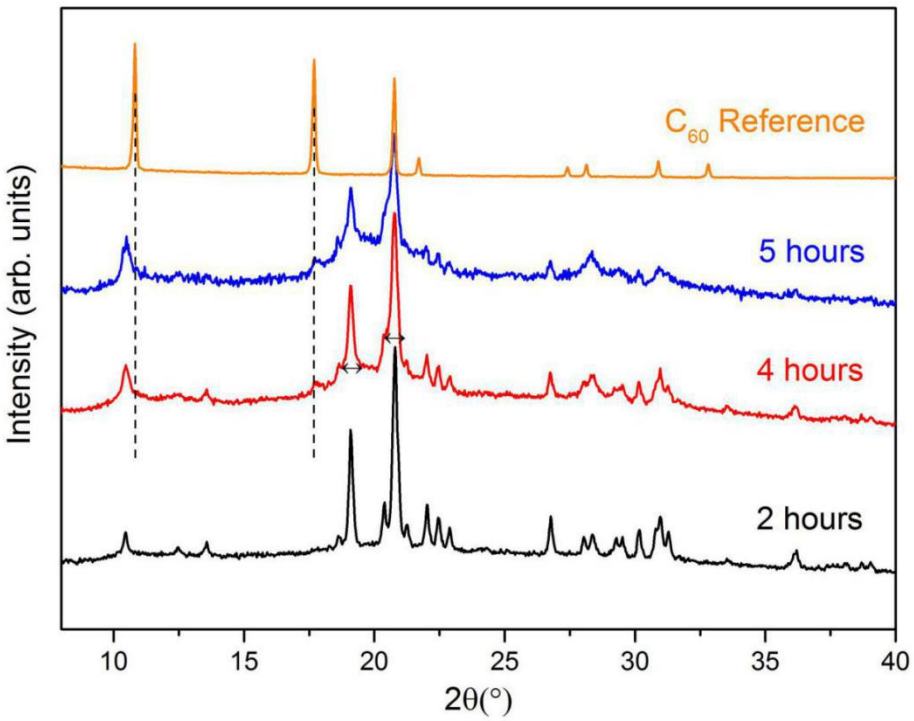

Fig. 7.2. X-ray diffraction profiles recovered at room temperature (303 K) after 2, 4 and 5 hours. The range between 40 and 115° is not shown due to the absence of Bragg peaks with significant intensity. In addition, the pattern of FCC C_{60} is provided on top as a reference.

To establish the stoichiometry of the solvate, the crystals were placed in pierced pans with an excess of mother liquid and submitted to TGA experiments. The heating process was preceded by an isothermal mass measurement at room temperature (303 K) being both processes represented in Fig. 7.3. The figure shows a very quick loss of mass finishing at point "**a**" that was assumed to be related with the complete evaporation of the liquid. This loss of mass is followed by a slower mass loss which tends to stabilize after 50 minutes. At this time the sample was heated at 5 K/min up to 550 K. The experimental loss of mass from "**a**" (see inset) was found around 26%, near the theoretical value of 27% for C_{60}:$CBrClH_2$ = 1:2 molar relation. Thus, the molar formula $C_{60}\cdot 2CBrClH_2$ (M = 979 g/mol) was ascribed to the solvate under examination.

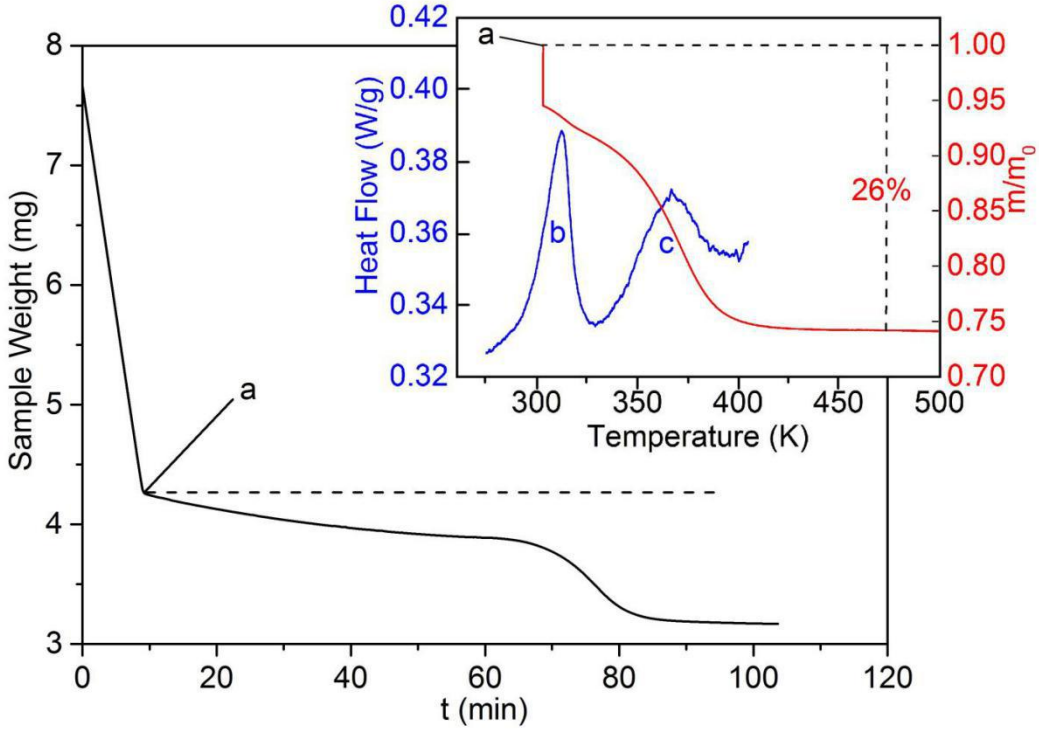

Fig. 7.3. Isothermal evaporation at 300 K and subsequent heating of C_{60}·2CBrClH$_2$ as a function of the time. The initial segment up to point "**a**" corresponds to the evaporation of the mother liquor. Insert: Thermogravimetric (right axis) curves and DSC (left axis) curves for C_{60}·2CBrClH$_2$ crystals. The dashed black lines indicate the point at which the sample was assumed to be free of mother liquor.

To establish the stoichiometry of the solvate, the crystals were placed in pierced pans with an excess of mother liquid and submitted to TGA experiments. The heating process was preceded by an isothermal mass measurement at room temperature (303 K) being both processes represented in Fig. 7.3. The figure shows a very quick loss of mass finishing at point "**a**" that was assumed to be related with the complete evaporation of the liquid. This loss of mass is followed by a slower mass loss which tends to stabilize after 50 minutes. At this time the sample was heated at 5 K/min up to 550 K. The experimental loss of mass from "**a**" (see

inset) was found around 26%, near the theoretical value of 27% for C_{60}:$CBrClH_2$ = 1:2 molar relation. Thus, the molar formula $C_{60}\cdot 2CBrClH_2$ (M = 979 g/mol) was ascribed to the solvate under examination.

To evaluate the desolvation enthalpy, co-crystals of $C_{60}\cdot 2CBrClH_2$ with an excess of mother liquid were placed in pierced pans and maintained in the TGA device until the liquid was evaporated, being immediately transferred to DSC. The DSC curve in Fig. 7.3, shows two broad endothermic effects. These results show that the desolvation process starts at low temperature, around 300 K, a fact that agrees with the starting desolvation observed at room temperature in the TGA device. Another common trend in both kinds of measurements is that around 322 K, the initial temperature of the second DSC endothermic effect there is a change in the mass loss rate in the TGA signal.

The desolvation enthalpy change, including peaks "**b**" and "**c**" in the DSC curve, was found to be near 84.7 J/g of solvate, i.e. 41.5 kJ/mol of solvent. The sublimation enthalpy of the solvent obtained by addition of the vaporization and melting enthalpies is around 38.5 kJ/mol, near to the value measured for the desolvation enthalpy. This indicates that the solvation occurs with no apparent extra-interaction between the C_{60} and solvent molecules in the solvate lattice [3].

To further investigate the behavior of this solvate, co-crystals with an excess of the mother liquid were introduced in stainless steel high-pressure pan, and submitted to heating ramps. The thermograms in Fig. 7.4, show three endothermic effects: the first peak **p**1 at 185 K, which corresponds to the melting of the crystalline $CBrClH_2$, and the remained peaks **p**2 at 322 K and **p**3 around 390 K, which must be related to some transformations involving exclusively the solvate.

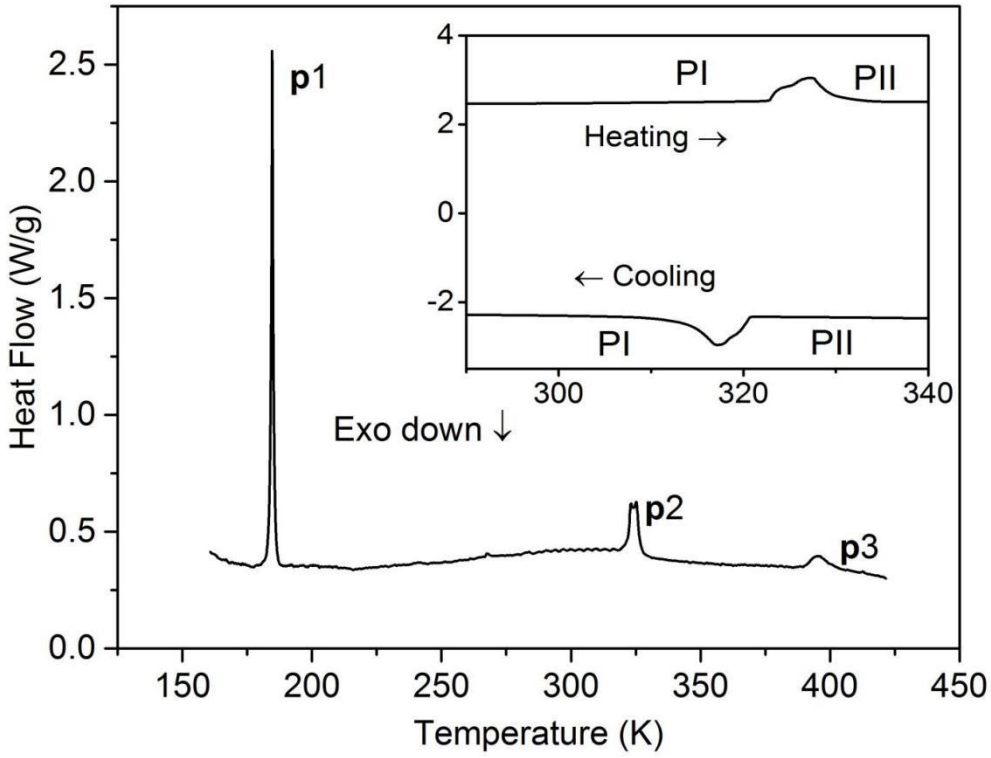

Fig. 7.4. Typical DSC curves for samples of C_{60}·2CBrClH$_2$ solvate with an excess of mother liquid in stainless steel high-pressure pans. Inset: DSC thermograph of C_{60}·2CBrClH$_2$ solvate upon cooling and heating between 290 and 340 K with the same heating rate 2 K/min.

To identify the structural changes associated with the DSC signals, X-ray measurements of co-crystals in the mother liquor in closed capillaries were undertaken. Fig. 7.5 shows the profiles recorded at 303 K, 333 K, 350 K and 393 K.

The changes in the spectra can be clearly seen in Fig. 7.5, were partial profiles (low angle) are presented. At 333 K a new spectra is obtained and it mimics the hexagonal profile of the C_{60}·2CBrHCl$_2$ solvate. In fact, the obtained spectrum can be indexed by a hexagonal lattice, group P6/mmm with a volume per molecule of around 900 Å^3, value of the same order as those found for other hexagonal solvates in this work.

Then, if there is no change in stoichiometry the second peak **p**2 at 322 K, must be related to a solvate transition from the monoclinic phase (PI, low-temperature phase) to a more symmetric hexagonal phase (PII, high-temperature phase).This would explain the reversibility of the signal **p**2 observed by DSC measurements (see inset figure of Fig. 7.4) and by X-ray measurements.

The profile at 350 K shows the reflections of the hexagonal phase together with that of FCC C_{60}, then the last DSC signal **p**3 (around 390 K) must concern the peritectic melting of this phase. The difference of temperatures obtained in both measurements techniques could be due to the fact that the capillary was not hermetically sealed and the desolvation process is already taking place at lower temperatures.

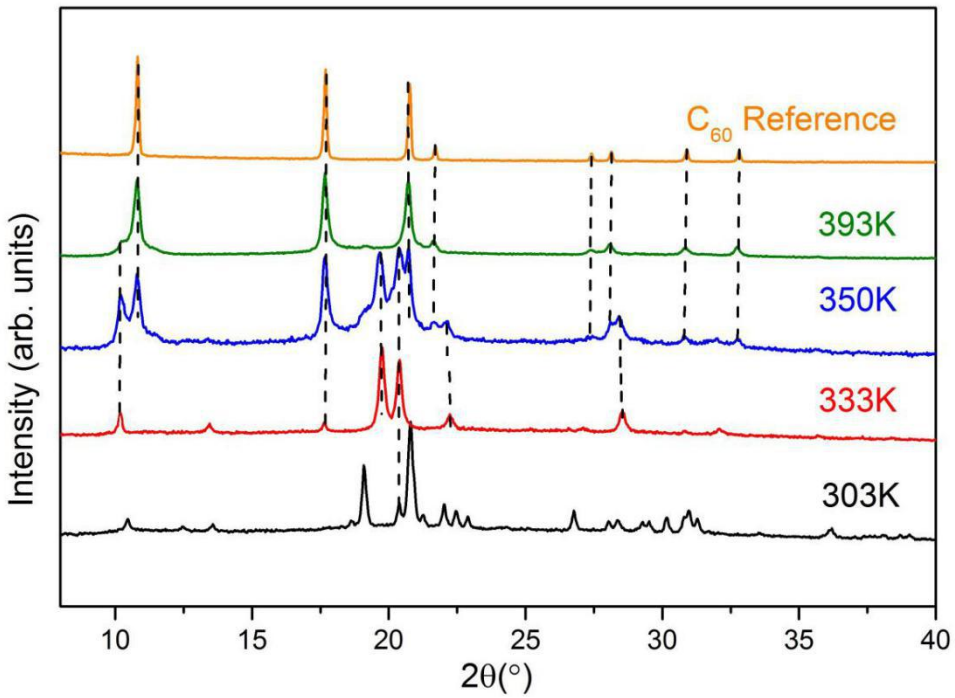

Fig. 7.5. Series of X-ray patterns of co-crystals in mother liquor in a closed capillary as a function of temperature. The experimental profile of FCC C_{60} phase has been represented for

reference. The range between 40 and 115° is not shown due to the absence of Bragg peaks with significant.

At this point, it is worth mentioning that in general when the solvate loses the solvent molecules the cubic C_{60} formed structure shows broad peaks related to defects and stacking faults [4-7]. On the contrary in this system, the recovered profile of the cubic C_{60} has shaped reflections as it is evidenced by the profile at 393 K in Fig. 7.5.

7.3 Discussion and structural characterization

Combining the former experimental results the binary phase diagram has been built up in Fig. 7.6 where the invariant temperatures have been determined from the DSC thermal events.

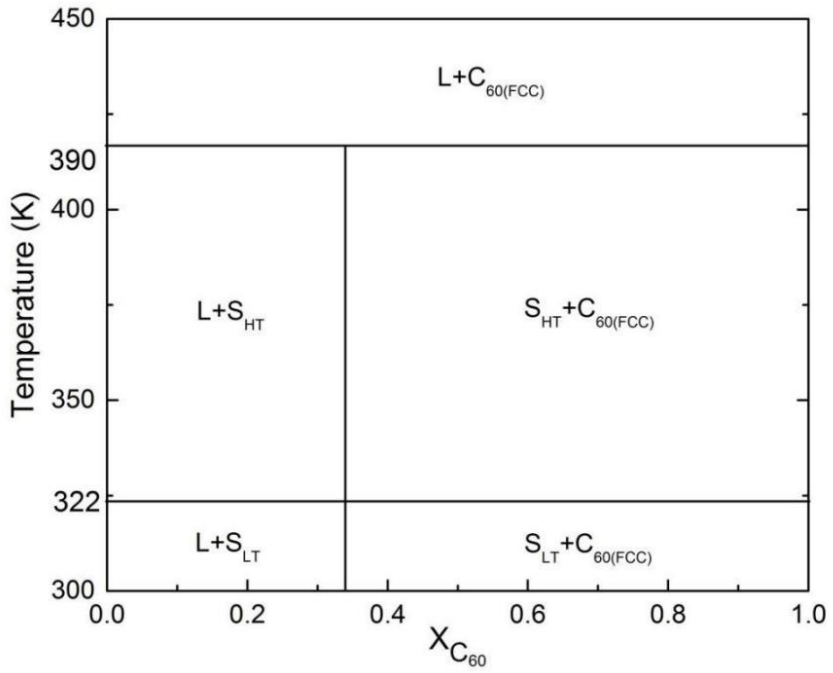

Fig. 7.6. C_{60}:$CBrClH_2$ phase diagram. S_{LT} and S_{HT} are the monoclinic and hexagonal phases of C_{60}·$2CBrClH_2$.

There is only one solvate formed between C_{60} and $CBrClH_2$, $C_{60}{\cdot}2CBrClH_2$, which corresponds to a mole fraction of X = 1/3. The solvate has a solid-solid phase transition from a low-temperature monoclinic phase (S_{LT}) to a high-temperature hexagonal phase (S_{HT}) at 322 K. The high-temperature phase undergoes a peritectic desolvation at 390 K.

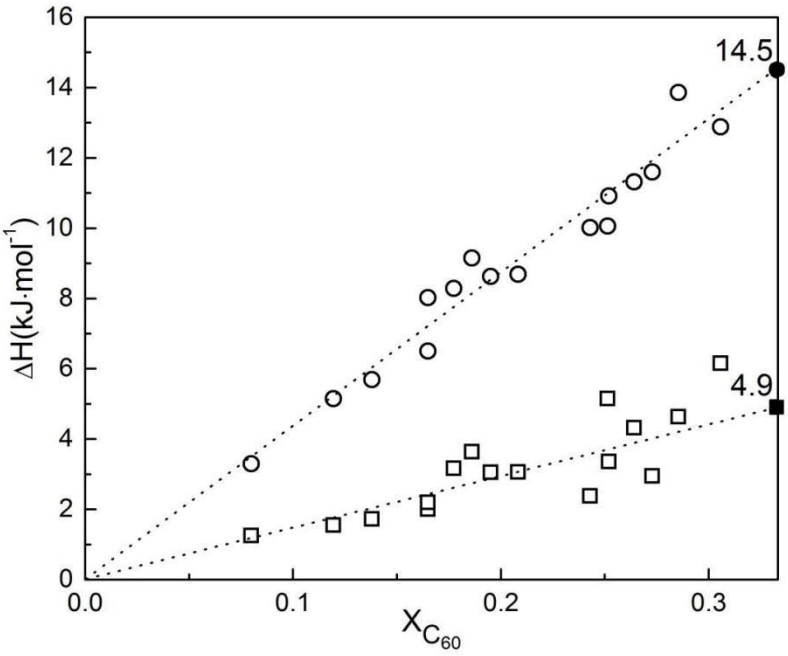

Fig. 7.7. Tammann diagram for the transition (empty squares) and melting (empty circles) of the $C_{60}{\cdot}2CBrClH_2$ at 322 and 390 K, respectively. Full symbols are extrapolated values at the solvate concentration.

To determine the energy involved in both, the transition and peritectic desolvation of co-crystal $C_{60}{\cdot}2CBrClH_2$, samples with variables quantities of the solvate and liquid solution were prepared in order of to measure concentrations ranged between 0 and 0.33. The DSC results are present in Fig. 7.7. The extrapolated values at the solvate concentration X = 0.33 are 4.9 J/g of solvate (4.8 kJ/mol of solvate) for the transition and 14.5 J/g (14.2 kJ/mol of

solvate) for the peritectic desolvation of $C_{60}{\cdot}2CBrClH_2$ (HT), respectively. Then, the calculated entropy changes in the solid-solid transition and peritectic would be, 44.1 J/K·mol and 36.4 J/K·mol. These values imply that the disorder generated at the solid-solid transition is higher than that at the peritectic desolvation of the hexagonal phase. Between the solvates obtained with halogenomethane derivatives only two, $C_{60}{\cdot}2CCl_4$ and $C_{60}{\cdot}2CCl_3(CH_3)$ undergo a solid-solid transition from a low symmetry phase to a hexagonal phase [8,9] with transition enthalpies values 4.5 and 1.3 kJ/mol of solvate, respectively. These values are similar to that obtained in the $C_{60}{\cdot}2CBrClH_2$ solvate.

The Rietveld refinement of the low-temperature phase was performed with Materials Studio, assuming a similar structure to that of $C_{60}{\cdot}2CBr_2H_2$. The orientationally ordered C_{60} molecule is located at the 2a Wyckoff position site of 2/m symmetry. The molecule of the solvent was modeled as a rigid body with the atom coordinates taken from Podsialdlo et al. [1]. The central carbon was located at the 4h Wyckoff position (0, y, 1/2) obtaining after refinement the final position of (0, 0.2768(2), 0.5). To make compatible the symmetry of the solvent molecule and that of the site, disorder between the two halogens was assumed. The position and orientation of the molecules were refined with a single overall isotropic displacement and preferred orientations using the March-Dollase formula [10]. The refined pattern together with the experimental one and difference between them are depicted in Fig. 7.8. In Table. 7.1, the values of the final Rietveld refinement are summarized.

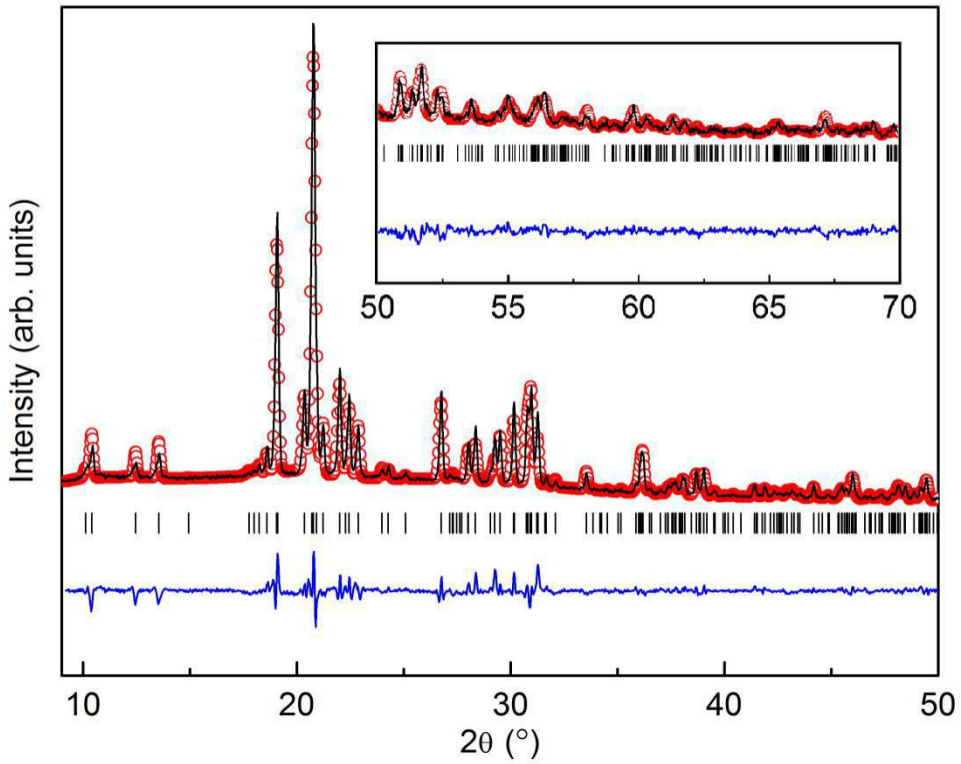

Fig. 7.8. Experimental **points**) and simulated (**black line**) X-ray diffraction Patterns together with Bragg reflections (**vertical sticks**) of C2/m monoclinic solvate C_{60}·2$CBrClH_2$(LT) at 300K.

The alternating stacking of the C_{60} and $CBrClH_2$ molecules is represented in Fig. 7.9. The solvent molecule has its 2-fold axis along the monoclinic axis **b** and the halogen ligands pointing along the longer diagonal of the *a*-*c* plane.

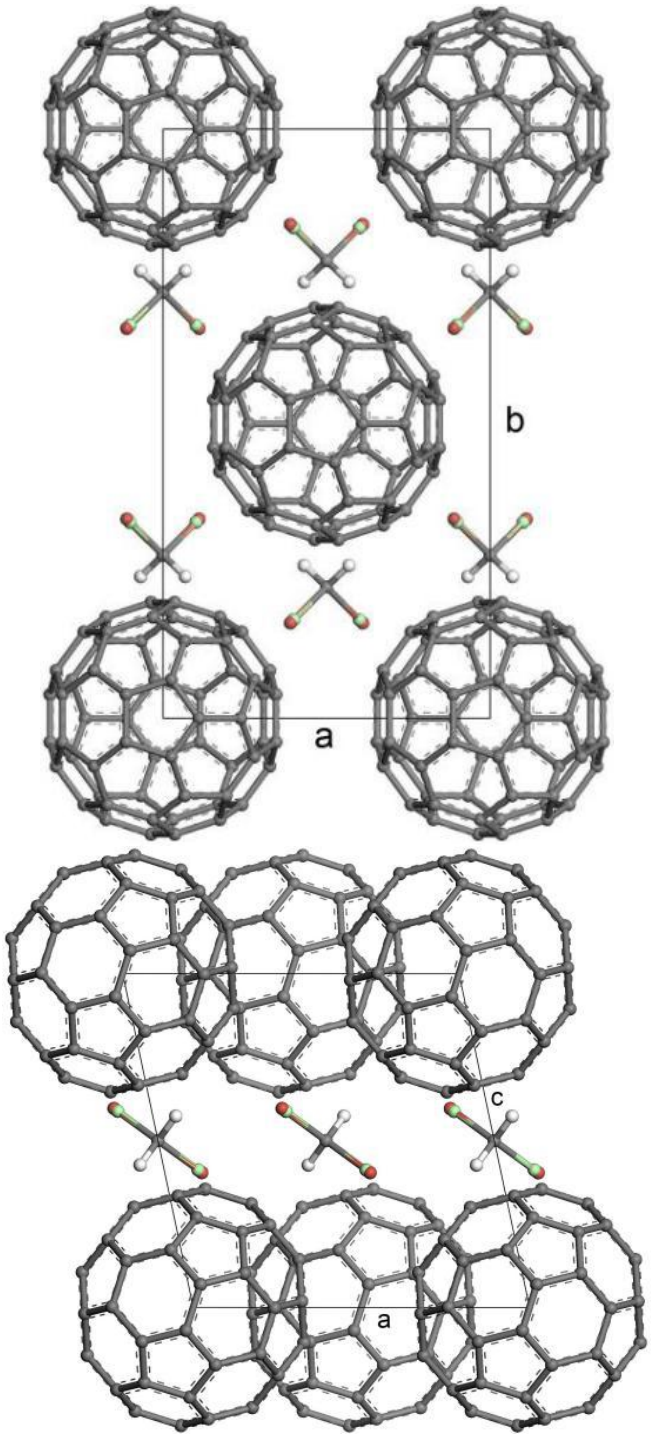

Fig. 7.9. Crystal structures of Monoclinic C_{60}·2$CBrClH_2$ in (001) plane (left panel), (010) plane (right panel) at 300 K.

The structure of the hexagonal HT phase has been analyzed using the FullProf Suite. The preliminary analyses by DICVOL reveal that systematic absences were compatible with the space group P6/mmm. The C_{60} molecule was modeled with spherical harmonics describing a homogeneous distribution 60 C- atoms located on a sphere of overall 3.59 Å radius. Like in the monoclinic phase the solvent molecule was described as a rigid body with the atom coordinates taken from Podsialdlo et al. [1]. For the Rietveld analysis, the center of C_{60} was positioned in the 1a Wyckoff site and the carbon of the tetrahedral $CBrClH_2$ molecule in the (1/3, 2/3, 1/2) position. The C-atom position and orientation of the molecule were refined, obtaining a final position of (0.329(6), 0.711(3), 0. 544(5)). The refined and experimental patterns are depicted in Fig. 7.10 and the final Rietveld results are summarized in Table. 7.1.

Table. 7.1. Crystal structures and the Rietveld refinement for the monoclinic and hexagonal phases of $C_{60}\cdot 2CBrClH_2$.

Chemical Formula	$C_{60}\cdot 2CBrClH_2$ (LT)	$C_{60}\cdot 2CBrClH_2$ (HT)
M /g·mol^{-1}	979	979
2 -Angular Range	5-80º	
Space group	C2/m	P/6mmm
a/Å	9.9153(6)	10.074(2)
b/Å	17.4119(12)	10.074(2)
c/Å	10.0478(6)	10.060(3)
α/º	90	90
β/º	101.966(3)	120
γ/º	90	90
V /Å^3	1697.02(1)	884.11(5)
Z	2	1
Temperature	303 K	333 K
Wavelength (CuKα1)	λ = 1.5406 Å	
2 -shift (zero correction)	-0.036(1)	0.0123
Reliability Parameters		
R_{wp}	5.26%	19.4%
R_p	3.83%	22.6%
Peak width parameters	U = 0.479, V = -0.304, W = 0.068	U = 5.346, V = -1.568, W = 0.249

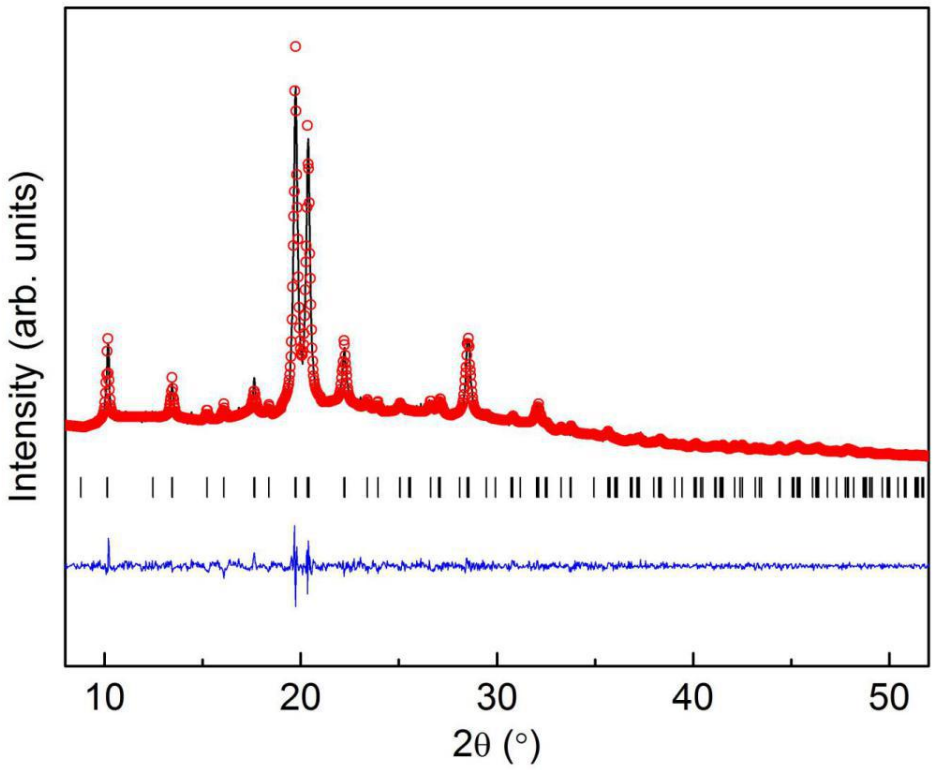

Fig. 7.10. Experimental (**points**) and simulated (**lines**) X-ray diffraction Patterns together with the difference profile(**bottom line**) and Bragg reflections (**vertical sticks**) of P/6mmm hexagonal solvate C_{60}·2CBrClH$_2$(HT) at 333K.

The mean volume available for the molecular unit in the monoclinic and hexagonal phases are V/Z = 848.5 Å^3 and 884.1 Å^3 per molecule, respectively. Taking for the solvent in its solid phase V/Z = 91.16 Å^3/molecule [1], and V/Z = 710 Å^3/molecule for the FCC C_{60}, a calculated value of V/Z = 892.32 Å^3 for C_{60}·2CBrClH$_2$ unit could be obtained following the additive scheme. Comparing the experimental and calculated values it can be inferred that monoclinic phase forms with a negative excess volume of -43.82 Å^3 per solvate molecule (-4.9%), whereas the hexagonal phase forms with -8.22 Å^3 per solvate molecule (-1%).

7.4 Conclusions

A C_{60}:halogenomethane co-crystal has been prepared and characterized both thermodynamically and structurally. Co-crystals C_{60}:$CBrClH_2$, after removed from the mother liquor reveal the existence of a monoclinic solvate with 1:2 stoichiometry, i.e., $C_{60}\cdot 2CBrClH_2$, with lattice parameters of a = 9.915(1) Å, b = 17.412(1) Å, c = 10.048(1) Å, β = 101.966(3)º. Interestingly enough this low-temperature solvate transforms reversibly on heating to a new Hexagonal phase, with lattice parameters of a = b = 10.074(2) Å, c = 10.060(3) Å at 322 K and with the same stoichiometry. Both solvates form with a negative excess volume: -43.82 (-4.9%) and -9.82 (-1.1%) respectively, which indicates that intermolecular interactions do appear between C_{60} and solvent molecules. On further heating, the hexagonal solvate disappears through a peritectic process at 390 K. Desolvation enthalpy (38.5 kJ/mol of solvent) is smaller than the sublimation enthalpy of pure solvent (41.5 kJ/mol), indication low intermolecular interactions between the C_{60} and $CBrCl_2H$ in the solvate lattice, in clear contradiction to the negative excess volumes found for both monoclinic and hexagonal solvates. Nevertheless, it should be mentioned that the hexagonal solvate, which finally desolvates at the peritectic invariant, forms with a low negative excess volume, about -1%, and that the desolvation enthalpy is just around 7% lower than the sublimation enthalpy. Thus, by assuming the errors for the aforementioned magnitudes, it can be concluded that, at least for the high-temperature hexagonal solvate, intermolecular interactions are quite weak.

7.5 References

[1] M. Podsiadło, A. Katrusiak, Isobaric, isochoric freezing of CH_2BrCl and isostructural relations between CH_2Cl_2, CH_2Br_2 and CH_2BrCl, Acta Crystallographica Section B, 63, 2007, 903.

[2] C. L. Yaws, Thermophysical Properties of Chemicals and Hydrocarbons, 2nd Edition, 2014, 497.

[3] A. Bondi, Heat of Sublimation of Molecular Crystals: A Catalog of Molecular Structure Increments, Journal of Chemical & Engineering Data, 8 (1963) 371.

[4] G. B. M. Vaughan, Y. Chabre, D. Dubois, Effect of stacking disorder on the orientational ordering transition of solid C_{60}, Europhysics Letters, 31, 1995, 525.

[5] S. Toscani, H. Allouchi, J. Ll. Tamarit, D. O. López, M. Barrio, V. Agafonov, A. Rassat, H. Szwarc, R. Céolin, Decagonal C_{60} crystals grown from n-hexane solutions: solid-state and aging studies, Chemical Physics Letters, 330, 2000, 491.

[6] P. Espeau, M. Barrio, D. O. López, J. Ll. Tamarit, R. Céolin, H. Allouchi, V. Agafonov, F. Masin, H. Szwarc, Phase Equilibria in the C_{60}+Ferrocene System and Solid-State Studies of the C_{60}:2Ferrocene Solvate, Chemistry of Materials, 14, 2002, 321.

[7] M. Barrio, D. O. López, J. Ll. Tamarit, P. Espeau, R. Céolin, Solid-State Studies of C_{60} Solvates Formed in the C_{60}-$BrCCl_3$ System, Chemistry of Materials, 15, 2003, 288.

[8] M. Barrio, D. O. López, J. Ll. Tamarit, H. Szwarc, S. Toscani, R. Céolin, C_{60}:CCl_4 phase diagram: polythermal behaviour of solvates C_{60}:12CCl_4 and C_{60}:2CCl_4, Chemical Physics Letters, 260, 1996, 78.

[9] R. Céolin, J. Ll. Tamarit, M. Barrio, D. O. López, P. Espeau, H. Allouchi, R.J. Papoular, Solid state studies of the C_{60}·2$(CH_3)CCl_3$ solvate, Carbon, 43, 2005, 417.

[10] W. A. Dollase, Correction of intensities for preferred orientation in powder diffractometry: application of the March model, Journal of Applied Crystallography, 19, 1986, 267.

8. Conclusion

In previous chapters, some thermodynamic and crystallographic properties of co-crystals formed between C_{60} and solvents of tetrahedral molecules $CBr_2(CH_3)_2$, CBr_2Cl_2, CBr_2H_2, $CBrCl_2H$ and $CBrClH_2$ have been studied.

In this chapter, we will present some common trends observed between the different studied solvates. Moreover, since other solvates involving tetrahedral molecules have been previously published, checking the reliability of our results the bibliographic information will be included in this chapter. The data that will be analyzed are those presented in Table 8.1 [1-7]. Some of these data have been introduced in the former chapters such as the excess volume defined by $\Delta V/V = [(V/Z)^{exp} - (V/Z)^{cal}] / (V/Z)^{cal}$, where $(V/Z)^{exp}$ and $(V/Z)^{cal}$ are the experimental and calculated volumes of the crystal lattice per molecular unit, respectively. Assuming a general expression C_{60}:n solvent for the solvate, the value $(V/Z)^{cal}$ has been calculated by means $(710 + n \cdot V/Z(solvent))$ where V/Z(solvent) is the volume for the molecular unit in the solid or orientational disordered solid phase of the solvent.

The solutions of C_{60} with four solvents CCl_4, CCl_3Br, $CBr_2(CH_3)_2$ and CBr_2Cl_2 produce metastable solvates of FCC cubic symmetry that become unstable and transform in FCC C_{60} as soon as they are removed from their mother liquors. Another solvent that forms a solvate not air stable is dichloromethane CCl_2H_2 [7]. This co-crystal of I-centered cubic symmetry and low stoichiometry transforms to a hexagonal polymorph of C_{60} spontaneously when extracted from the solution. As it is shown in Table 8.1 positive excess volumes have been obtained for all these cubic solvates even if the dichloromethane co-crystal forms with a weakly negative excess volume.

Solvates of lower symmetry (Hexagonal, Orthorhombic and Monoclinic) are formed with negative values of excess volume. These negative excess volumes suggest that strong interactions between the molecules of C_{60} and solvent molecules appear in the stable co-crystals.

Then the excess volumes are in line with the observed lower stability of the cubic co-crystals relative to the more stable lower symmetry co-crystal in the air.

Another parameter to account for the interactions in the crystal is the Packing Coefficient. This parameter was introduced by Kitaigorodskii [8-9] in relation with the Principle of close-packing. According to this principle, a molecule may be represented by a combination of intersecting atomic spheres whose radii are equal to the van der Waals atomic radii. These molecules are closely packed in the crystal lattice in such a way that each molecule is located into the hollows of its neighbors. The degree of space filling of the unit cell is accounted by the packing coefficient:

$$\eta = \frac{V_m}{V / Z}$$

Table. 8.1. Crystallographic data for solvates involving tetrahedral solvent molecules.

C_{60}:nSolvent (nSolvent)	V/Z (Å^3) Solvate	V_{vdw} (Å^3) Solvent	Excess volume (%)	Packing coefficient	Structure
12CCl_4 [1]	2568.50	86.55	+12.0%	0.611	Cubic
2CCl_4 [2]	957.60	86.55	-7.8%	0.731	Hexagonal
12CCl_3Br [1]	2625.50	91.05	+9.3%	0.634	Cubic
2CCl_3Br [1]	973.50	91.05	-4.6%	0.735	Hexagonal
2CCl_3H [1]	892.0	71.20	-9.0%	0.749	Hexagonal
2$CCl_3(CH_3)$ [3]	962.0	91.0	-2.7%	0.736	Hexagonal
1.5CBr_2ClH [4]	848.25	80.96	-7.4%	0.760	Orthorhombic
2CBr_2ClH [4]	906.40	80.96	-8.8%	0.755	Hexagonal
2CBr_3H [5]	924.0	85.43	-7.8%	0.753	Hexagonal
CBr_3H [6]	790.93	85.43	-13.7	0.772	Orthorhombic
CCl_2H_2 [7]	788.94	57.66	+0.1%	0.740	Cubic
2CCl_2H_2 [2]	783.0	57.66	-10.6%	0.820	Tetragonal
2CBr_2H_2	850.80	66.30	-5.5%	0.773	Monoclinic
12$CBr_2(CH_3)_2$	2827.70	103.43	+5.0%	0.630	Cubic
2$CBr_2(CH_3)_2$	995.60	103.43	-4.3%	0.74	Hexagonal
12CBr_2Cl_2	2710.10	100.11	+2.0%	0.640	Cubic
2CBr_2Cl_2	982.70	100.11	-5.0%	0.739	Hexagonal
2$CBrClH_2$(LT)	848.50	61.85	-4.9%	0.765	Monoclinic
2$CBrClH_2$(HT)	882.50	61.85	-1.1%	0.736	Hexagonal
2$CBrCl_2H$	900.77	76.42	-3.7%	0.754	Hexagonal
$CBrCl_2H$	801.37	76.42	-2.5%	0.752	Monoclinic

Where Z is the number of formula units per unit cell, V_m is the volume of an isolated molecule and V/Z is the volume of the crystal lattice per molecule. The volume of the statistical entity is given by $V_m = V(C_{60}) + n \cdot V_s$, where $V(C_{60})$ and $n \cdot V_s$ are the van der Waals volume of C_{60} and the n solvent molecules in the co-crystal, respectively.

The van der Waals volume of C_{60} is known to be 526 $Å^3$ (the volume of a sphere with a ca. 5 Å radius), whereas for the solvent molecule it has been determined through the Kitaigorodsky method [9] or from Yaws's book [10].

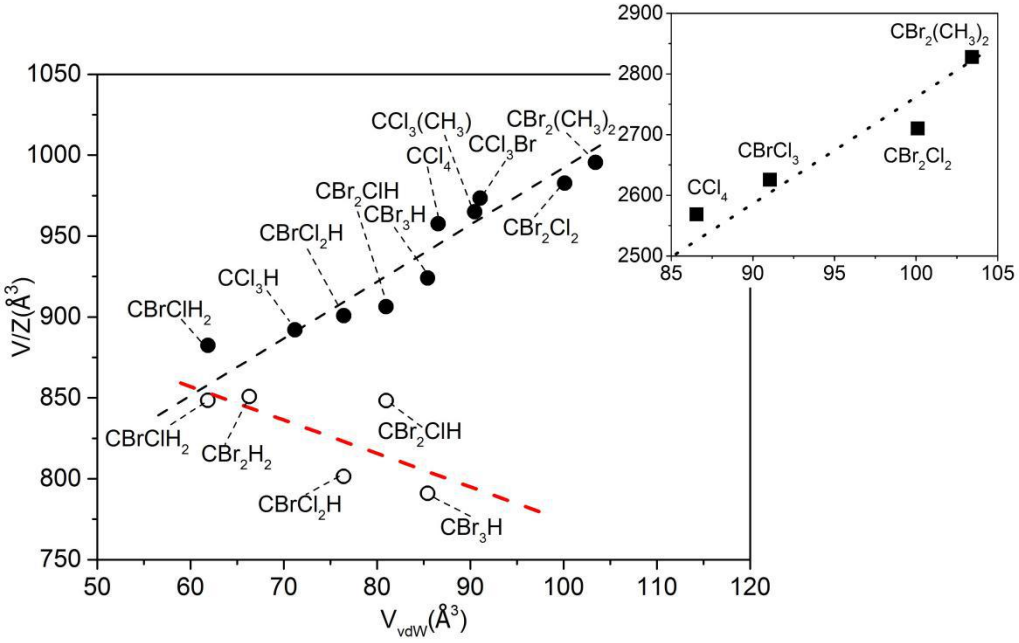

Fig. 8.1. Volume per molecular unit (Z) of the stable solvates as a function of the van der Waals volume of a single solvent molecule with different lattice symmetries: (●) hexagonal (○) monoclinic and orthorhombic. Inset: The same graph for the metastable FCC cubic (■) co-crystals. The lines are fits for the hexagonal (black dashed line), monoclinic and orthorhombic (red dashed line) and cubic(black dotted line) data.

Fig. 8.1 shows the volume per molecular unit in the co-crystals as a function of the van der Waals volume of the solvent molecule. For the FCC cubic co-crystals corresponding to the stoichiometry 1:12 (inset of Fig. 8.1), the volume of the unit cell is governed by the molecular size of the solvent i.e. the larger the guest molecule, the larger is the unit cell of the co-crystal. The same trend observed for the hexagonal co-crystals, result in the independence of of the dipole moment of the guest molecule, as can be inferred from the fact that they range from 0.2 D (for CCl_3Br and CBr_2Cl_2) to 2.11 D (for $CCl_3(CH_3)$) [11-13].

For co-crystals of lower symmetry, monoclinic and orthorhombic, lower V/Z values can be observed for the similar size of the van der Waals volumes. Then a better packing of the solvent molecules between the C_{60} layers of the co-crystals (see structural results in previous chapters) can be inferred. Assuming that solvents involved in these co-crystals have similar dipolar moments or lower that the involved in the hexagonal ones this behavior cannot be explained by the dipolar moment of the solvents. Nevertheless, the overall orientational order in the low symmetry solvates would allow a better packing in the unit cell. In relation to this assertion, the packing coefficient represented in Fig. 8.2 shows that both cubic and hexagonal co-crystals have lower packing than the orientationally ordered co-crystals. Moreover, for the hexagonal co-crystals, two different trends are observed.

For co-crystals with solvent molecules without an H-atom bound to the central carbon (CCl_3Br, $CCl_3(CH_3)$, CBr_2Cl_2 $CBr_2(CH_3)_2$ and CCl_4), the packing coefficients are much lower than for co-crystals possessing an H-atom attached to the central carbon atom. It implies that the molecules CCl_3H, CBr_3H, CBr_2ClH, $BrCl_2H$ and $CBrClH_2$ fit better in the interstitial layers between the layers of C_{60} molecules stacked along the *c* axis. In previous chapters, it has been shown that the solvent molecules fill the prismatic hexagonal voids in the primitive hexagonal lattice (space group P6/mmm) of the co-crystals. It has been demonstrated that for the CCl_3H and CBr_3H molecules, with C_{3v} symmetry, a disorder concerning a three-fold axis exists [14]. For the CBr_2ClH, $CBrCl_2H$ and $CBrClH_2$ molecules this kind of disorder can be simulated assuming disorder between the halogen atoms. Thus, taking the molecules in Fig. 8.2 with a three-fold molecular symmetry axis and an H-atom bonded to the central carbon atom, the more efficient packing can be explained by placing their three-fold axes, i.e. along the C-H bond, parallel to the c axis of the hexagonal unit cell.

This hypothesis is supported by the observed C_{60}-C_{60} distances in the [00l] hexagonal planes. Fig. 8.3 depicts the hexagonal lattice parameters as a function of the van der Waals volume of single solvent molecules. A clear anisotropy of the hexagonal lattice exists for the [001] planes and (001) direction. The C_{60}-C_{60} distances in the [001] planes, i.e. the *a* lattice parameter, are virtually constant irrespective of the solvent volume (the average hexagonal lattice parameter is 10.13 ± 0.05 Å for all analyzed co-crystals), whereas the hexagonal lattice strongly increases along the ***c*** direction when increasing the van der Waals volume of the solvent molecule; however, this effect is almost absent for the co-crystals with the C-H three-fold (or pseudo) symmetry axis. Any increase in the lattice parameter ***a*** as a function of the van der Waals volume is most likely due to disorder around the C-H three-fold axis. For the other solvent molecules, the disorder appears to extend over all four positions, explaining the increase of the lattice parameter c with the solvent size.

For the low-symmetry solvates is difficult to establish a straightforward correlation as for the hexagonal solvates, assuming that different stoichiometries and symmetries are involved. In any case, one of the highest packings is shown for the C_{60}:$2CBr_2H_2$ solvate (0.77), for which the structural characterization in Chapter V showed that both C_{60} and solvent molecules are orientationally ordered. The only comparably sized solvate that exhibits orientational order for C_{60} and the solvent molecule too, the low- temperature orthorhombic solvate with CS_2 has a similar packing coefficient, 0.78, while the high-temperature monoclinic solvate which exhibits orientational disorder possesses a considerable lower packing coefficient 0.76 [15]. Then the high packing coefficients obtained in the studied monoclinic solvates could be ascribed to the orientational order of the solvent molecule in the co-crystal.

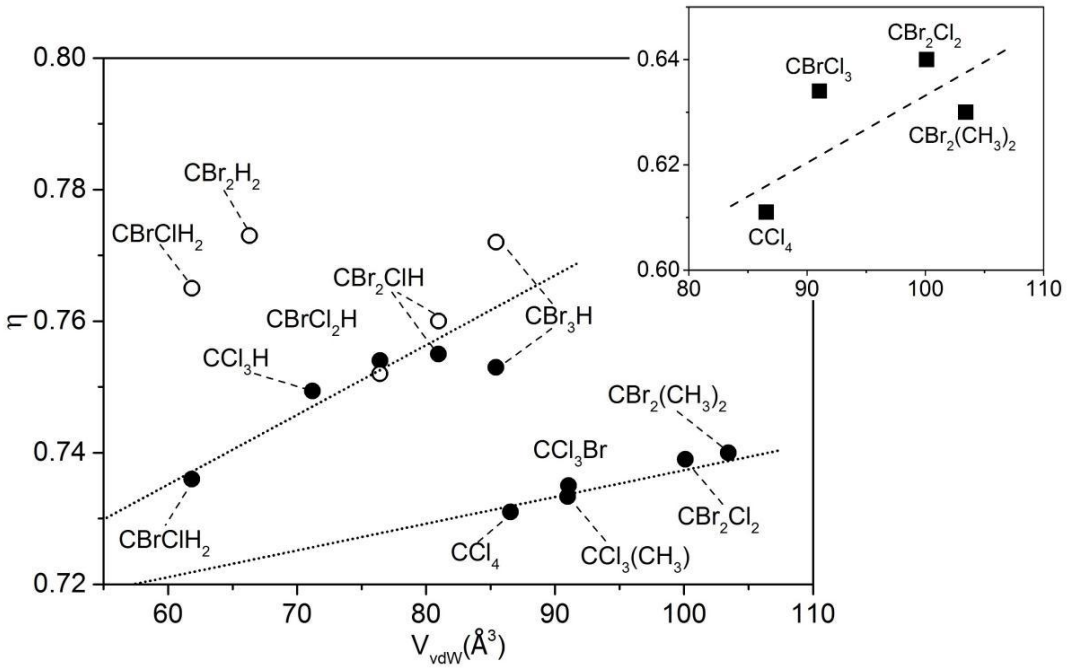

Fig. 8.2. Packing coefficient of the stable solvates as a function of the van der Waals volumes of a single solvent molecule with different lattice symmetries: (●) hexagonal (○) monoclinic and orthorhombic. Inset: The same graph for the metastable FCC cubic (■) co-crystals. The lines are fitting for the hexagonal (black dotted line), and cubic(black dashed line) data.

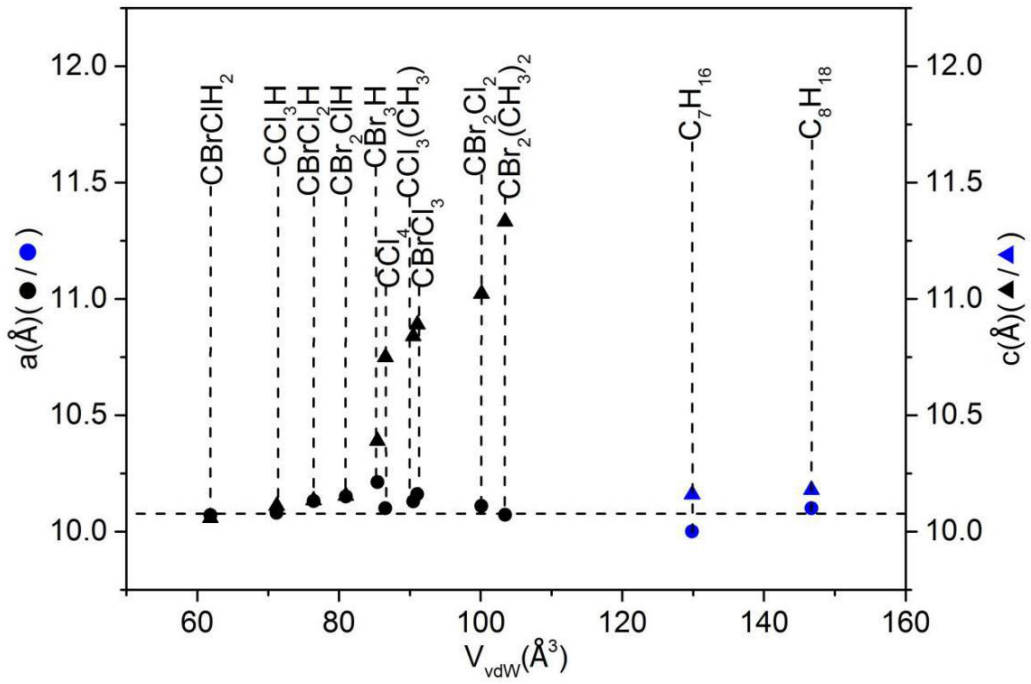

Fig. 8.3. Hexagonal lattice parameters as a function of the van der Waals molecular volumes of the solvents with tetrahedral molecules (**a** (●), **c** (▲)). Two data related to n-alkane solvents are included for comparison (**a** (●), **c** (▲)).

To establish whether similar relationships emerge in solvates co-crystallized with solvent molecules of different geometry, a bibliographic search was carried out. Unfortunately, in no case, there is a study as extensive as that for tetrahedral molecules. In the Tables 8.2, 8.3 and 8.4 crystallographic data for halogen ethane derivatives, alkanes and benzene derivatives are shown. Additional crystallographic data for all the co-crystals that appear in this chapter are presented in Tables 8.6, 8.7 and 8.9 at the end of the chapter.

Table. 8.2. Crystallographic data for solvates involving halogen ethane derivatives.

C_{60}:nSolvent (nSolvent)	V/Z ($Å^3$) Solvate	V_{vdw} ($Å^3$) Solvent	Excess volume (%)	Packing coefficient	Structure
$C_2Cl_2H_4$ [16] 1,2 dichloroethane	793.25	97.0	-2.8%	0.784	Orthorhombic
C_2Cl_3H [17] Trichlorethylene	810	85.0	-4.9%	0.753	Orthorhombic
$C_2Cl_3H_3$ [18] 1,1,2-Trichloroethane	808.0	91.0	-6.7%	0.760	Orthorhombic

Table. 8.3. Crystallographic data for solvates involving n-alkanes molecules.

C_{60}:nSolvent (nSolvent)	V/Z ($Å^3$) Solvate	V_{vdw} ($Å^3$) Solvent	Excess volume (%)	Packing coefficient	Structure
C_5H_{12} [19]	813.75	96.15	-4%	0.764	Orthorhombic
C_6H_{14} [20, 21]	816.0	113.39	-6.2%	0.785	Orthorhombic
C_7H_{16} [22]	838.83	129.85	-6.2%	0.782	Orthorhombic
C_7H_{16} [22]	879.90	129.85	-1.6%	0.744	Hexagonal
C_8H_{18} [23]	899.30	146.70	-2.6%	0.747	Hexagonal
$2/3C_9H_{20}$ [24]	835.5	164.26	-3.1%	0.756	Orthorhombic

Table. 8.4. Crystallographic data for solvates involving benzene derivatives and cyclohexane.

C_{60}:nSolvent (nSolvent)	V/Z ($Å^3$) Solvate	V_{vdw} ($Å^3$) Solvent	Excess volume (%)	Packing coefficient	Structure
$12C_6H_{12}$ [2,25] cyclohexane	2794.0	101.99	+1.6%	0.633	Cubic
$4C_6H_6$ [26] Benzene	1147.0	80.40	-2.4%	0.739	Triclinic
$C_6H_5(CH_3)$ [27] Toluene	830.0	98.85	-2.5%	0.753	Orthorhombic
$2C_6H_5Br$ [28] Bromobenzene	943.50	99.80	-2.5%	0.77	monoclinic

Checking the symmetry of the co-crystals introduced in the new tables only a cubic solvate appeared in Table 8.4 concerning cyclohexane solvent. This solvent, consisting of pseudo-globular molecules, forms with C_{60} a solvate of cubic (FCC) symmetry and stoichiometry (1:12). The values of V/Z and η match up the evolution observed in the cubic solvates involving tetrahedral molecules (Fig. 8.4 and Fig. 8.5).

The remaining solvates are mostly of low symmetry, only two alkanes C_7H_{16} and C_8H_{18} form co-crystals of hexagonal symmetry. The parameters *a* and *c* of the former solvates, are shown in Fig. 8.3 together with the hexagonal co-crystals of tetrahedral molecules. The packing of the C_{60} molecules in the [001] planes, i.e. the *a* lattice parameter, are quite similar irrespective of the symmetry and shape of the solvent. In the n-alkane solvates, the V/Z values (Fig. 8.4) do not reveal strong differences as a function of the symmetry of the co-crystals or of the van der Waals volumes of the solvents although higher values of V/Z are obtained for the hexagonal lattices. On the contrary, the packing is lower in the hexagonal that in the orthorhombic solvates. For solvates involving tetrahedral molecules lower V/Z values and higher packing coefficients have been obtained for the orientationally disordered solvates. Unfortunately, in the n-alkanes case, the structures have not been determined and it is not possible to correlate the degree of disorder in the co-crystals with the volume and packing coefficient values.

For the halogen ethane derivatives, van der Waals volumes do not change so much as to stablish a trend as a function of the variation of the V/Z values. The V/Z values are closed to those of the co-crystal of low symmetry formed by solvents of tetrahedral molecules (Fig. 8.4) although the packing is quite similar to that obtained for the highly packed hexagonal solvates. It has recently been shown that the two conformers *trans* and *gauche* of $C_2Cl_3H_3$ are present in the solvate where they occupy the largest interstitial holes between the C_{60} molecules, displaying both conformers orientational disorder [29].

Benzene solvate with a stoichiometry (1:4) shows higher V/Z value than their derivatives toluene and bromobenzene in spite of its lower van der Waals volume. In benzene co-crystal, the molecules of C_{60} lie in an approximately hexagonal close-packed arrangement cohabit with

disordered benzene molecules [26]. The higher number of the solvent molecules in the lattice and the disorder could be related to the higher values of V/Z and the lower packing coefficient.

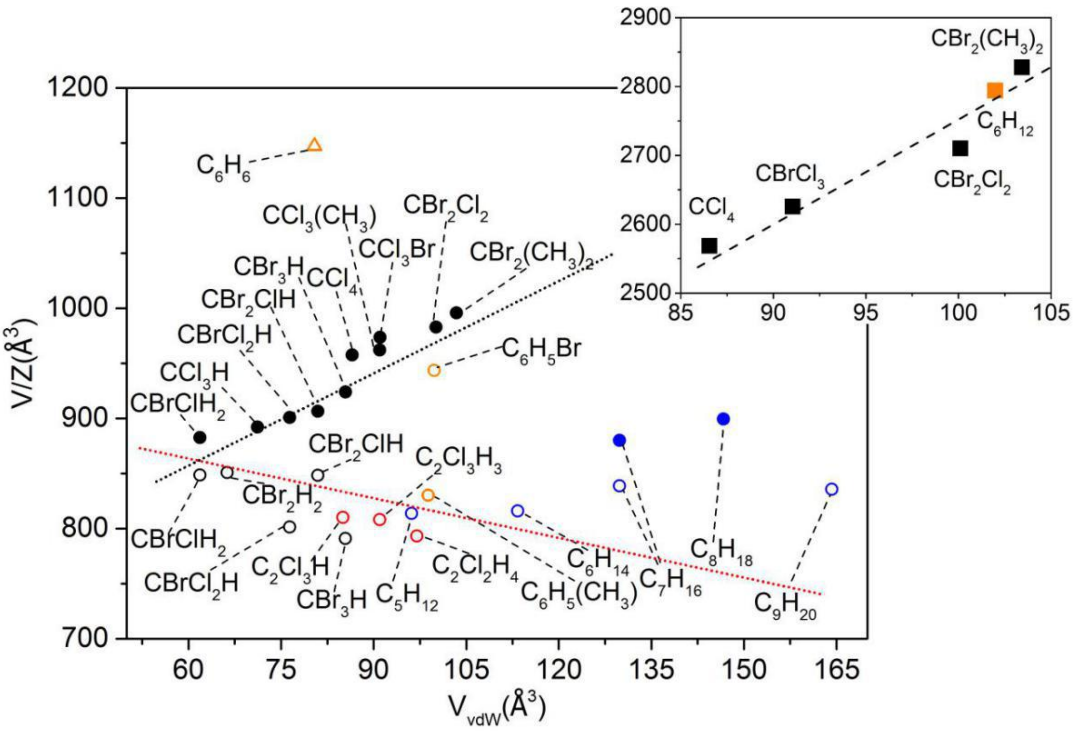

Fig. 8.4. Volume per molecular unit (Z) of several solvates as a function of the van der Waals volumes. Different colors represent different solvent families: (●)hexagonal, (○) monoclinic and orthorhombic for tetrahedral molecules, ((○) orthorhombic) for halogen ethane molecules, ((○) orthorhombic, (●) hexagonal) for n-alkane molecules and ((○)monoclinic and orthorhombic, (△)triclinic) for benzene derivatives. Inset: The same graph for the metastable FCC cubic co-crystals ((■) for tetrahedral molecules, (■) for cyclohexane. The lines are fits involving only the tetrahedral molecules.

A negative excess volume and a high packing coefficient suggest strong interactions between C_{60} and solvent molecules. In fact, positive excess volumes and low packing

coefficient have been obtained for the unstable solvates in line with this idea. The desolvation process involves the transformation of the solvate in cubic C_{60} plus vapor. High desolvation enthalpies are related to strong C_{60}-solvent interactions in the co-crystals. The difference between desolvation enthalpies and sublimation enthalpies of the pure solvents allows to compare the C_{60}-solvent interactions in the co-crystals and between the solvent molecules in their lattice from a thermodynamic point of view.

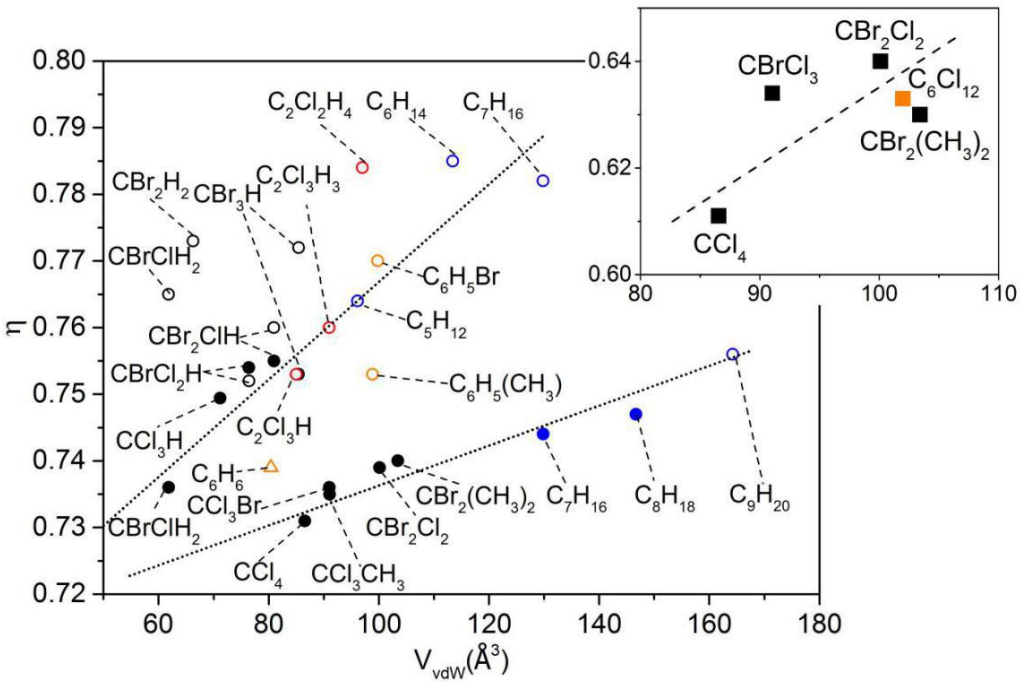

Fig. 8.5. Packing coefficient as a function of the van der Waals volumes of a single solvent molecule. Different colors represent different solvent families: (●)hexagonal, (○) monoclinic and orthorhombic for tetrahedral molecules, ((○) orthorhombic) for halogen ethane molecules, ((○) orthorhombic, (●) hexagonal) for n-alkane molecules and ((○)monoclinic and orthorhombic (△)triclinic) for benzene derivatives. Inset: The same graph for the metastables FCC cubic co-crystals ((■) for tetrahedral molecules (■) for cyclohexane. The lines are fits involving only the tetrahedral molecules.

Both kinds of energies have been compiled in Table 8.5 for some of the co-crystals introduced previously that are stable out of the solution with negative excess volumes. The desolvation enthalpies are near (or even smaller than) the sublimation enthalpy of pure solvents. This indicates that solvation occurs with no apparent extra-interaction between the C_{60} and solvent molecules in the solvate lattice. Then in some cases, the thermodynamic results are in contradiction with the results that can be extracted from the volumes excess and packing coefficients. Nevertheless, it is worth mentioning that the error for the desolvation enthalpy is quite large (it can be even up to 30%) whatever the solvate is considered. Despite this regard, the difference between desolvation and sublimation enthalpies exceeds far away the error and, for those cases, the desolvation enthalpy is much lower than the corresponding sublimation enthalpy, a fact that highlights even more the contradiction with the conclusions derived from the structural analysis.

Table. 8.5. Thermodynamic data for some C_{60}:nSolvent solvates. The enthalpies are given for a mol of solvent.

C_{60}:nSolvent (nSolvent)	Desolvation enthalpy (kJ/mol)	Sublimation enthalpy (kJ/mol)	Structure
$2CCl_4$	37.0 [30]	36.56 [10]	Hexagonal
$2CCl_3Br$	15.64 [2]	39.28 [2]	Hexagonal
$2CCl_3H$	56.0 [31]	38.59 [10]	Hexagonal
$2CCl_3(CH_3)$	44.5 [3]	42.66 [3]	Hexagonal
$1.5CBr_2ClH$	44.0-55.0 [4]	39.62 [10, 32]	Orthorhombic
$2CBr_2H_2$	41.95	46.20 [33]	Monoclinic
$2CBr_2(CH_3)_2$	34.0	68.29 [34, 10]	Hexagonal
$2CBr_2Cl_2$	22.0	44.09 [10, 11]	Hexagonal
$2CBrClH_2$	41.50	38.5	Monoclinic
$2CBrCl_2H$	18.74	40.40	Hexagonal
C_6H_{14}	48.6-52.6 [34]	50.80 [35]	Orthorhombic
C_7H_{16}	35.50 [22]	37.30 [22]	Hexagonal
C_8H_{18}	50.0 [23]	55.0 [23]	Hexagonal
$C_2Cl_2H_4$	45.0 [16]	41.0 [16]	Orthorhombic
C_2Cl_3H	43.7 [17]	40.6 [17]	Orthorhombic
$C_6H_5(CH_3)$	45.0 [35]	40.0 [36]	Orthorhombic

Table. 8.6. Lattice parameters for hexagonal co-crystals.

Hexagonal				
C_{60}:nSolvent (nSolvent)	a (Å)	c (Å)	V_{vdw} (Å^3)	V/Z (Å^3)
$2CCl_4$ [2]	10.10	10.76	86.55	957.60
$2CBr_2(CH_3)_2$	10.07	11.33	103.43	995.60
$2CCl_3Br$ [1]	10.16	10.90	91.05	973.50
$2CCl_3H$ [1]	10.08	10.31	71.20	892.00
$2CCl_3(CH_3)$ [3]	10.13	10.84	90.47	965.00
$2CBr_2Cl_2$	10.11	11.02	100.11	982.70
$2CBr_2ClH$ [4]	10.15	10.34	80.96	906.40
$2CBr_3H$ [5]	10.21	10.39	85.43	924.00
$2CBrClH_2$(HT)	10.06	10.07	61.85	882.50
$2CBrCl_2H$	10.13	10.134	76.42	900.77
C_7H_{16} [22]	10.00	10.16	129.85	879.90
C_8H_{18} [23]	10.10	10.18	146.70	899.30

Table. 8.7. Lattice parameters for orthorhombic co-crystals.

Orthorhombic					
C_{60}:nSolvent (nSolvent)	a (Å)	b (Å^3)	c (Å)	V_{vdw} (Å^3)	V/Z (Å^3)
C_5H_{12} [19]	10.16	31.71	10.10	96.15	816.0
$C_2H_4Cl_2$ [16]	10.07	31.34	10.06	83.0	793.25
C_2HCl_3 [17]	31.47	10.07	10.22	82.36	807.0
$C_6H_5(CH_3)$ [27]	10.34	31.53	10.18	59.51	829.75
C_7H_{16} [22]	10.07	10.22	48.90	129.85	838.83
$1.5CS_2$ [37]	24.97	25.52	9.98	51.83	795.0
$1.5CBr_2ClH$ [4]	23.01	12.65	11.66	80.96	848.25
C_6H_{14} [21]	10.24	10.18	31.31	113.39	816.0

Table. 8.4. Unit-cell parameters and symmetry for co-crystals C_{60}:Solvent in room temperature.

Monoclinic						
C_{60}:nSolvent (nSolvent)	a (Å)	b (Å^3)	c (Å)	Beta (°)	V_{vdw} (Å^3)	V/Z (Å^3)
$2C_6H_5Br$ [28]	17.23	10.16	11.34	108.12	99.8	943.5
$2CBr_2H_2$	9.90	17.45	10.10	102.77	66.30	850.80
$2CBrClH_2$(LT)	9.92	17.41	10.05	101.97	61.85	848.50
$CBrCl_2H$	10.14	31.23	10.12	90.21	76.42	900.77

The conclusions reached in this thesis should provide a basis for further investigations of the co-crystals C_{60}:nSolvent, and they bring further insights as to the solid-state physical chemistry of C_{60} solvation. The outstanding common features remain to be checked through systematic studies sharing thermodynamic, dynamic and structural aspects.

8.1 References

[1] M. Barrio, D. O. López, J. Ll. Tamarit, P. Espeau, R. Céolin, Solid-State Studies of C_{60} Solvates Formed in the C_{60}-$BrCCl_3$ System, Chemistry of Materials, 15, 2003, 288.

[2] M. Jansen, G. Waidmann, Darstellung und Charakterisierung der Fulleren-Kokristallisate $C_{60}\cdot 12C_6H_{12}$, $C_{70}\cdot 12C_6H_{12}$, $CC_{60}\cdot 12CCl_4$, $C_{60}\cdot 2CHBr_3$, $C_{60}\cdot 2CHCl_3$, $C_{60}\cdot 2H_2CCl_2$, Zeitschrift für anorganische und allgemeine Chemie, 14, 1995, 621.

[3] R. Céolin, J. Ll. Tamarit, M. Barrio, D. O. López, P. Espeau, H. Allouchi, R. J. Papoular, Solid state studies of the $C_{60}\cdot 2(CH_3)CCl_3$ solvate, Carbon, 43, 2005, 417.

[4] R. Céolin, D. O. López, B. Nicolaï, P. Espeau, M. Barrio, H. Allouchi, J. Ll. Tamarit, Solid-State Studies of C_{60} Solvates formed with Chlorodibromomethane, Chemical Physics, 342, 2007, 78.

[5] C. Collins, J. Foulkes, A. D. Bond, J. Klinowski, Crystalline $C_{60}\cdot 2CHBr_3$ solvate: A solid-state study, Physical Chemistry Chemical Physics, 1, 1999, 5323

[6] M. J. Hardie, R. Torrens, C. L. Raston, Characterisation of a new 1:1 (C_{60}) ($CHBr_3$) intercalation complex, Chemical Communications, 15, 2003, 1854.

[7] R. Céolin, J. Ll. Tamarit, M. Barrio, D. O. López, S. Toscani, H. Allouchi, V. Agafonov, H. Szwarc, Solid-State Studies on a Cubic 1:1 Solvate of C_{60} Grown from Dichloromethane and Leading to Another Hexagonal C_{60} Polymorph, Chemistry of Materials, 13, 2001, 1349.

[8] A. I. Kitaigorodskii, Molecular Crystals and Molecules, Academic Press, New York and London, 1973, 20.

[9] A. I. Kitaigorodskii, Mixed Crystals; Berlin: Springer-Verlag, 1984, 62.

[10] C. L. Yaws, Thermophysical Properties of Chemicals and Hydrocarbons, 2nd Edition, 2014, 497.

[11] M. Barrio, J. Ll. Tamarit, P. Negrier, L. C. Pardo, N. Veglio, D. Mondieig, Polymorphism of CBr_2Cl_2, New Journal of Chemistry, 32, 2008, 232.

[12] L. C. Pardo, M. Barrio, J. LlTamarit, D. O. López, J. Salud, A. J. Oonk, Orientationally Disordered Mixed Crystals Sharing Methylchloromethanes [(CH_3)4-nCCln, n=0, ⋯ , 4], Chemistry of Materials, 17, 2005, 6146.

[13] B. Parat, L. C. Pardo, M. Barrio, J. LlTamarit, P. Negrier, J. Salud, D. O. López, D. Mondieig, Polymorphism of $CBrCl_3$, Chemistry of Materials, 17, 2005, 3359.

[14] R. E. Dinnebier, O. Gunnarsson, H. Brumm, E. Koch, A. Huq, P. W. Stephens, M. Jansen, Structure of Haloform Intercalated C_{60} and Its Influence on Superconductive Properties, Science, 296, 2002, 109.

[15] B. Morosin, P. P. Newcommer, R. J. Baughman, E. L. Venturini, D. Loy, J. E. Schirber, On the "orthorhombic form of C_{60}" molecular crystals containing CS_2, Physica C: Superconductivity, 184, 1991, 21.

[16] F. Michaud, M. Barrio, S. Toscani, D. O. López, J. Ll. Tamarit, V. Agafonov, H. Szwarc, R. Céolin, Solid-state studies on single and decagonal crystals of C_{60} grown from 1,2-dichloroethane, Physical Review B, 57, 1998, 10351.

[17] V. V. Gritsenko, O.A. D`Yachenko, N. D. Kushch, N. G. Spitsina, E. B. Yagubskii, N. V. Avramenko, M. N. Forlova, Crystal solvate of C_{60} with tricloroethylene, $C_{60}\cdot C_2HCl_3$, Russian Chemical Bulletin, 43, 1994, 1183.

[18] F. Michaud, M. Barrio, D. O. López, J. Ll. Tamarit, V. Agafonov, S. Toscani, H. Szwarc, R. Céolin, Solid-State Studies on a C_{60} Solvate Grown from 1,1,2-Trichloroethane, Chemistry of Materials, 12, 2000, 3595.

[19] G. Oszlanyi, G. Bortel, G. Faigel, S. Pekker, M. Tegze, Dynamic origin of the orthorhombic symmetry of C_{60}-n-pentane, Solid State Communications, 89, 1994, 417.

[20] J. M. Hawkins, T. A. Lewis, S. D. Loren, A. Meyer, J. R. Heath, R. J. Saykally, F. J. Hollander, A crystallographic analysis of C_{60} (Buckminsterfullerene), Journal of the Chemical Society, Chemical Communications, 1991, 775.

[21] R. Céolin, V. Agafonov, R. Moret, C. Fabre, A. Rassat, A. Dworkin, D. Andre, H. Szwarc, A. J. Schierbeek, P. Bernier, A. Zahab, The decagonal twinning in C_{60} crystals grown from n-hexane, Carbon, 30, 1992, 1121.

[22] R. Céolin, V. Agafonov, B. Bachet, A. Gonthier-Vassal, H. Szwarc, S. Toscani, G. Keller, C. Fabre, A. Rassat, Solid-state studies on C_{60} solvates grown from n-heptane, Chemical Physics Letters, 244, 1995, 100.

[23] R. Céolin, V. Agafonov, S. Toscani, M. F. Gardette, A. G. Vassal, H. Szwarc, C_{60} Hexagonal Solvate Grown from n-Octane: Solid-State Studies, Fullerene Science and Technology, 5, 1997, 559.

[24] R. Céolin, D. O. López, M. Barrio, J. Ll. Tamarit, P. Espeau, B. Nicolaï, H. Allouchi, R. Papoular, Solid state studies on C_{60} solvates formed with n-alcanes:orthorhombic C_{60}·2/3 n-nonane, Chemical Physics Letters, 399, 2004, 401.

[25] S. M. Gorun, K. M. Creegan, R. D. Sherwood, D. M. Cox, V. W. Day, C. S. Day, R. M. Upton, C. E. Briant, Solvated C_{60} and C_{60}/C_{70} and the low-resolution single crystal X-ray structure of C_{60}, Journal of the Chemical Society, Chemical Communications, 1991, 1556.

[26] M. Meidine, P. B. Hitchock, H. W. Kroto, R. Taylor, D. R. M. Walton, Single crystal X-ray structure of benzene-solvated C_{60}, Journal of the Chemical Society, Chemical Communications, 1992, 1534.

[27] R. A. Assink, J. E. Schirber, D. A. Loy, B. Morosin, G. A. Carlson, Intercalation of molecular species into the interstitial sites of fullerene, Journal of Materials Research, 7, 1992, 2136.

[28] M. V. Korobov, A. L. Mirakian, N. V. Avramenko, E. F. Valeev, I. S. Neretin, Y. L. Slovokhotov, A. L. Smith, G. Olofsson, R. S. Ruoff, C_{60}·Bromobenzene Solvate: Crystallographic and Thermochemical Studies and Their Relationship to C_{60} Solubility in Bromobenzene, The Journal of Physical Chemistry B, 102, 1998, 3712.

[29] E. Mitsari, M. Romanini, N. Qureshi, J Ll.Tamarit, M. Barrio, R Macovez. C_{60} solvate with 1,1,2-trichloroethane: a cocrystal with dynamic statistical disorder, Journal of Physical Chemistry C, 120, 2016,12831.

[30] M. Barrio, D. O. López, J. L1. Tamarit, H.Szwarc, S.Toscani, R.Céolin, C_{60}-$CC1_4$ phase diagram: polythermal behaviour of solvates $C_{60}\cdot 12CC1_4$ and $C_{60}\cdot 2CC1_4$, Chemical Physics Letters, 260, 1996, 78.

[31] R. Windiks, A. Bill, B. Delley, V. Z. Kresin, Crystal Structures and Electronic Properties of Haloform-Intercalated C_{60}, Physical Review B, 33, 2002, 195418.

[32] Fact Sheet Correcting the Henry`s Law Constant for Soil Temperature, United States Environmental Protection Agency, 2001.

[33] W. Acree. Jr, J. S. Chickos, Phase Transition Enthalpy Measurements of Organic and Organometallic Compounds. Sublimation, Vaporization and Fusion Enthalpies From 1880 to 2010, Journal of Physical and Chemical Reference Data, 39, 2010, 043101.

[34] A. Wurflinger, L.C. Pardo, Thermodynamic Measurements on CH_3CCl_3, $(CH_3)_2CBr_2$, and on $nC_{20}H_{42}$ at High Pressures, Zeitschriftfür Naturforschung, A Journal of physical sciences, 57, 2002, 177.

[35] S. Toscani, H. Allouchi, J. Ll. Tamarit, D. O. López, M. Barrio, V. Agafonov, A. Rassat, H. Szwarc, R. Céolin, Decagonal C_{60} crystals grown from n-hexane solutions: solid-state and aging studies, Chemical Physics Letter, 330, 2000, 491.

[36] K. M. Kadish, R. S. Ruoff, Rencent Advances in the Chemistry and Physics of Fullerenes and Related Materials, Fullerenes volume 5, 1997, 373.

[37] B. Morosin, P. P. Newcommer, R. J. Baughman, E. L. Venturini, D. Loy, J. E. Schirber, On the “orthorhombic form of C_{60}” molecular crystals containing CS_2, Physica C: Superconductivity, 184, 1991, 21.

List of Publications

J. Ye, M. Barrio, R. Céolin, N. Qureshi, I. B. Rietveld, J. Ll. Tamarit, Van-der-Waals based solvates of C_{60} with CBr_2Cl_2 and $CBr_2(CH_3)_2$, Chemical Physics, 477, 2016, 39.

J. Ye, M. Barrio, Ph. Negrier, N. Qureshi, I. B. Rietveld, R. Céolin, J. Ll. Tamarit, Orientational order in the stable buckminster fullerene solvate $C_{60}{\cdot}2CBr_2H_2$, The European Physical Journal Special Topics, 226, 2017, 857.

Acknowledgements

This thesis becomes a reality with the support and help of many individuals. I would like to express my sincere thanks to all of them.

My deepest gratitude goes first and foremost to my supervisor Maria del Barrio, for her constant encouragement and guidance. She has walked me through all the stages of the writing of this thesis. Without her consistent and illuminating instruction, this thesis could not have reached its present form. Thank you for all!

Second, I would like to express my heartfelt gratitude to Prof. Josep Lluís Tamarit, who led me into the GCM group, this big families. Thank you for all your invaluable help and generous encouragement. I am also greatly indebted to all the friends in GCM group, who is working here right now, and was working here. Thank you for everything I could have an unforgettable six years.

Last my thanks would go to my beloved family and Di for supporting me throughout these years, especially my grandpa.

谢谢！Thank you! Gracias!